NANOGAP BASED LABEL-FREE IMPEDIMETRIC BIOSENSORS

A THESIS
SUBMITTED TO THE DEPARTMENT OF ELECTRICAL AND ELECTRONICS ENGINEERING
AND THE GRADUATE SCHOOL OF ENGINEERING AND SCIENCE
OF BILKENT UNIVERSITY
IN PARTIAL FULLFILMENT OF THE REQUIREMENTS
FOR THE DEGREE OF
MASTER OF SCIENCE

By
Oğuz Hanoğlu
July 2012

I certify that I have read this thesis and that in my opinion it is fully adequate, in scope and in quality, as a thesis for the degree of Master of Science.

Assist. Prof. Dr. Ali Kemal Okyay (Supervisor)

I certify that I have read this thesis and that in my opinion it is fully adequate, in scope and in quality, as a thesis for the degree of Master of Science.

Prof. Dr. Ergin Atalar

I certify that I have read this thesis and that in my opinion it is fully adequate, in scope and in quality, as a thesis for the degree of Master of Science.

Assist. Prof. Dr. Necmi Bıyıklı

I certify that I have read this thesis and that in my opinion it is fully adequate, in scope and in quality, as a thesis for the degree of Master of Science.

Assoc. Prof. Dr. Mustafa Özgür Güler

I certify that I have read this thesis and that in my opinion it is fully adequate, in scope and in quality, as a thesis for the degree of Master of Science.

Prof. Dr. Gönül Turhan-Sayan

Approved for the Graduate School of Engineering and Science:

Prof. Dr. Levent Onural
Director of the Graduate School

ABSTRACT

NANOGAP BASED LABEL-FREE IMPEDIMETRIC BIOSENSORS

Oğuz Hanoğlu
M.S. in Electrical and Electronics Engineering
Supervisor: Assist. Prof. Dr. Ali Kemal Okyay
July 2012

Despite lots of research going on to find a hope, *cancer* is still a major cause of death in today's world. It has been reported that cancer has some *biomarkers* in human body and detecting these biomarkers timely can pave the way for *early detection* and *successful treatments*.

Point-of-care biosensors are highly promising for this mission. If these biosensors can achieve sensitivity and reliability with a low-cost and simple platform, they can address a large mass of people who are at the early stages of cancer without any clear symptoms yet.

For this purpose, various biosensing mechanisms can be used to convert the signal coming from the recognition elements on the biosensor surface to the digital domain for signal processing. One of these mechanisms, *impedimetric (impedance based) sensing* is a very appealing electrical biosensing method since this method can offer label-free, low-cost, low-power requirement, miniaturizable, and chip-integrable detection platforms. However, impedimetric sensing in liquid medium is problematic, since during the electrical measurements, ion-based undesired layers (*electrical double layers*) are formed over the electrodes in the target liquid. Unfortunately, these layers act like a shield against the applied electric field to the liquid and can prevent the detection of the target biomarkers.

In this thesis, a *nanogap based label-free biosensor* structure is designed and using this design *impedimetric sensing in liquid medium* is demonstrated at *low frequencies (1 kHz – 100 kHz)*. Low frequency platforms are quite amenable to low-cost applications like point-of-care biosensing.

The designed structure utilizes nanometer scale electrode separation (*nanogap*). Theoretical calculations show that nanogap reduces the undesired effect of electrical double layer. Moreover, nanogap also helps in minimizing the volume of the required liquid for the measurement.

Design, fabrication, surface functionalization and biotinylation stages of the biosensor are realized in a cleanroom environment and biomimetic materials laboratory. The fabricated biosensor is tested by introducing the target molecules (streptavidin) in a phosphate-buffered saline solution. A parameter analyzer with a capacitance-voltage unit and a probe station are used for the impedance measurements.

With these biosensors, *label-free detection of streptavidin* is observed for 100 µg/mL, 10 µg/mL, 1 µg/mL, 100 ng/mL and 10 ng/mL concentrations. This is, to the best of our knowledge, the first demonstration of streptavidin detection in nanogap based label-free impedimetric biosensors. The above-mentioned concentrations show that these biosensors are promising for commercial applications. *Sensitivity to the dielectric constant of the target medium* is measured to be 132 pF per unit change in the dielectric constant at 10 kHz measurement frequency. *Reliability tests* are performed: *stable and repeatable* operation of the sensors are checked and verified.

In conclusion, this *proof-of-concept study* shows that nanogap based biosensors would be a suitable and appealing choice for sensitive, reliable, simple, low-power and low-cost point-of care biosensing applications. Next step would be utilizing the platform presented in this work in detecting specific cancer biomarkers like PSA or CA125. Thereby, developed further and commercialized, *nanogap based label-free impedimetric biosensors* can act in the battle of human being against cancer in the future.

Keywords: biosensor, early detection, point-of-care detection, impedimetric, nanogap, label-free, electrical double layer, cancer, streptavidin, biotin

ÖZET

NANOARALIK TEMELLİ ETİKETSİZ ÇELİÖLÇER BİYOALGILAYICILAR

Oğuz Hanoğlu

Elektrik ve Elektronik Mühendisliği Bölümü, Yüksek Lisans

Tez Yöneticisi: Yar. Doç. Prof. Dr. Ali Kemal Okyay

Temmuz 2012

Bir çare bulmak adına yapılan onca araştırmaya rağmen, *kanser* günümüzde halen temel ölüm nedenleri arasında yer almaktadır. Araştırmalar göstermiştir ki kanser vücutta bazı *biyoişaretçilere* sahiptir ve bu biyoişaretçileri zamanında tespit edebilmek *erken tanıya* ve *başarılı tedavilere* olanak sağlayabilir.

Yerinde tanı yapabilen biyoalgılayıcılar bu görev için oldukça ümit vadedicidirler. Eğer bu biyoalgılayıcılar, duyarlılığı ve güvenilirliği düşük maliyetli ve basit bir yapı ile sağlayabilirlerse, kanserin erken aşamalarında bulunan ve henüz ciddi bir belirtiye sahip olmayan geniş kitlelere hitap edebilirler.

Bu amaçla, biyoalgılayıcı yüzeyindeki algılama elemanından gelen sinyali sinyal işleme amacıyla sayısal alana dönüştürmeye yarayan çeşitli biyoalgılama mekanizmaları kullanılabilir. Bu mekanizmalardan biri olan *çeli temelli algılama* çok cazip bir biyoalgılama yöntemidir; çünkü bu yöntem etiketsiz, düşük maliyetli, düşük güç gerektiren, küçültülebilir ve çiple tümleştirilebilir algılama platformları sunabilir. Ancak, çeli temelli algılama sıvı ortamlarda sorunludur çünkü elektriksel ölçümler esnasında, hedef sıvıdaki elektrotlar üzerinde iyon temelli istenmeyen katmanlar (*elektriksel çift katmanlar*) oluşmaktadır. Ne yazık ki, bu katmanlar sıvıya uygulanan elektriksel alana karşı bir kalkan gibi davranmakta ve hedef biyoişaretçilerin algılanmasını önleyebilmektedir.

Bu tezde *nanoaralık temelli etiketsiz bir biyoalgılayıcı* yapısı tasarlanmış ve bu tasarım kullanılarak *sıvı ortamda* ve *düşük frekanslarda (1kHz – 100 kHz) çeli temelli algılama* gösterilmiştir. Düşük frekanslı platformlar yerinde tanı yapabilen biyoalgılayıcılar gibi düşük maliyetli uygulamalara oldukça yatkındırlar.

Tasarlanan yapı nanometre düzeyinde elektrot ayrımı (*nanoaralık*) kullanmaktadır. Teorik hesaplamalar nanoaralığın, elektriksel çift katmanın istenmeyen etkisini azalttığını göstermiştir. Buna ek olarak, nanoaralık ölçüm için kullanılan sıvı hacmini asgari düzeye çekmeye de yardımcı olmaktadır.

Biyoalgılayıcının *tasarım, üretim, yüzey etkinleştirme ve biyotinleme* aşamaları temizoda ortamında ve biyomimetik malzeme laboratuarında gerçekleştirilmiştir.Üretilen biyoalgılayıcılar hedef moleküllerin (streptavidin) fosfat tamponlu bir tuzlu su çözeltisi içinde tanıtılması ile test edilmiştir. Çeli ölçümleri için sığa-gerilim ölçüm birimli bir parametre inceleyici ve bir ölçüm istasyonu kullanılmıştır.

Bu biyoalgılayıcılarla, *etiketsiz streptavidin algılaması* 100 µg/mL, 10 µg/mL, 1 µg/mL, 100 ng/mL ve 10 ng/mL derişimlerinde gözlemlenmiştir. Bu, bildiğimiz kadarıyla, nanoaralık temelli etiketsiz çeliölçer biyoalgılayıcılarla streptavidin algılanmasının ilk gösterimidir. Yukarıda belirtilen derişimler bu biyoalgılayıcıların ticari uygulamalar için ümit vadettiğini göstermektedir. *Hedef ortamın dielektrik sabitine duyarlılık*, 10 kHz ölçüm frekansında dielektrik sabitindeki birim değişikliğe karşı 132 pF olarak ölçülmüştür. *Güvenilirlik testleri* gerçekleştirilmiştir; algılayıcıların *kararlı ve tekrarlanabilir* çalışırlığı kontrol edilmiş ve doğrulanmıştır.

Sonuç olarak, bu *kavramsal ispatlayıcı çalışma* nanoaralık temelli biyoalgılayıcıların duyarlı, güvenilir, basit, düşük güç ve düşük maliyet gerektiren biyoalgılama uygulamaları için uygun ve cazip bir seçenek olabileceğini göstermektedir. Bundan sonraki adım, bu çalışmada tanıtılan platformu PSA ya da CA125 gibi belirli kanser biyoişaretçilerini algılamada kullanmak olabilir. Böylece, daha da geliştirilir ve ticarileştirilirse, *nanoaralık* *temelli etiketsiz çeliölçer biyoalgılayıcılar* gelecekte insanoğlunun kansere karşı savaşında yer alabilirler.

Anahtar Sözcükler: biyoalgılayıcı, erken tanı, yerinde tanı, çeliölçüm, nanoaralık, etiketsiz, elektriksel çift katman, kanser, streptavidin, biyotin

If you fail to attain self knowledge, what good is there in your studies?

Yunus Emre (13^{th}-14^{th} centuries)

Acknowledgements

I am full of gratitude as you will see in this part. Wherever possible, I list my thanks in alphabetical order of the surnames.

I would like to start by expressing my thanks to those who somehow contributed to this thesis and/or to my career at Bilkent. Although I may not list you by name in the following lines, please forgive me and note that I give you the first place in my acknowledgements.

No words could ever do justice to express my thanks and gratitude to my beloved family. So, I will not even begin expressing how their love, guidance, support, encouragement, warmth, comfort, joy, inspiration, affection, help, advice… played a critical role in this work.

Rudyard Kipling said *“I keep six honest serving-men (They taught me all I knew); their names are What and Why and When and How and Where and Who.”* Thanks to my six men whom I had the opportunity to meet a long time ago. I am grateful to each of you for you have stayed with me up to now. It is my pleasure to share in this thesis what you taught me during my research.

Thanks to my supervisor, Prof. Ali Kemal Okyay. I would like to express my deepest graduate to you for being a wonderful supervisor to me. You were involved in every aspect of my research, helped enormously by sharing your invaluable experience and enlightened my path with your guidance and support. You were not only a supervisor teaching me how to do research but you were also a mentor showing and explaining how to be an academician, how to run a research team and how to collaborate with other researchers. You have given me freedom to explore many areas and have always been open to provide advice and support. I am more than grateful to you for your confidence in my abilities, your gentle and pleasing demeanor, your genuine thoughtfulness, and for the magnificent opportunities you provided me.

I would like to thank Prof. Ergin Atalar, Prof. Necmi Bıyıklı, Prof. Mustafa Özgür Güler and Prof. Gönül Turhan Sayan for being members of my thesis committee, reading my thesis, providing suggestions and helping me making it better.

The work described in this thesis is result of a collaborative effort. I would like to thank our collaborators Prof. Necmi Bıyıklı and Prof. Mustafa Özgür Güler for their productive and rewarding collaboration. Your encouragement, guidance, useful and timely comments, expertise and lab opportunities have all been essential to achieve the research results in this thesis. Thanks to Prof. Sedat Ağan from Kırıkkale University for his contributions and assignment of his students to our nanogap project. I would like to deeply thank Handan Acar, a PhD student of Dr. Güler and the princess of our project. You managed every detail in the surface functionalization and biotinylation parts of our project very well. You have introduced various laboratory equipments (ellipsometer, scanning electron microscope, etc.) to me and have kindly shared your experience. It has been a privilege to work with you and has been a delight to experience your humorous and well-disciplined working style. I would also like to thank Selim Sülek for his friendship and contributions including the XPS measurements.

There are special people who have played a critical role in my career. They are *"the wonders of my academic world"*. I would like to bestow my special thanks to Prof. Haluk Külah, Prof. Ahmet Rumeli and Prof. Gönül Turhan-Sayan (Gönül Hocam, literally). You have always made me feel comfortable and welcome whenever I visited you and I asked you for advice. I have left your offices pretty much every time with a precious piece of advice and a smile on my face. I hope I will always carry the wisdom you taught me and apply it in my life.

I would like to express my deep appreciation to Prof. Haldun Özaktaş for answering my curious six men on numerous subjects varying from the academic world to the blinking stars. I truly appreciate your time and interest. I would like to thank Prof. Tayfun Akın, Prof. Abdullah Atalar, Prof. Nesim Erkip, Prof. Özay Oral and Prof. Yusuf Ziya Özcan for generously sharing their experience, ideas and recommendations concerning my career. You have been very instrumental in my career decisions. I would like to thank Prof. Ekmel Özbay for showing how diligence and intelligence can achieve wonderful things with the opportunities in Turkey. You have been a great inspiration to me.

I would like to acknowledge the administrative and technical staff of our department, especially Ergün Hırlakoğlu and Mürüvet Parlakay.

I think there are amazing elements of doing research in a *nano*technology research center; one of them is you see how to be happy with the smallest of things. I had this opportunity and witnessed that *re*search shows the meaning of its prefix countless times up until you reach the end and then, you truly appreciate the whole process. Confucius said *"I hear and I forget; I see and I remember; I do and I understand."* Now, I deeply understand the whole process and see, with admiration, how *with every hardship comes ease*.

I owe a great many thanks to the wonderful, talented, smart, and fun people who were with me during this instructive process. Dear Fatih Bilge Atar, Fırat Yılmaz and Mustafa Yüksel, I feel privileged and honored to have worked with you. You have contributed a lot to our project with your diligence and intelligence. The joy you have brought into my everyday life (or the joy you have brought into my everyday life ☺) has been a powerful driving force. You have been great friends and have made up many of my best times I have had at Bilkent.

I want to extend my thanks to the past and present members of our research team including Sabri Alkış, Levent E. Aygün, Enes Battal, Temmuz Ceyhan, Furkan Çimen, Ş. Burç Eryılmaz, Mohammad Ghaffari, Abdullah Gülle, Yunus Emre Kesim, A. Cahit Köşger, Burak Mert, Efe Onaran, M.Cengiz Onbaşlı, Feyza Bozkurt-Oruç, K. Gürkan Polat, Ferhat Taşdemir, Onur Tidin, , Ahmet Turnalı, Ahmet D. Usta, Habip K. Üsküdar, Alper Yeşilyurt, T. Alper Yoğurt. Thanks to Yunus Emre Kesim for the useful discussions. Thanks to Feyza Bozkurt-Oruç for her help in the ALD and lithography processes. Thanks to

Mohammad Ghaffari for the SEM images. Thanks to all of my teammates for their pleasant friendship.

Special thanks to Alper Yeşilyurt and Aslı Ünlügedik-Yılmaz, who were my first mentors in the cleanroom and Elif Aydoğdu, who was the other. In addition, UNAM (Institute of Materials Science and Nanotechnology) researchers and staff helped me greatly. Thanks to them including Çağla Özgit-Akgün, Engin Çağatay, İnci Dönmez, Deniz Kocaay, Fikret Piri, Mustafa Kemal Ruhi, Adem Saraç and Semih Yaşar. I am grateful to all of you for your assistance and for being my precious friends.

The poem says *"Come, let us be friends for once; let us make life easy on us…" (Yunus Emre)*. I would like to thank my friends for making life easy on me: Volkan Açıkel, Mehmet Eren Ahsen, Halil Akçalı, İbrahim Akçalı, Shahab Akhavan, Ahmet Emin Akosman, Deniz Aksoy, Alexandra Zehra Aksu, Sinan Alemdar, Umut Aradağ, Damla Ateş, Gökçe Osman Balkan, Gamze Baykaldı, Bayram Bütün, Seymur Cahangirov, Mustafa Rıdvan Cantaş, O. Orkun Cellek, Ahmet Fatih Cihan, Tuğrul Ç. Cinkara, Cemil C. Coşkun, Atilla Özgür Çakmak, Hümeyra Çağlayan, Neslihan Çiçek, Evrim İ. Çolak, Oğuzcan Dobrucalı, Hüseyin Duman, Burak Dura, Çağlar D. Emiroğlu, Talha Erdem, Gülesin Eren, Yavuz Nuri Ertaş, Hatice Ertuğrul, Ruslan Garifullin, Behnam Ghassemiparvin, Sayım Gökyar, Erdal Gönendik, T. Cihad Gülcü, Aşkın Güler, Mert Gülleroğlu, Kıvanç Güngör, Burak Güzeltürk, Berna Hanoğlu, Ali Nail İnal, Mehmet Kanık, Murat Kayserilioğlu, Yusuf Keleştemur, Ceyhun Kelleci, Tural Khudiyev, Veli Tayfun Kılıç, Evren Mutlugün, Sedat Nizamoğlu, M. Alican Noyan, Selim Olçum, S. Figen Öktem, Burak Özbey, Şule Öztürk, Johanna Sandberg, Emre Sarı, M. Akın Sefünç, Volkan Şirin, Orkun Tunçel, Bilal Turan, Özhan Turgut, Erdem Ulusoy, Can Uran, Kadir F. Uyanık, Okan Ünlü, Mustafa Ürel, Duygu Yalçın, Mahmut Yavuzer, M.Oğuzhan Yayla, Neval A. Cinel-Yılmaz, Murat C. Yüksek, Gülis Zengin, Taner Zorbay and many others whose names I forget to list. I would like to add this list to my ECD (electronic circuit design course) students with whom we *"Enjoy ECD"*. The poem goes on *"... let us be lovers and loved ones; the earth shall be left to no one."* I thank all of you

for being "lovers and loved ones" and making my graduate experience memorable.

Thanks to Dr. Joshua T. Nevill for kindly sharing his experience at UC Berkeley and for the discussion (and coffee) at the cafe of San Francisco. Your PhD thesis has become an inspiring motivation for me and the discussions with you enlightened my research path.

I would like to acknowledge TÜBİTAK for supporting my masters study. I very much appreciate their generous support, which has been a strong driving force. Also, I would like to acknowledge the IEEE Electron Devices Society for their financial and moral support.

Finally, I would like to acknowledge my hats… There are many roles we are expected to play on the stage of life. At TEGV (Educational Volunteers), this is explained to children by wearing different colored hats on top of each other, each hat corresponds to a different role like "citizen", "daughter" and "gamer". Looking from this perspective, I have worn quite a few hats at Bilkent, including but not limited to: "the researcher hat", "the graduate student hat", "the teaching assistant hat", "the assistant coordinator hat", "the (recitation) instructor hat", "the (undergraduate) advisor hat" as well as "the goalkeeper hat", "the (novice) gardener hat" and in general, "the Bilkenteer hat". Thank you my dear hats for making my time at Bilkent so much more beneficial and enjoyable. You have been priceless opportunities for me to improve myself. I am truly grateful.

This is the end of my acknowledgements, which is, to my experience, one of the most read parts of a thesis. The following parts of this thesis will be expectedly more technical. Albert Einstein said *"Everything should be made as simple as possible, but not simpler"* I have tried a lot to keep it simple and straightforward (the kiss principle). Naturally, there are a lot of details left out since it is quite difficult to fit everything in one thesis. Nevertheless, I hope this thesis will present to you a coherent story of our biosensors and I hope that you will enjoy reading it.

To the Honeybee who knows how to thank a daisy,
To the Daisy who knows how to thank a honeybee, and

To Him who teaches me how to thank…

Table of Contents

List of Figures

List of Tables

Chapter 1

Introduction

1.1 Motivation

Cancer is still a major leading cause of death in today's world. Despite lots of research going on to find a hope, it has been reported that 7.6 million people died worldwide (approximately 13% of all deaths) because of this disease in 2008 and the annual death toll is projected to be 13.1 million in 2030 [1], [2]. Unfortunately, current technology on cancer diagnosis and treatment is far from helping millions of cancer patients [3–5]. Figure 1.1 illustrates the disappointing truth by the cancer incidence and mortality numbers of 2008. Only the five cancer diseases (pancreas, liver, lung, oesophagus and gallbladder) with the highest mortality/incidence rates are shown.

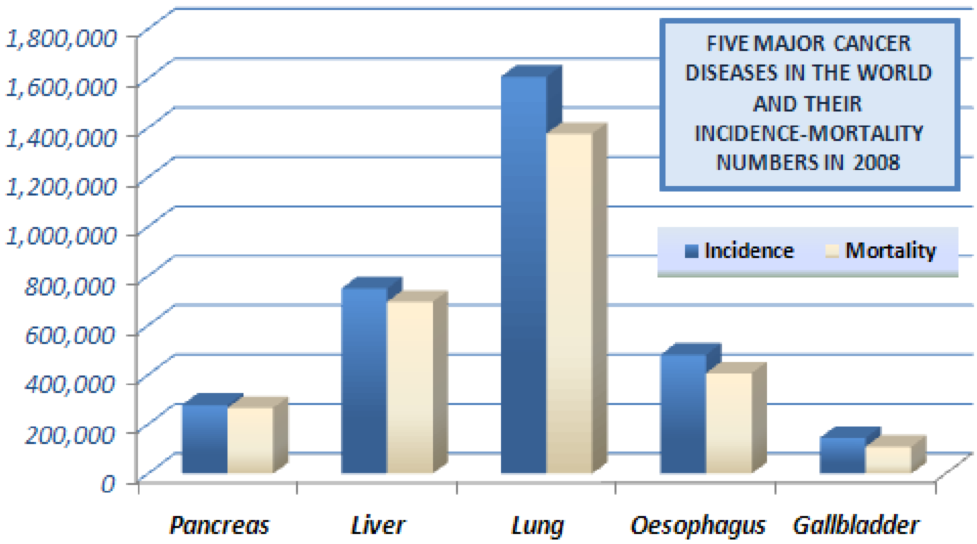

a) Cancer numbers in the world

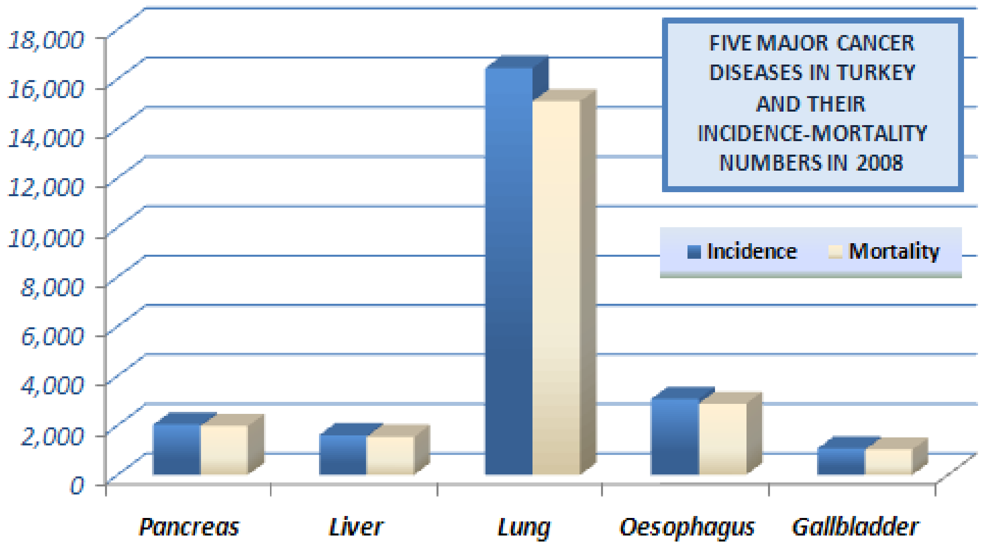

b) Cancer numbers in Turkey

Figure 1.1 Incidence and mortality numbers of the five major cancer diseases with highest mortality/incidence rates in 2008 (after [2])

The problem lies in the strategy of this smart enemy. *Cancer* is defined as uncontrolled and abnormal cell growth that leads to the formation of tumor mass [4]. Even after the formation, tumor may progress in stealth mode usually without any symptoms and turning out to a fatal risk over time by spreading to the other parts of the body. This is called *metastasis*. After metastasis, symptoms starts appearing, though at this stage it is very difficult to remove the millions of cancer cells from the body [4].

It is for no doubt that *early detection* is extremely important in the battle of the human against cancer. The determined and industrious warriors of this battle, scientists and doctors have discovered over the years of intense research that some cancer indicators in human blood called *cancer biomarkers* can be used in the early detection if human body is constantly monitored. Cancer biomarkers are great allies not only for the early detection of cancer; but also monitoring the progress of its treatment [4]. Some cancer biomarkers discovered so far are listed in Table 1.2.

Cancer	**Biomarker**
Prostate	PSA,PAP
Breast	CA15-3, CA125, CA27.29, CEA, BRCA1, BRCA2, MUC-1, CEA, NY-BR-1, ING-1
Leukemia	Chromosomal abnormalities
Testicular	α-Fetoprotein (AFP), β-humanchorionic gonadatropin, CAGE-1, ESO-1
Ovarian	CA125, AFP, hCG, p53, CEA
Bladder	BAT, FDP, NMP22, HA-Hase, BLCA-4, CYFRA21-1
Colon and pancreatic	CEA, CA19-9, CA24-2, p53
Lung	NY-ESO-1, CEA, CA19-9, SCC, CYFRA21-1, NSE
Melanoma	Tyrosinase, NY-ESO-1
Liver	AFP, CEA
Gastric carcinoma	CA72-4, CEA, CA19-9
Esophagus carcinoma	SCC
Trophoblastic	SCC, hCG
Any solid tumor	Circulating tumor cells in biological fluids, expression of targeted growth factor receptors

Table 1.1 Biomarkers associated with cancer diseases [6]

Clearly the idea of monitoring the cancer biomarker cannot be labeled ‘original’ considering the well-known operation principles of the immune system. Nevertheless, mimicking the immune system is not as easy as it seems.

There is variety of molecular origins for biomarkers (i.e. proteins, enzymes, DNA, RNA) depending on a specific cancer and more importantly, their presence in human blood may not always be a direct indication of cancer. To illustrate, one of the biomarkers of prostate cancer is prostate specific antigen (PSA). However, its presence in human blood correlates with cancer beyond the threshold level of 4 ng/mL; below this is considered normal [4–6].

Cancer biomarker	**Threshold**
PSA	4 ng/mL
CEA	3 ng/mL
NSE	12.5 μg/mL
ALP	~0
SCCA	1.5 ng/mL
Ferritin	250 ng/mL
AFP	10 ng/mL

Table 1.2 Some cancer biomarkers and their threshold levels in human serum [6]

In conclusion, there are two headlines in the issue: Although the exact mechanism beyond the cancer and its metastasis is still unknown, early detection (before the metastasis) is promising for successful treatments. Cancer biomarkers play a key role in early cancer detection and, although not easy, it is essential to periodically monitor them in such a way that the alarm bell should not be set ringing unless their levels exceed the threshold.

In the world of electrical engineer, these words evoke the term “sensor”; which can be used for both detection and quantification of cancer biomarkers in the body. These sensors, more specifically called *biosensors*, should not necessarily be as accurate or sensitive as to replace the complex, bulky and costly equipments in the hospitals and medical laboratories; but, instead they can support them by addressing a larger mass of people, who are at the early stages of cancer without any symptoms yet. Obviously, the gold requirements are to be low-cost, fast, and small. They should be easily accessible at the home site and usable without any complex sample handling or any kind of special expertise. The sensors serving these purposes are called *point-of-care* (POC) *biosensors*.

Research is still going on developing them for early cancer detection applications. This thesis is a part of this research and hopefully be a good contribution to it. This work investigates an electrical detection platform for which a benign protein pair (streptavidin and biotin) is used as a proof-of-concept demonstration. The presented detection platform, in principle, can be tailored for a specific cancer type using the related cancer biomarker and recognition element pair.

1.2 Organization of this thesis

This thesis will continue by elaborating on *biosensors*, related concepts and performance metrics in Chapter 2. In Chapter 3, *impedimetric sensing* will be introduced as an efficient tool for developing electrical based biosensors that can be miniaturized and suited to POC applications. A crucial part of the theme underlying this thesis, utilizing *nanogap* concept of device fabrication in impedimetric sensing, will also be analyzed in this chapter. The fruits of this idea, *nanogap based impedimetric biosensors*, will be presented thoroughly in Chapter 4. Their operation principles, sensor layout, fabrication, surface functionalization and biotinylation will be the topics covered in this chapter. Chapter 5 will build upon the previous chapter and offer detailed information about *the measurement setup*, *sensor performance results* in terms of *sensitivity* and *reliability*, as well as *critical discussions* on these results. The final chapter will briefly summarize this work with its *key achievements* and the thesis will be concluded by some discussion on *future directions* of this work.

Chapter 2

Biosensors, Related Concepts and Performance Metrics

2.1 Introduction

Biosensors are devices designed for detection or quantification of biological components like specific proteins or DNA sequences [7]. An interesting historical note about the biosensors is that one of the oldest biosensors was a canary used by coal miners (Figure 2.1). In the 19^{th} century, coal miners were taking a canary in a cage with them while going underground. Canaries can quickly metabolize odorless toxic gases like methane and carbon monoxide and thereby, warn the coal miners by stopping singing in the mine [8]. Though, eco-friendliness is a big concern for these sensors.

Figure 2.1 Canaries as one of the oldest biosensors from the 19^{th} century [8]

Since then, biosensor technology has advanced significantly by utilizing the outputs of various sciences like electronics, physics, biology, chemistry and material sciences. Today, they have application areas in many fields: *Environmental applications* include harmful organisms' detection in air and water. *Food applications* include monitoring food-borne pathogens in the food. *Military applications* include detecting threats in a biological warfare. *Health applications* include the early detection of diseases and monitoring the effects of treatments [4–9]. Among the health applications, glucose measuring sensors are perhaps the most well-known, commercialized examples. These sensors address the large market of diabetic people constituting 1-2% of world's population. They generally utilize electrochemical detectors with an enzyme called glucose oxidase and are used by placing a drop of blood on a test strip which has an interface with the sensor (Figure 2.2 a-b). Others can be in the form of a wristwatch and utilize reverse iontophoresis to extract glucose level over the skin tissue (Figure 2.2c). In this case, monitoring of glucose level can be done periodically like in every 10 minutes, stored in the device memory and reported as a function time at the end of the day [9], [10].

a) GlucoSure™ [11] b) OneTouch Ultra® [12] c) GlucoWatch® [10]

Figure 2.2 Some of the commercial glucose biosensors

2.2 Biosensor Related Concepts

2.2.1 Parts of a biosensor

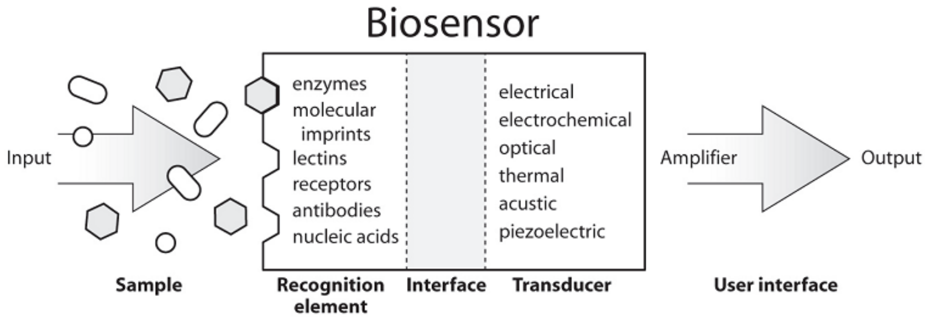

Figure 2.3 Parts of a biosensor [13]

A biosensor is composed of several parts (Figure 2.3). *Target molecules* in the sample can be of various biological origins like nucleic acids, proteins and bacteria. These molecules vary in size from nanometer to micrometers scale. As far as cancer detection is considered, target molecules (cancer biomarkers) are chosen such that they indicate the presence of a specific type of cancer (Table 1.2).

To recognize these target molecules, biosensor's sensing areas are modified with *recognition elements*. A range of recognition elements is used for cancer biomarker detection. Antibody molecules related to specific target molecules are widely investigated in the literature. In addition, synthetic recognition elements are also fabricated and used. These elements include synthetic peptides, aptamers and metal oxide materials[6].

As a result, *recognition elements* act as an interface between the *target molecules* and the *transducer*. Transducer senses the signal coming from the recognition elements and transfers this to the digital domain for signal processing. Finally, the processed signal is displayed at the *output*.

2.2.2 Biosensor transduction mechanisms

Transduction can be realized via numerous mechanisms including light based [6], [14–17], magnetoresistance based [18–22] and electrical based [23–29] detection. Among these mechanisms, electrical based detection outshines as a strong candidate for point-of-care health applications since it offers simplicity, chip-integrability; and, moreover it is quite inclined to low-cost, low-power platforms [7]. In this work, electrical based detection is used for transduction.

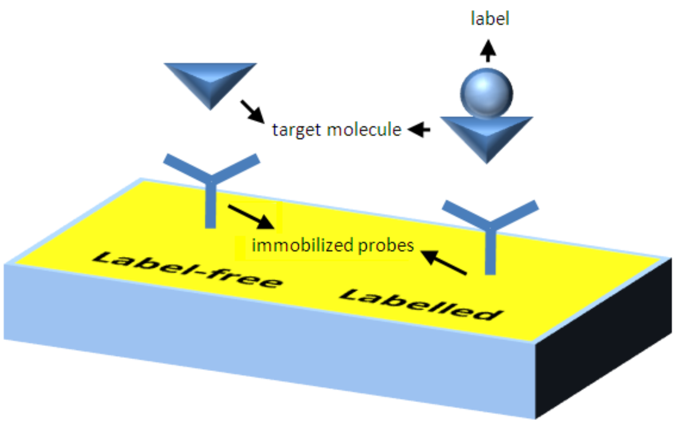

Figure 2.4 Label-free and Labelled detection

An important distinction in biosensor transduction is having labelled or label-free detection mechanism (Figure 2.4). *Labelled biosensors* require target molecules to be labelled. In these sensors, the output of the transducer corresponds to the amount of label and this is assumed to give the number of bound targets. Anything allowing convenient detection like magnetic beads [30], fluorophores [31] or enzymes [32] can be used as a label. Labelled biosensors are frequently used in immunoassay technologies. Enzyme-linked immunosorbent assay (ELISA) sensor is one of the oldest examples [33]. Unfortunately, these sensors generally require an expert for sample handling and an additional time for labelling process. Besides, labelling process may decrease target molecules' affinity to immobilized probes and this is problematic especially in low concentration detection [7], [34]. All of these issues as well as the higher cost of labelled sensors make *label-free biosensors* rather attractive for cancer monitoring applications. Label-free biosensors are able to detect the target directly in a sample with no or very little sample preparation.

As a result, labelled detection based biosensors are not much suitable for point-of-care health monitoring applications due to sample handling, time and cost issues; whereas label-free biosensors, allowing simpler, faster and low-cost detection, are more prone to this kind of applications [7]. In this work, label-free biosensing is studied.

2.2.3 Selectivity and its crucial role in biosensing

*Selectivity***,** sometimes termed *specificity***,** is the ability of specifically responding of the sensor to the target analyte. It is one of the biggest challenges in all label-free sensors. If the active surface of the sensor is not developed to ensure higher specific than non-specific binding, the output signal would carry uncertainty and this would result in poor biosensing performance. To illustrate, blood serum typically contains ca. 70 mg/mL total protein content. For the case of prostate cancer, prostate specific antigen (PSA) to be detected in blood serum is several ng/mL, that is “detecting 1 in 10,000” [35], [36]. This contrast is terrifying; but, fortunately, there are a number of strategies developed to find the needle in the haystack. Non-specific binding which results from the adhesion of undesired molecules to the active biosensing area, can be prevented by coating *blocking agents* around the active biosensing area. These agents can adsorb the molecules that would nonspecifically bind to the sensing area [selectivity folder]. Bovine serum antigen (BSA) and salmon serum DNA are well-known examples in the literature. Another strategy is purifying the human blood from interfering proteins. However, for point-of-care applications, this is only meaningful if purification can be completed in a simple setting at patient site. *Micro-total analysis systems* (μTAS, or *lab-on-a-chip* (LoC)) technology is promising for this purpose [37–39]. They can allow the non-expert to do complex analyses by miniaturizing the laboratory tools on a chip. Finally, non-specificity can be circumvented to a certain extent by a “rinse” step before taking measurement and such a “rinse” step would remove the nonspecifically bound molecules, leaving specifically bound ones, which are typically so strongly bound that such a rinse does not reverse them [40], [41].

2.3 Biosensor Performance Metrics

Performance metrics that will be analyzed in this work are mainly sensitivity, dynamic range, upper and lower limits of detection, reliability, stability, response time and repeatability**.** They will be defined in this section and used frequently in Chapter 5 while the results are discussed.

Sensitivity can be defined in two ways: [42]

When target molecule sensing is considered, it is defined as the minimum detectable change in the response of the sensor per the associated change in the analyte concentration. Sensitivity depends on various factors like the affinity and selectivity of binding process, transduction mechanism and amplification and noise of the readout circuitry. Either of these can limit the overall sensitivity. *Dynamic range* includes the concentrations for which the target molecule can be detected. Dynamic range of a sensor defines the variety of applications that a sensor can be used (Figure 2.5). For example, whereas the range required for metabolites is in μmol/L and mmol/L, for viral or tumor antigens like PSA this is in the order of pmol/L. Dynamic range is bounded by *upper and lower limit of detections*. Both of these limits depend on the sensor as well as the specific target and recognition molecules of interest. For example, a commercial enzyme-linked immunosorbent assay (ELISA) sensor exhibits different dynamic ranges depending on the targets used [33].

Another and more general definition of sensitivity is the change in the output signal with respect to a unit change in the input parameter. Mathematically, this equals to the slope of the output characteristic curve. This definition will be used while analyzing the sensitivity of produced biosensors with respect to dielectric constant of the solution.

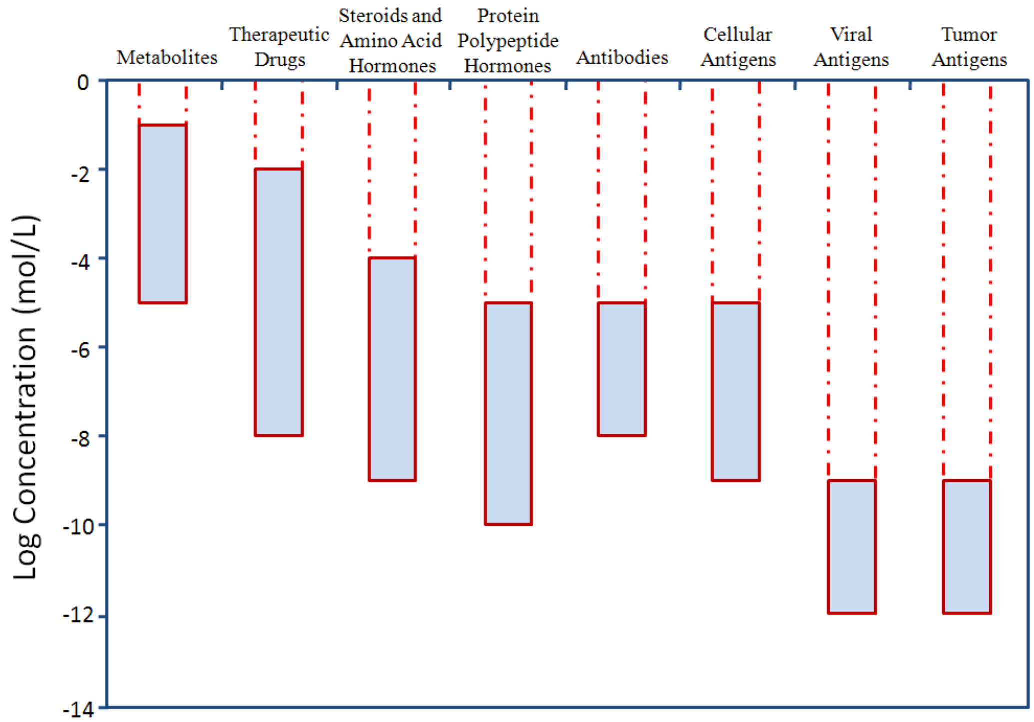

Figure 2.5 Dynamic ranges associated with some clinically important analytes [After 43].

Sensitivity in biosensors can be limited by either the binding of the desired target molecule to the surface or the transduction mechanism for detecting this binding [7]. In this work, the focus is on the demonstration of nanogap based impedimetric detection as a transduction mechanism and thus, streptavidin-biotin pair (instead of a specific cancer related pair) is used for the proof-of-concept.

Reliability is defined as the sensor's ability to produce consistent results with respect to time. For commercialization purposes, reliability is at least as important as sensitivity. However, unfortunately, it is generally not reported in the biosensor studies in the literature [7]. Reliability has two aspects: stability and repeatability.

Stability is settling to a constant response after the sample solution is introduced. Biosensors do not change output state immediately after the sample solution is applied due to delays related to the transduction mechanism.

Response time is the time required for the output response to reach its final value within the tolerance band. It is simply illustrated in Figure 2.6.

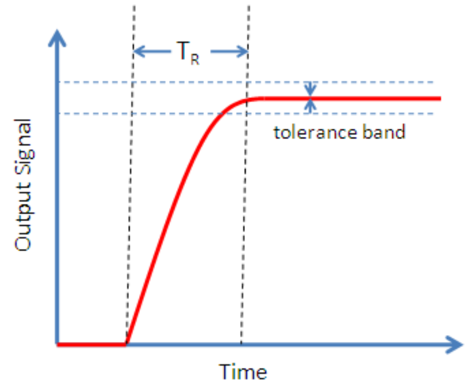

Figure 2.6 Illustration of the response time (T_R) and tolerance band. Response time consists of the time period starting from the application of sample solution and ending with the output signal to reach its final value within tolerance band.

Repeatability is providing same output response when same measurements are performed repeatedly.

Verification of the reliability can be done by observing the output signal while successive target application and removal steps are conducted. This is illustrated on a figurative output signal versus time plot in Figure 2.7.

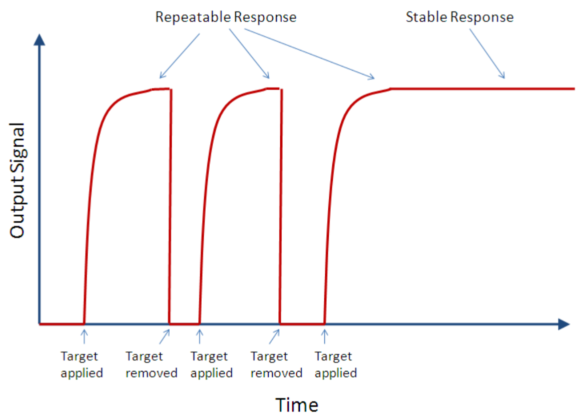

Figure 2.7 Illustration of repeatable and stable responses on a reliable sensor.

2.4 Conclusion

Biosensor technology utilizes many academic disciplines and addresses to a variety of sectors. Health industry is one of them. Label-free and electrical based biosensors are promising for point-of-care health applications. Selectivity is an important concern which should be satisfied by simple methods that can be implemented at patient’s site rather than complex clinical settings and without any special expertise. Performance metrics define the application areas of a biosensor. For a biosensor to be utilized in early cancer detection, sensitivity metrics associated with the specific biomarker of the targeted cancer should be satisfied. As for all sensors, reliability is an essential performance metric for point-of-care biosensors and it should definitely be demanded from any candidate.

Chapter 3

Impedimetric Sensing for Biosensor Applications

3.1 Introduction

Impedimetric (impedance based) sensing is an electrical based technique for characterizing systems of interest. It offers advantages like label-free, low cost, low power requirement, miniaturizable, and chip-integrable detection platforms, which are extremely appealing for point-of-care applications. This chapter starts by introduction of this efficient technique and continues with explanation of the concepts related to it. Unfortunately, impedimetric sensing in ionic solutions is hampered by a charge layer called electric double layer. The rest of the chapter handles this problem and offers nanogap based biosensors as an effective solution.

Impedimetric sensing deals with impedimetric response of samples. Response depends on sample's permittivity and resistivity and thereby, gives insight about sample. *Impedance* (Z) is a measure of how a sample responds to an applied sinusoidal (AC) voltage and it is a function of the frequency of the AC voltage.

If an AC voltage is applied to a sample media with linear constituents, a current signal is sustained through it. Impedance can be calculated by using these voltage and current signals.

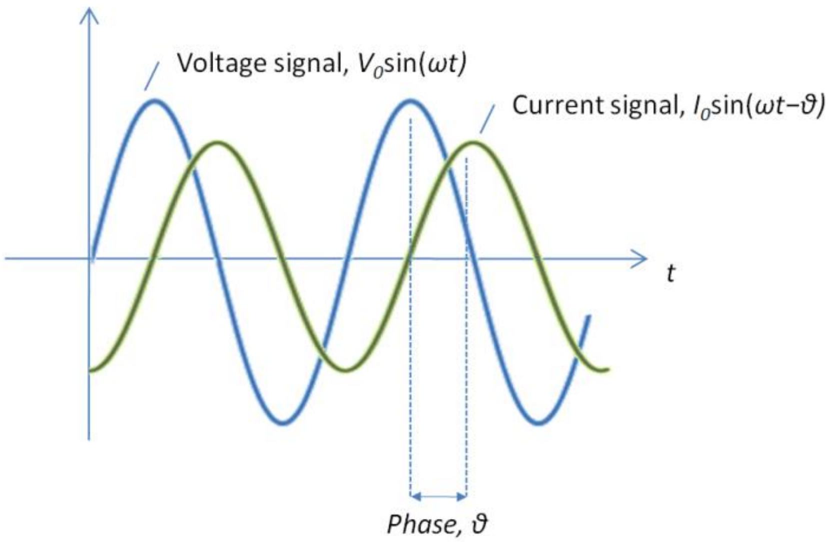

Figure 3.1 Representative figure showing voltage and current signals on a sample. V_0 and I_0 are the magnitudes of voltage and current signals respectively and θ is the difference in phase angles of both signals

Amplitudes V_0, I_0 of the signals as well as the phase difference θ can be obtained and related to sample's impedance by the relation

$$Z = \frac{V_0}{I_0} e^{j\theta} \tag{3.1}$$

Impedance is a complex quantity defined as the ratio of voltage phasor V to current phasor I of the sample.

$$Z \triangleq \frac{V}{I} \tag{3.2}$$

It can be better visualized on the complex plane.

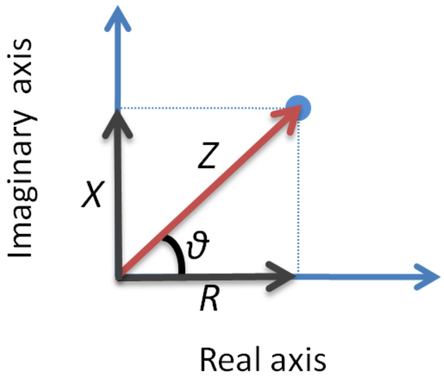

Figure 3.2 Graphical representation of the impedance on the complex plane. Impedance is related to sample's resistance (R) and reactance (X).

Once impedance is obtained, it can be converted to the other fundamental electrical notions as shown in Table 3.1.

$Z = R + jX$	$R = \|Z\|cos\ (\theta)$	Z, Impedance R, Resistance X, Reactance θ, Phase Angle	Y, Admittance G, Conductance B, Susceptance
$\|Z\| = \sqrt{R^2 + X^2}$	$X = \|Z\|sin(\theta)$		
$\theta = arctan\ (\frac{X}{R})$	$Y = \frac{1}{Z} = G + jB$		

Table 3.1 Fundamental equations and definitions related to the impedance

3.2 Impedimetric Sensing Concepts

Three fundamental concepts of impedimetric sensing in this work are dielectric constant, parallel plate capacitor and electrical double layer; these concepts will be introduced in this section.

3.2.1 Dielectric Constant (Relative Permittivity, ϵ_r):

Dielectric constant (ϵ_r) is used as equivalent to the more general term relative permittivity. Thus, the method preferred in this part is to define permittivity first, and then, state its relation to dielectric constant.

Fundamental law of electrostatics, stated by French scientist Charles-Augustin de Coulomb in 1787, describes the electrostatic interaction between two electrically charged particles [44].

$$|F| = k\frac{|q_1q_2|}{r^2} \tag{3.3}$$

In this law (known as Coulomb's law) F is the force acting on point charges q_1 and q_2, r is the separation distance, and k is the proportionality constant. Force F created by a point charge q on a unit charge of distance r is defined as the electric field (E). Thus, Coulomb's law can also be stated as

$$|E| = k\frac{|q|}{r^2} \tag{3.4}$$

k, the proportionality constant, depends on the medium. In free space, k is $\frac{1}{4\pi\epsilon_0}$, which is also known as Coulomb's constant and approximately equal to 8.9876×10^9 N m^2 C^{-2}. ϵ_0 is called permittivity of free space and in a dielectric, it is multiplied by the relative permittivity of the dielectric (ϵ_r).

The origin of permittivity belongs to dipoles in a dielectric. Although a molecule in a dielectric is macroscopically neutral, small displacements in its positive and negative charges results when an external electric field is applied and so, it becomes a dipole. This kind of molecules which behave like a dipole in the presence of an electric field is called nonpolar molecules. On the other hand, some molecules like H_2O, can exhibit the polarization effect even without any electric field due to structural formation of their atoms. These are called polar molecules [45].

In a dielectric material, no polarization effect is observed even if the polar molecules exist. This is because these molecules are randomly oriented, and macroscopically, their effects are cancelled on the average. When an electric field is applied, however, dipoles experience a force and randomness in their alignments disappears since all tend to align in parallel to the external field (Figure 3.3).

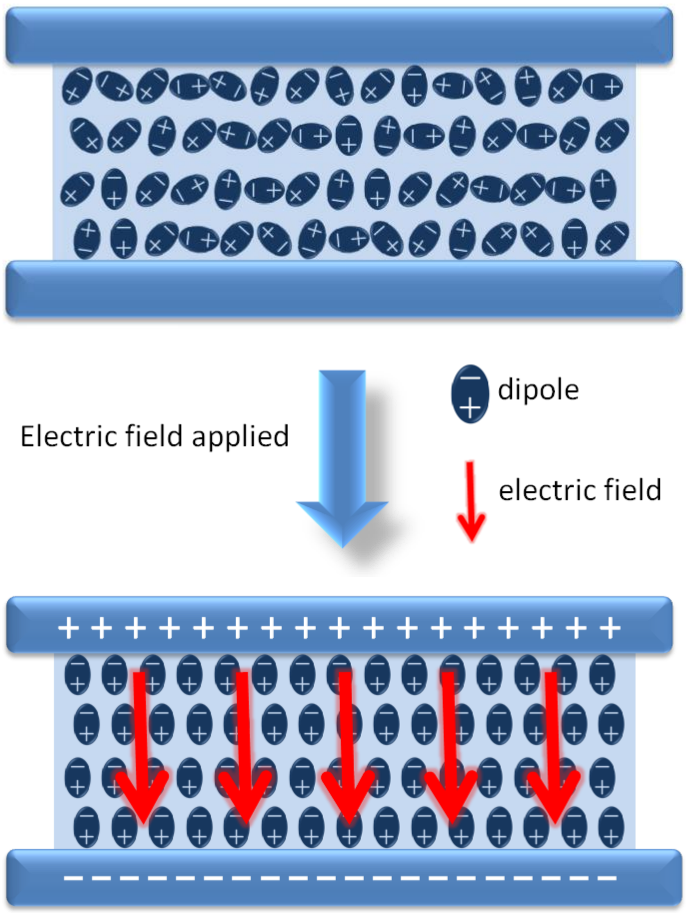

Figure 3.3 Illustration of how dipoles in a sample media orient themselves in parallel to the applied electric field. Permittivity is a term related to this orientation phenomenon.

This is known as dielectric polarization and its resultant effect can be observed in macroscopic scale as a new electric field opposing the applied electric field. This explains the inverse proportionality between the permittivity ϵ and proportionality constant k.

Permittivity is a function of the applied frequency of excitation. This is because as the field intensity and direction change, dipoles will try to follow the electric field by reorienting themselves accordingly. Since the response of matter is not instantaneous, as the frequency increases, dipoles start to be less successful in the pursuit of applied electric field and there will be a frequency beyond which the material cannot respond as quickly as the excitation frequency of the signal and permittivity starts decreasing. Since this is at very high frequencies (such as around 2.5 GHz for water molecules [46]) with respect to the frequency range of 1 kHz – 100 kHz considered in this work, relative permittivity of the materials involved are assumed constant within the low frequency (1 kHz – 100 kHz) range. Relative permittivity of a dielectric is frequently called dielectric constant at low frequencies, so the term dielectric constant will be used throughout this thesis.

Name	**Dielectric constant**
Deionized water	80
Methanol	33
Isopropanol	18
Al_2O_3 (ALD)	8
SiO_2 (PECVD)	5
Biotin	2
Streptavidin	2
Air	1

Table 3.2 Dielectric constants of the solutions, materials and biological entities used in this work. Reported values are roughly stated [47–50].

3.2.2 Parallel-Plate Capacitors

Capacitance is charge-storing ability of a system and c*apacitor* is the name of the element used for this purpose. Capacitance (C) of a capacitor is defined as the amount of charge stored (Q) per unit voltage applied to it (V).

$$C = \frac{Q}{V} \tag{3.5}$$

which is informally called the ice-cream formula (

).

One of the most commonly used capacitors is parallel-plate capacitor. It is not only useful as a discrete device in electric circuits; but more importantly, it is an essential part of modeling various capacitance-based phenomena. The concept can be utilized in anywhere (semiconductors, photodetectors or biosensors) where two planes of charges in parallel are considered.

In this capacitor, two conductor parallel plates of area A are separated by a uniform distance d. The space between the plates is filled with a material of dielectric constant ϵ_r (Figure 3.4)

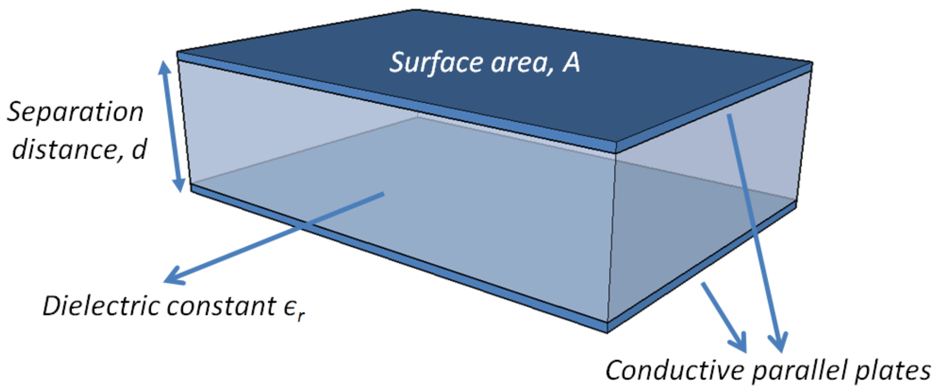

Figure 3.4 Parallel plate capacitor

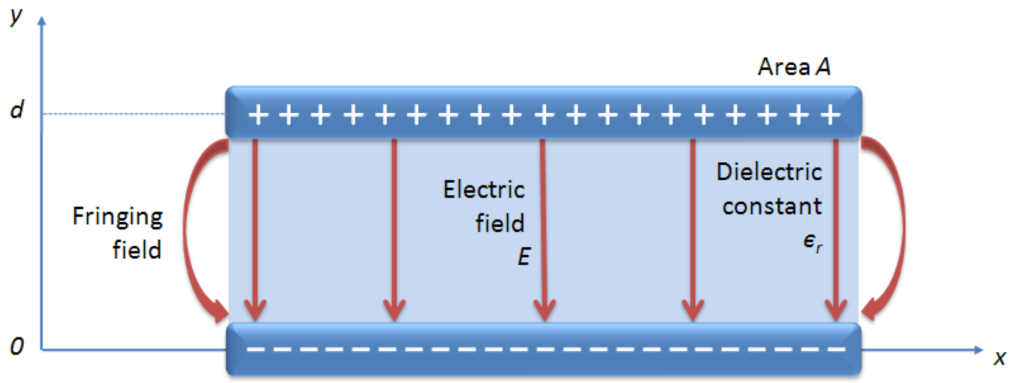

Figure 3.5 Cross section of a parallel-plate capacitor

Electric field is created when voltage is applied to the electrodes (Figure 3.5). Fringing fields at the edges of the plates can be neglected if the distance *d* is sufficiently small when compared to dimensions of the plates [51]. Then, the electric field is confined to the space where dielectric material is filled and it can be found by utilizing Gauss's law [52]

$$\oint E \cdot ds = \frac{Q}{\varepsilon} \tag{3.6}$$

This is a closed surface integral asserting that total outward flux of the E-field over any closed surface is equal to total charge Q enclosed in that surface divided by the material permittivity ϵ. To get the electric field between the two plates, a hypothetical closed surface is placed as shown in Figure 3.6.

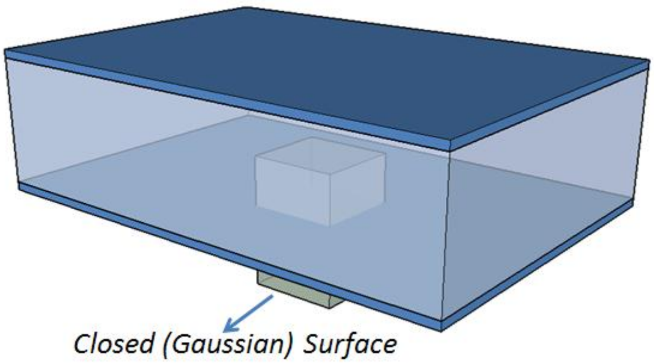

Figure 3.6 A hypothetical closed surface is placed to apply Gauss's law on parallel-plate capacitor.

When equation 3.6 is applied on the six faces of the rectangular box, it is seen that the electric field lines are parallel to the side faces of the box (Figure 3.6) and thus, $E \cdot ds$ is zero on those surfaces. Similarly, the bottom face has zero contribution since no electric field exists in that region. Consequently, only the top face contributes to the left part of equation 3.6, and since electric field is perpendicular to the top face and uniform over it, left part of equation 3.6 turns out to a multiplication

$$|E| \times S = \frac{Q_{enc}}{\varepsilon} \tag{3.7}$$

where S is the surface area of the top face and $Q_{enc}$is the charge enclosed in the hypothetical box. Q_{enc} can be expressed in terms of the total charge on the plate as

$$Q_{enc} = \frac{Q \times S}{A} \tag{3.8}$$

Combining equation 3.7 and 3.8, electric field magnitude is obtained to be

$$|E| = \frac{Q}{\varepsilon \times A} \tag{3.9}$$

Electric field does not depend on the height of the box as far as the top face is in between the plates. Thus, electric field is constant within the dielectric medium. This is used in calculation of the voltage (*V*) between the capacitor plates (Figure 3.5) as

$$V = \int_0^d E \cdot dy = |E| \times d \tag{3.10}$$

Combining this with equation 3.9,

$$V = \frac{Q \times d}{\varepsilon \times A} \tag{3.11}$$

Finally, using equation 3.5 and 3.11, capacitance of a parallel-plate capacitor can be obtained as

$$C = \varepsilon \frac{A}{d} = \varepsilon_0 \varepsilon_r \frac{A}{d} \tag{3.12}$$

This is a very useful formula, used in capacitance estimation of various phenomena where two conductive layers exist in parallel. However, care must be taken when *d* gets close to the dimensions of the plates so that fringing fields cannot be neglected.

3.2.3 Electrical Double Layer

Looking at the discussion on parallel plate capacitors in the previous section, it can be expected that when two plates of area A and separation distance d are placed in a dielectric liquid solution with dielectric constant ϵ_r, the resultant capacitance will be equal to equation 3.12. However, in general there is more to it than this simplified view.

This is due to two layers of ions accumulated in the close vicinity of the plates: When an electric field is applied, ions in the liquid react to this and move towards oppositely polarized plates. Thereby, a layer of mobile charges is formed in the liquid near each plate and it is called diffuse layer [46].

Figure 3.7 illustrates the neighborhood of a negatively charged plate, where diffuse layer is formed by accumulation of positive ions solvated in water. ‘Solvated ions’ refer to those surrounded with water (solvent) molecules.

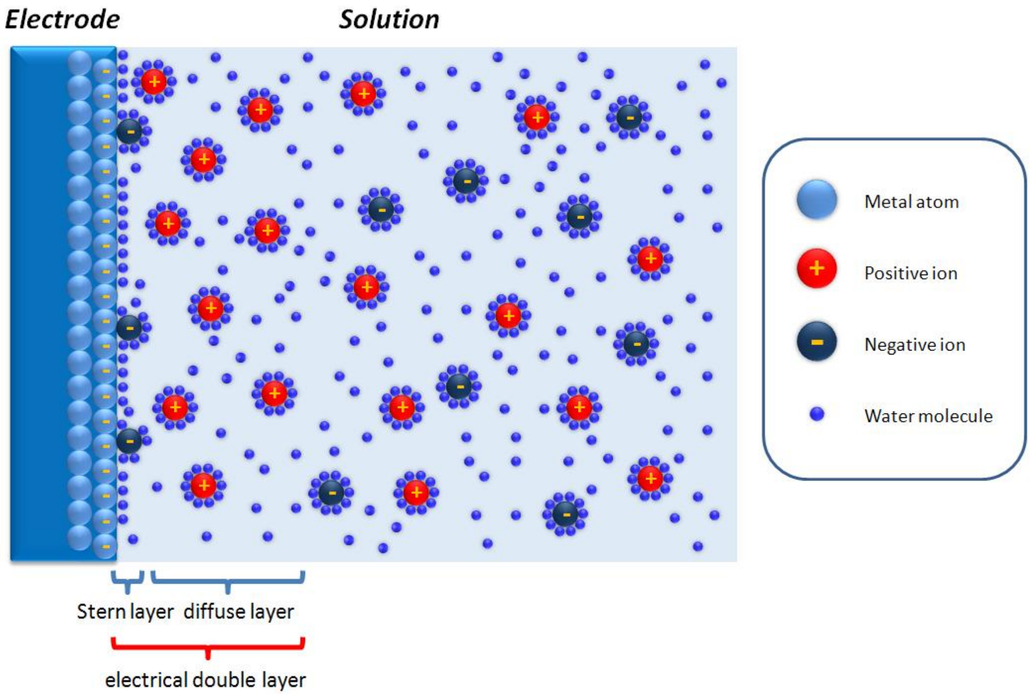

Figure 3.7 Electrical double layer formed in the vicinity of a negatively charged plate

Water, a polar molecule, first orients itself such that its negatively charged portion is closer to a positive ion and then attaches to it forming a complex (opposite for a negative ion). This is the mechanism behind the dissolution of ions (easily) in a polar solvent like water [53].

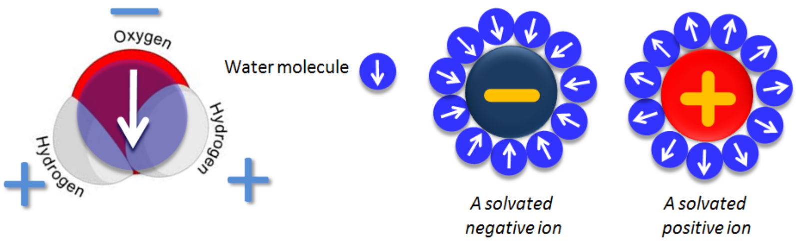

Figure 3.8 Solvation of ions in water.

In addition to solvated ions, there is also a layer of unsolvated ions on the negatively charged plate as shown in Figure 3.7. These are immobile ions directly adsorbed to the surface. Adsorption, similar to surface tension, is a consequence of surface energy. Simply stated, unlike the metal atoms in the bulk of the plate, the metal atoms at the surface are not wholly surrounded by other metal atoms and thus, can attract atoms in the liquid solution. The exact nature of this attraction is beyond the scope of this work; however, the consequence of it is a layer of immobile ions immediately adjacent to the surface. This layer is called Stern layer, after Otto Stern who contributed to its theory.

To summarize the explanations so far, when two metal plates are immersed in a liquid solution and a voltage is applied to them, ions in the solution start to accumulate near the plates. They are solvated, mobile ions forming the diffuse layer. In addition to this, there is a layer of immobile ions on the plates forming the Stern layer. Two layers together are called electrical double layer, which is the secret behind the surplus in the capacitance of a parallel plate capacitor immersed in a solution.

The reason of the surplus can be understood by assuming the electrical double layers as separate plates immersed in the solution and placed very closely to the present plates. They essentially decrease the separation distance d in equation 3.12 and as a result, the capacitance increases. Since the separation distance resulted from electrical double layer is in the order of nanometers, huge capacitance values can be obtained using this idea as in the case of super capacitors (also known as ultracapacitor, or electrical double layer capacitor) [54]. These are commercially available products going up to several 1000 Farads and can be used in various sectors like in uninterruptible power supplies [55] or in electrical cars [56]. However, electrical double layer is not always a desirable thing as will be shown in the next section.

3.3 Impedimetric Sensing in a Nanogap

One of the protagonists in this thesis is nanogap. It refers to the gap formed between the two electrodes with the separation distance of the order of nanometers. At the beginning of this chapter, impedimetric sensing is introduced as a label-free, low-cost, low power requirement, miniaturizable, chip-integrable, electrical based detection technique such that it can be applied to point-of-care biosensor applications. However, in applications working with liquid-based samples (like human blood), the problem of electrical double layer arises. This problem with its possible solution based on nanogap will be discussed in this section.

Electrical double layer is a complex phenomenon; however, thanks to research efforts for more than a century on it, several models are developed explaining its formation and macroscopic effects [57–59]. The model deployed in this work is Gouy-Chapman model. This model assumes the ions behaving as point charges and employs the Poisson-Boltzmann equation to predict potential distribution in the solution. It does not take into account the finite size of the ions; neither does it consider the fact that permittivity of water decreases around the solvated ions since the water molecules surrounding the ions cannot respond freely to the applied electric field anymore. Some more drawbacks leading to imperfections such as neglecting the effect of Stern layer may be considered for this model. Nevertheless, this model provides relatively good predictions for solutions with ionic strengths less than 0.2 M and for applied electrical voltages below 50-80 mV [60]. Thus, it is sufficient for this work where ionic strength is in the order of 10^{-7} M and applied rms voltage is 10 mV.

For the simple case of sufficiently large planar electrode surface, the potential cannot change in directions parallel to it because of the symmetry. Using this information, one dimensional solution of the electric potential with respect to distance from the electrode surface can be obtained by Gouy-Chapman model as [60]

$$\phi(x) = \phi_0 e^{(-\frac{x}{\lambda_D})}$$

(3.13)

Electric field intensity can be calculated by taking derivative of electric potential $\phi(x)$ with respect to x.

$$|E| = \left|-\frac{d\phi(x)}{dx}\right| = \frac{\phi_0}{\lambda_D} e^{(-\frac{x}{\lambda_D})}$$

(3.14)

Electric field intensity in the neighborhood of a negatively charged electrode is illustrated in Figure 3.9.

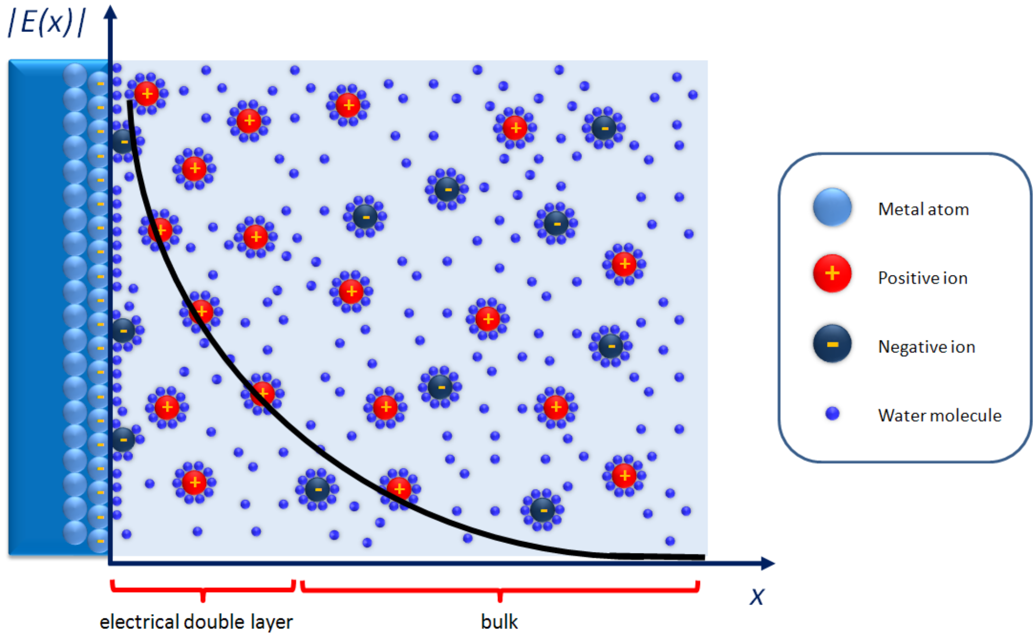

Figure 3.9 Electric field intensity with respect to the distance from the electrode surface

Electric field decays exponentially with increasing distances from the electrode (equation 3.14). The decaying constant λ_D is called Debye length. The effect of ionic concentration on it will be discussed in the following pages. For now, it is necessary to observe that within five Debye lengths from the electrode, the electric field almost vanishes (becomes less than 1% of $\frac{\phi_0}{\lambda_D}$) in the solution.

In essence, electrical double layer acts as a shield against the applied electrical field. This causes a major problem for the biosensor applications since the electric field applied by the electrodes does not appear on the significant portion of the target medium as shown in Figure 3.10.

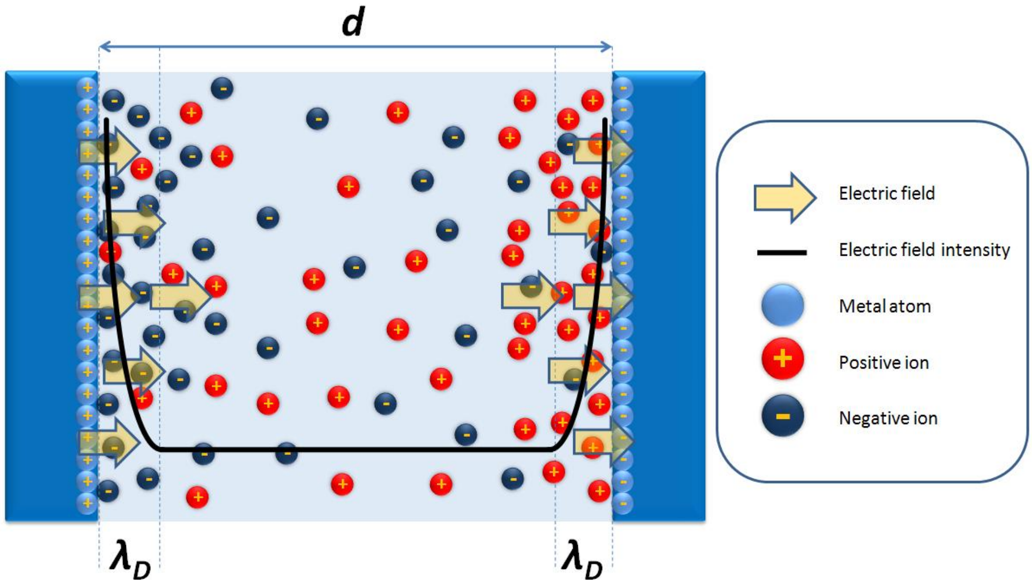

Figure 3.10 Electric field intensity between the two electrodes in a solution

There are two ways of dealing with this problem, which are increasing the Debye length λ_D and decreasing the electrode separation distance d. For simplicity, these two are combined in a single dimensionless parameter

$$S = \frac{\lambda_D}{d} \tag{3.15}$$

Using equation 3.14, electric field intensity can be obtained for the single electrode. Since it will be similar (symmetric with respect to the midpoint of the electrodes) for the other electrode and since electric fields related to both electrodes are superimposable due to the linearity of the system at low voltages, total electric field in the solution can be obtained. It is plotted for different S parameters in Figure 3.11.

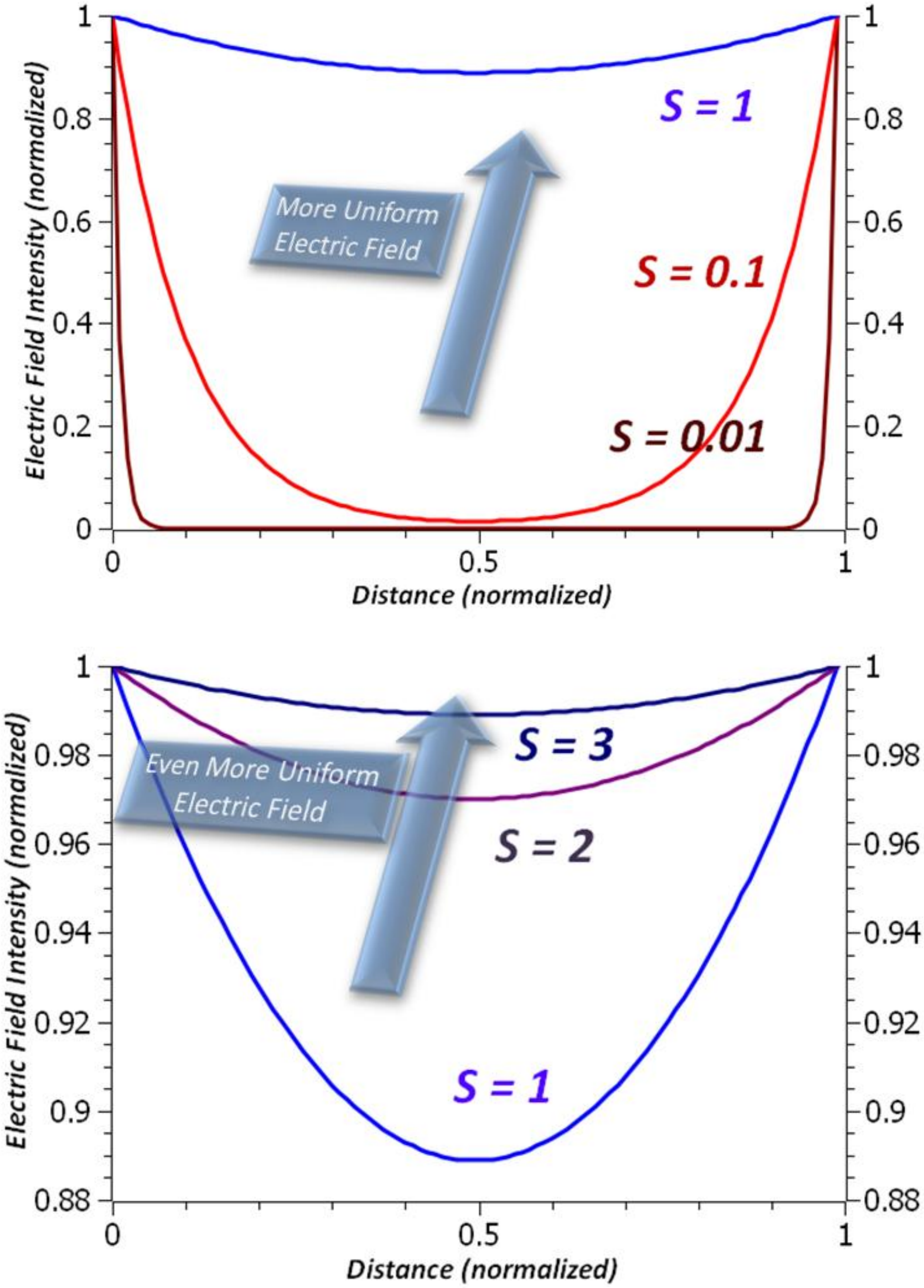

Figure 3.11 Electric field intensity with respect to distance.

S denotes the ratio between Debye length and electrode separation distance.

Increasing S parameter produces more uniform electric fields in the sample media (Figure 3.11). For the sensor applications that are considered, in the regions with higher electric field, sensor is more sensitive to the changes in the permittivity of the medium. Thus, the uniformity in electric field is essential for the sensor to be equally sensitive to the whole sample media. As an example, when S=0.01, there is almost no electric field in the midst of the two electrodes as seen in Figure 3.11. This means even if the permittivity of the sample in this region is changed, it will hardly be possible to detect it at the output.

Increasing S parameter is possible by increasing the Debye length. For the water at 25°C, Debye length is

$$\lambda_D = \frac{0.34\ \mathrm{nm}}{\sqrt{C\ \ \mathrm{L/mol}}} \tag{3.16}$$

where C is the ionic strength (a measure of the concentration of ions in a solution) [60]. This is tabulated for ions with single valence electrons (monovalent ions, like Na^+ or OH^-) in Table 3.3. For example, Debye length of a 1 mM aqueous NaCl solution at 25 °C is about 10 nm.

Molarity (M)	**Debye lengths (nm)**
10^{0}	0.3
10^{-1}	1
10^{-2}	3
10^{-3}	10
10^{-4}	30
10^{-5}	96
10^{-6}	304
2×10^{-7} (min.)	760

Table 3.3 Ionic concentrations and corresponding Debye lengths for monovalent ions in water.

Debye length is inversely proportional with the molar concentration of ions. This is expected since more ions means stronger electric field shielding and lesser Debye length. When Debye length for human blood plasma is calculated; it appears to be 0.78 nm. This is because human blood plasma is like an ion cocktail with the ingredients as 143 mM Na^{+}, 5 mM K^{+}, 2.5 mM Ca^{+2}, 1mM Mg^{+2}, 103 mM Cl^{-}, 27 mM ${HCO_3}^{-1}$, 1 mM ${HPO_4}^{-2}$, and 0.5 mM ${SO_4}^{-2}$. This means the applied electric field will be shielded within an extremely short distance (a typical atomic radius is of the order of 0.1 nm) and the impedimetric measurement will not be sensitive to the rest of the liquid. Thus, it is hardly possible to apply impedimetric sensing in human blood as the sample medium. On the other hand, deionized (DI) water is perhaps the most appropriate choice for obtaining the largest Debye length and thus, the most uniform sensitivity results in the whole sample medium (Figure 3.11). DI water is purified from its mineral ions such as sodium, calcium, iron, copper, chloride and bromide. This presents a less ionic medium and looking at equation 3.16 one might conclude that very high (more than a micrometer) Debye lengths can be obtained by deionization. However, deionization does not remove the hydroxide or hydronium ions from water, which are the self-ionization products of water ($2H_2O \rightarrow H_3O^{+} + OH^{-}$) and therefore those ions are impossible to remove. As a result, the ion concentration in water cannot decrease below 2x10^{-7} M. Moreover, in reality, it is even higher than this considering additional practical issues like unpurified ionic impurities, dissolution of CO_2 in water or pH being different from pH 7. Thus, practically even in DI water, Debye length is no more than a few 100 nms [60].

Revisiting the *S* parameter, decreasing the separation distance *d* is also a path for improving *S*. This is where the nanogap takes to the stage. Nanogap sets the distance to the same order with Debye length so that S parameters can reach beyond 1. Thereby, linear potential distribution (thus, uniform electric field) can be realized in the target liquid (Figure 3.12).

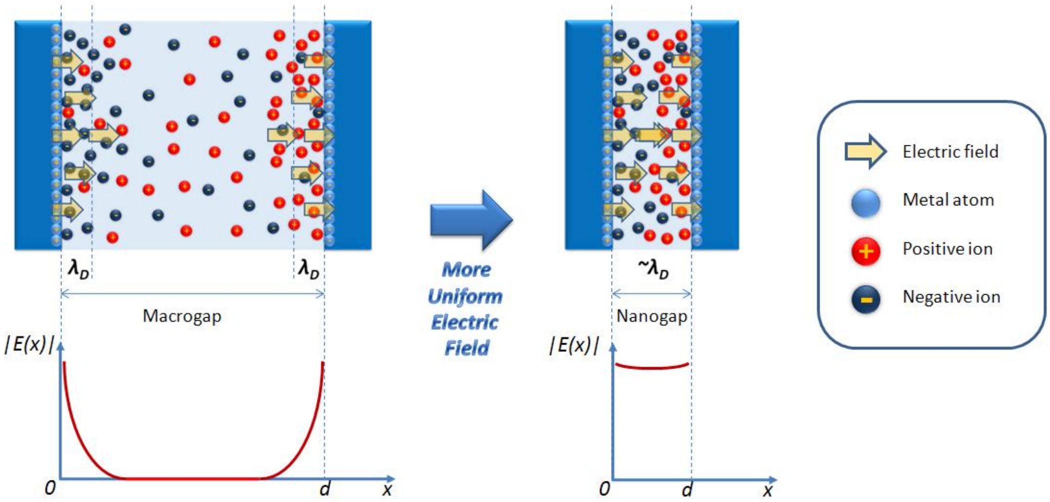

Figure 3.12 Potential distribution within a macroscale electrode gap and nanogap

An almost uniform electric field can be obtained by utilizing nanogap. This is not the case in macrogap where a parasitic bulk region with no electric field remains. Nanogap concept, in addition to using DI water as the sample medium, enables all molecules filling the gap experience almost identical electrical conditions, thus producing more uniform sensitivity results. In addition to this, since even a single molecule can occupy a reasonable percentage of the tiny volume inside the nanogap, nanogap biosensors can be extremely sensitive to DNA's, proteins and other biological molecules, which are all in nanoscale [46]. Therefore, the ability of shrinking measurement volumes to nano dimensions is also an appetizing reason for using nanogap based impedimetric sensing in detection of low amounts of target molecules such as cancer biomarkers.

3.4 Conclusion

Impedimetric sensing can be utilized in point-of-care biosensor applications. It has many benefits like label-free and low-cost detection; however, impedimetric sensing requires dealing with the electrical double layer observed in ionic liquid solutions. Electrical double layer is undesired since it disturbs the electric field uniformity in the sample media. The undesired effect of electrical double layer can be circumvented by (1) using DI water as sample medium so that high Debye length is obtained and (2) utilizing nanogap in impedimetric sensing. Nanogap helps reducing the undesired effect of electrical double layer and serves the purpose of minimizing the measurement volume, which is an appealing feature for cancer biomarker detection.

Chapter 4

Nanogap Based Impedimetric Biosensors

4.1 Introduction

Benefits of nanogap in impedimetric sensing are discussed in the previous chapter. Nanogap provides a uniform electric field and minimized sample volume so that sensitive detection of even very few target molecules can be achieved. This chapter will consider realization of this idea by producing a nanogap based impedimetric biosensor. First, the nanogap fabrication techniques will be discussed. Then, this will be followed by the sequence of sections explaining the design, fabrication, surface functionalization and biotinylation processes.

4.2 Nanogap Fabrication Techniques

Benefits of nanogap in impedimetric sensing can be realized by nanogap devices. Numerous nanogap devices with various fabrication techniques are reported in the literature [61]. These devices can be categorized as planar or vertical nanogap devices (Figure 4.1 and 4.2).

Planar devices are fabricated by techniques like lithography or chemical deposition. Although it has been reported that some outstanding results can be obtained with these techniques, they are in general not suitable for high-throughput fabrication. Standard optical lithography, which is compatible with batch processing, is not efficient in forming submicron scale distances. However, it is still possible to utilize standard optical lithography in micron scale target detections like bacteria. In that case, very high frequencies should be used so that ions in the liquid solution do not have time to form electrical double layer [62]. Relaxation frequency for ions in DI water is around 280 kHz [53], [63]. Thus, dealing with high frequency parasitic effects and high-cost measurement tools like network analyzer are required. Shadow evaporation technique uses lithography by tilting the sample to enhance the resolution [64]. Nevertheless, it is not suitable for high-throughput fabrication. E-beam lithography is an alternative which presents nanoscale resolution in gap formation, but with a high fabrication cost and long fabrication time per device [65]. Deep UV lithography achieves electrode separation distances down to 250 nm [51], but the associated production system costs are prohibitive for low-cost biosensor applications. Electrochemical deposition methods also offer nanogap formation but they have difficulty in providing well-defined patterns [66]. In conclusion, planar nanogap devices seem inappropriate for point-of-care biosensor applications until the inherent problems like low yield and high cost are resolved.

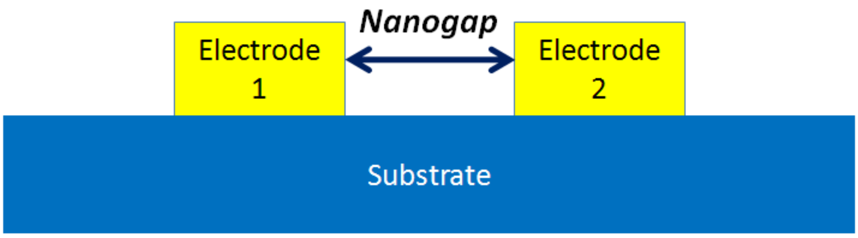

a)

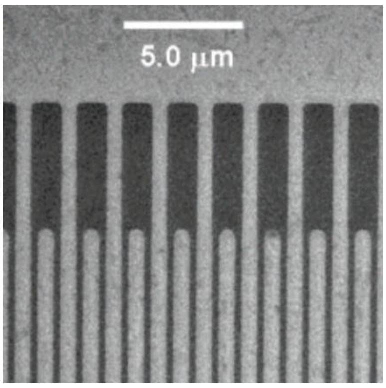

b)

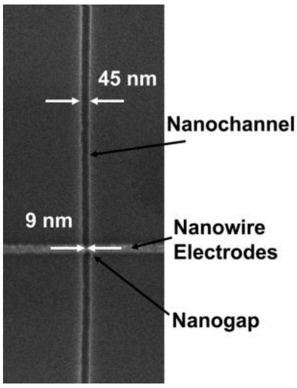

c)

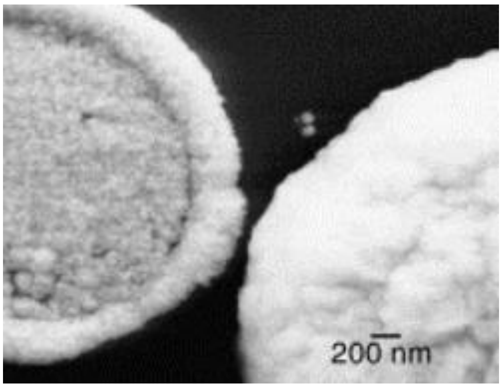

d)

Figure 4.1 Planar nanogap devices a) Cross-sectional view of a typical planar nanogap device. Some of the nanogap devices from the literature ([67],[64], [66], respectively)

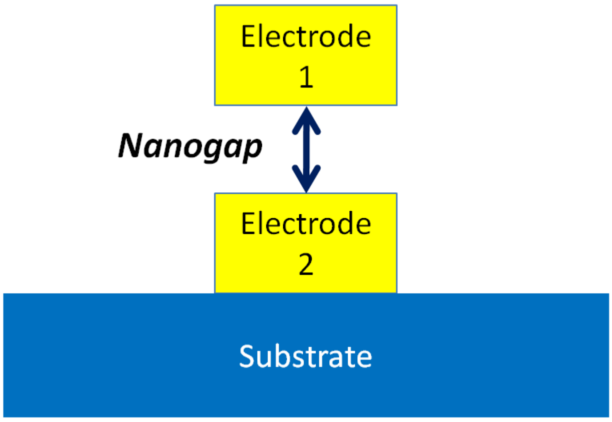

a)

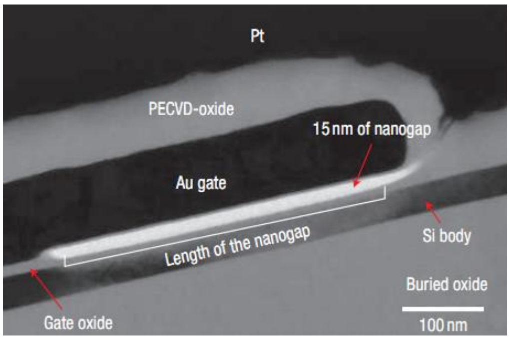

b)

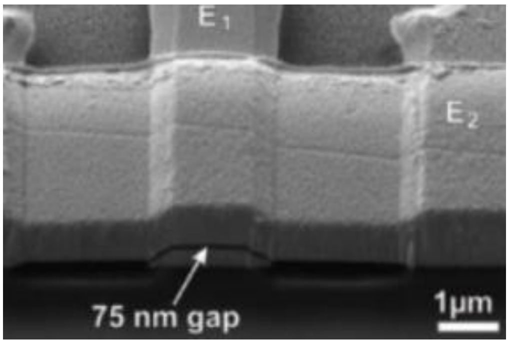

c)

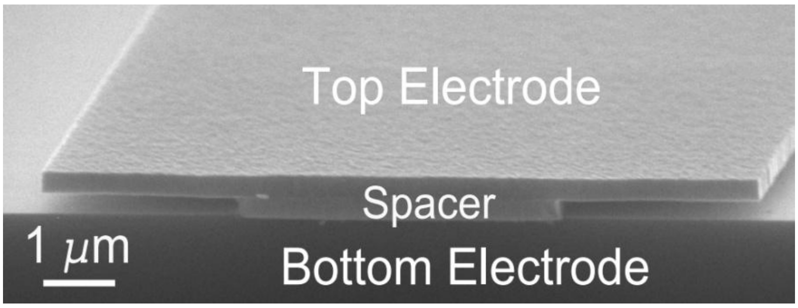

d)

Figure 4.2 Vertical nanogap devices a) Cross-sectional view of a typical vertical nanogap device b,c,d) Some of the nanogap devices from the literature ([50], [68], [69],respectively)

Vertical nanogap devices are formed by vertically situated electrodes (Figure 4.2a). They are usually formed by incorporating nanometer-high sacrificial layers between the electrodes. Nanogap is formed by removing this sacrificial layer [68]; though, some of it may be preferred to remain as a spacer between the electrodes [50], [69]. The strong advantage of these devices is they can use low-cost, mature thin film growth techniques for nanoscale-high sacrificial layer. These versatile techniques offer great thickness uniformity and control in addition to cost effectiveness. Thus, vertical nanogap devices are preferred in designing the nanogap based impedimetric biosensors in this work.

4.3 Sensor Design

The principle of operation is to detect impedimetric changes when target molecules are bound to the recognition elements (Figure 4.3a). For this purpose, the vertical nanogap device structure is designed (Figure 4.3). Recognition elements will be placed on the dielectric layer in between. This dielectric layer will function as a separator for two electrodes, as well as a holder for receptor molecules.

Measurements are taken in DI water medium. Target molecules replace the portion of DI water over recognition elements when bound to them; and, this results in a change of nanogap impedance. DI water offers high Debye length. This, in addition to nanoscale electrode separation, reduces the undesired shielding effect of electrical double layer such that uniform electric field can be obtained in the whole nanogap. Fringing fields are neglected since the electrode sizes are much larger than the nanoscale separation distance. The measured impedance between the electrodes is equally sensitive to the changes over any recognition elements in the gap. This means whether a target molecule is bound to the upper or lower part of the nanogap will make the same effect on the overall impedance.

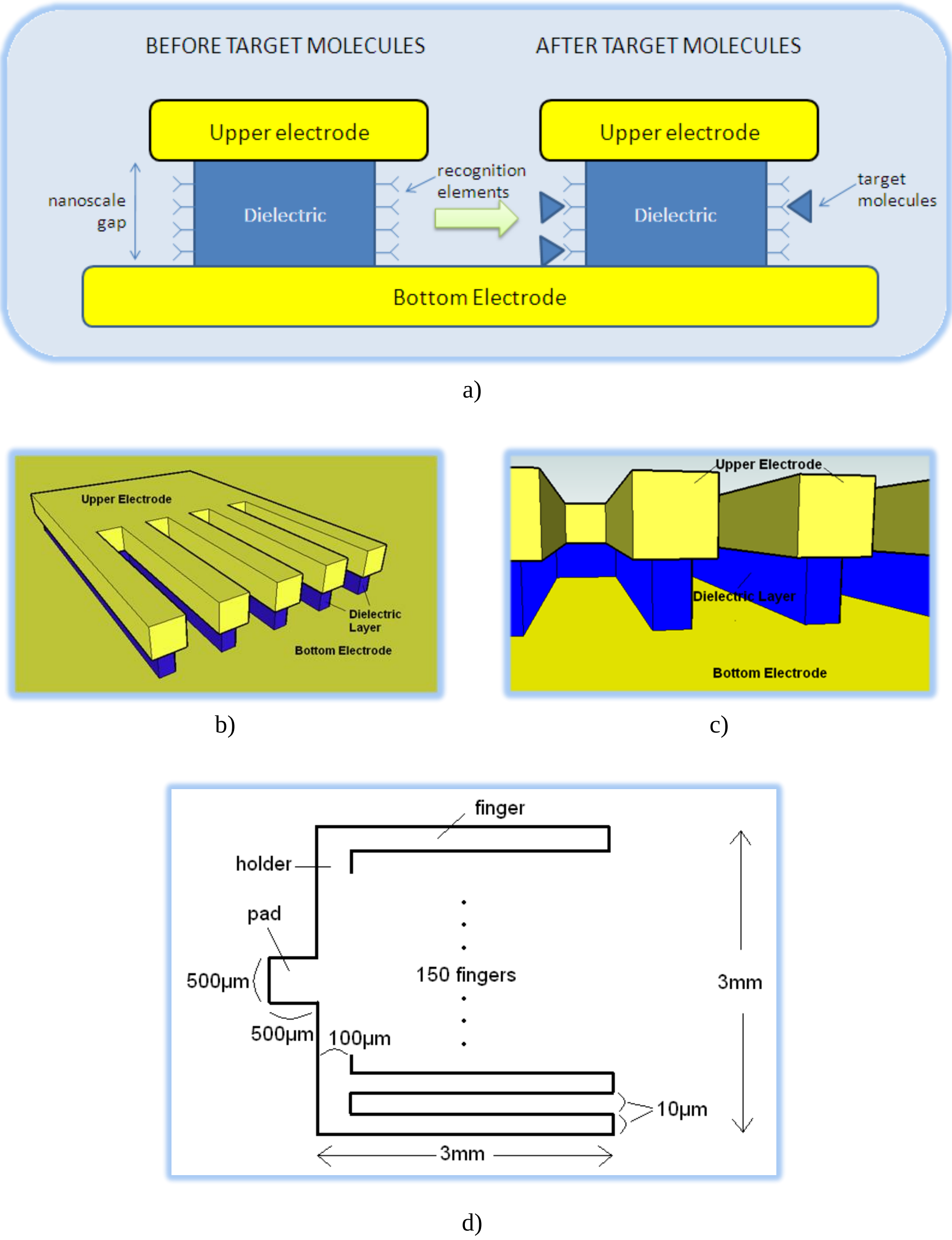

Figure 4.3 Operation principles and various views of the designed sensors

As a proof of concept, streptavidin and biotin are studied as target molecule and recognition element pair. This is because streptavidin and biotin are known to have one of the strongest non-covalent interactions in the nature (Dissociation constant K_d is on the order of $\approx 10^{-14}$ mol/L) [70]. In section 4.5, their molecular structure is introduced in detail. Streptavidin has a dielectric constant (ϵ_r) of about 2 [50]. The contrast between the dielectric constants of streptavidin and DI water (ϵ_r=80) is another advantage of DI water as a measurement medium. Thanks to this contrast, greater impedance change occurs after streptavidin-biotin binding when compared to other alternatives with less contrasts like air (ϵ_r=1).

Nanogap focuses the sensitivity on nanoscale dimensions, where the biomolecular events realize. The measurement volume and surface area of the recognition elements can be adjusted by sensor geometry. The electrode geometry in Figure 4.2d serves the purpose of increasing the percentage of the (target molecule sensing) nanogap area with respect to (insensitive) dielectric material volume which contributes constant impedance to the overall impedance. The structure in Figure 4.2c increases the ratio of sensor perimeter (proportional to nanogap volume) versus sensor area (proportional to dielectric volume) by about 145 fold when compared to a square pad occupying the same area. In this design, fingers (high perimeter/area ratio) comprise the 89 percent of the whole area (Table 4.1).

Parts	**Unit Size**		**Quantity**	**Total Area**	**Area (%)**
	W(μm)	H(μm)	#	(μm^2)	
Fingers	10	3000	150	4,500 x 10^3	89
Holder	100	3000	1	300 x 10^3	6
Pad	500	500	1	250 x 10^3	5
Electrode				5,050 x 10^3	100

Table 4.1 Geometrical dimensions of designed sensor

Alternative sensor layouts would be as shown in Figure 4.4. Increasing the finger lengths (Figure 4.4b) can increase the overall perimeter/area ratio when compared to the current layout (Figure 4.4a); although it will not be much effective since finger area is already 89% percent of the total area. Additionally, long fingers would be beneficial to increase the overall nanogap volume and increase the detectable amount of target molecules. This means increasing the saturation concentration of the sensor and engineering the dynamic range, which is defined in Chapter 2. However, problem in Figure 4.4b would be the resistance of the long fingers. This can deteriorate the overall sensitivity by adding resistive noise of fingers which is analyzed by Dr. Nevill [46]. A method for eliminating this concern is to place electrodes to all sides (Figure 4.4c). Scaling up and down the layouts without changing the ratios of the dimensions can be another alternative to engineer the dynamic range and sensitivity. The effects of these and various layouts on the sensitivity and other sensor metrics can be analyzed as a future work.

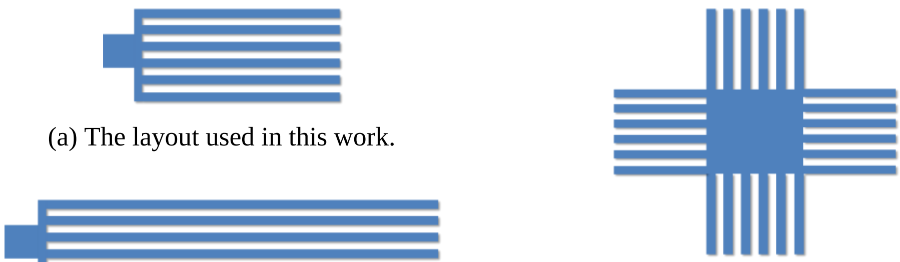

(a) The layout used in this work.

(b) Long fingers

(c) Short fingers in four sides.

Figure 4.4 Alternative sensor geometries

In order to analyze the impedance measurements, designed biosensor structure is modeled with an equivalent circuit model (Figure 4.5). Since two electrodes are separated by a distance of the order of the Debye length (a few 100 nms for DI water), the complex effect of electrical double layer is significantly reduced. Thus, electrical double layer is ignored in this design and the overall nanogap is modeled with only its capacitance and resistance connected in parallel.

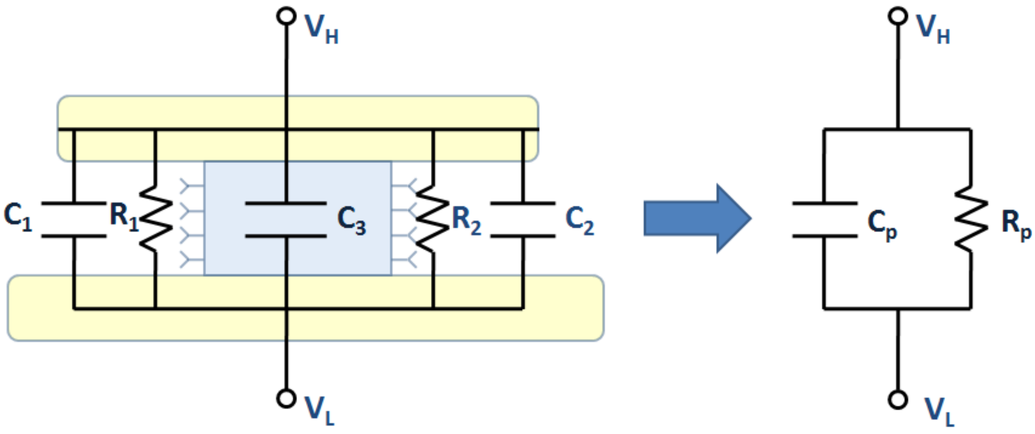

a) b)

Figure 4.5 Equivalent circuit model for the nanogap biosensors in this work a) Nanogap is modeled with a capacitor (C_1 or C_2) and resistor (R_1 or R_2) in parallel, whereas dielectric layer is modeled with a capacitor (C_3). b) A more compact equivalent circuit obtained by combining the capacitors and resistors.

The two models in Figure 4.5 are related to each other by the equations

$$C_p = C_1//C_2//C_3 = C_1 + C_2 + C_3$$
$$R_p = R_1//R_2 = \frac{R_1 R_2}{R_1 + R_2} \tag{4.1}$$

Since C_1 and C_2 will be filled with the same medium, parallel combination of C_1 and C_2 can be represented by a single capacitor C_{ng}.

$$C_{ng} \triangleq C_1//C_2 = C_1 + C_2 \tag{4.2}$$

As will be explained in the next section, two different materials (SiO_2 and Al_2O_3) are used in forming the biosensor’s dielectric layer. Associated capacitors of them can be incorporated into equation 4.1 as a series equivalent C_{dl}.

$$C_{dl} \triangleq C_3 = \frac{C_{Al_2O_3} C_{SiO_2}}{C_{Al_2O_3} + C_{SiO_2}} \tag{4.3}$$

Using equations 4.2 and 4.3, C_p can be expressed as

$$C_p = C_{ng} // C_{dl} = C_{ng} + C_{dl} \tag{4.4}$$

Each capacitor in this relation can be calculated by the parallel plate capacitor model introduced in section 3.2.2.

$$C = \frac{\epsilon_0 \epsilon_r A}{d} \tag{4.5}$$

where A is the area of the plate, d is the distance between the plates, ϵ_0 is the electric constant (8.854×10^{-12} F m^{-1}) and ϵ_r is dielectric constant of the medium between the plates. Dielectric constants that will be used in these calculations are presented in Table 3.2.

4.4 Sensor Fabrication

Fabrication starts with a bare wafer and ends up with an array of biosensor devices on a single wafer. It includes deposition of metal electrodes and dielectric layers as well as formation of the nanogap. These processes are done in the 5000 sq ft Class 100 clean room facility at UNAM (Institute of Materials Science and Nanotechnology).

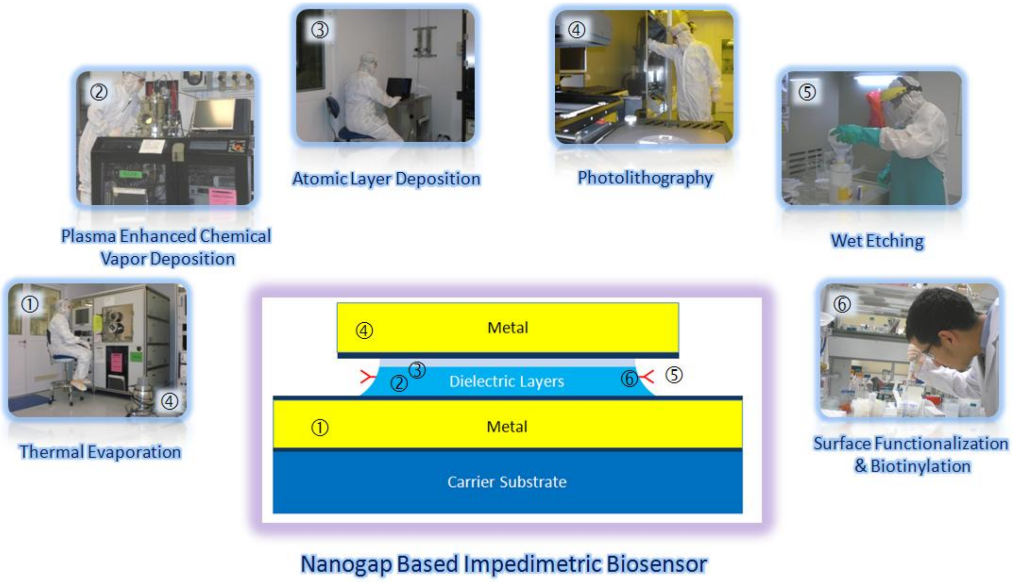

a)

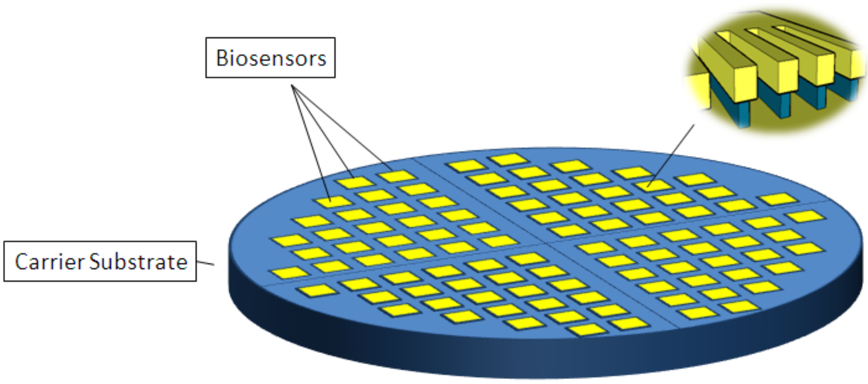

b)

Figure 4.6 Illustration of the fabrication steps and the biosensor arrays obtained at the end. More than 50 devices can be produced in a single run.

4.4.1 Substrate and Surface Preparation

The fabrication can be done on various types of wafers like Silicon, Quartz or Pyrex wafers. This is because the resistivity of the substrate in this work is not important thanks to the high conductivity of the gold bottom layer coating. Thus, the only function of substrate in this work is to carry devices. The wafer should stand to temperatures up to 250°C, which is the maximum temperature used in this fabrication. Also, the wafer should be well polished so that the surface roughness is no more than several nanometers.

Surface preparation before device fabrication is important to avoid contaminants like dusts, organic particles on the wafer. For this purpose, substrate is ultrasonically agitated in acetone ($(CH_3)_2CO$) and isopropyl alcohol ($(CH_3)_2CHOH$) for about 5 minutes each. Ultrasonic agitation improves attacking of solutions to the wafer surface and thus, increases the efficiency of contaminant removal. This clean ensures clean surface for the fabrication.

4.4.2 Formation of the Bottom Electrode

Thermal evaporation (VAKSIS, PVD Vapor–3S Thermal) is used for the formation of the bottom electrode. Gold (Au) is used as the material of the electrodes for two reasons: (1) Au is a highly conductive material so that the resistance associated with it can be neglected in impedance measurements. This eliminates the additional complexity in modeling and noise related with electrode resistance. (2) Au is a noble material and it does not react directly with oxygen. These make it a good electrode material choice for biosensing applications, where stability and repeatability are important considerations. Especially in this work, stability of Au in water and dry air is important since successive dry-wet cycles will be applied during the measurements.

100-nm-thick Au is evaporated with 10-nm-thick layer of chromium (Cr) before and after it. A very thin layer of Cr enhances the adhesion of Au with other layers.

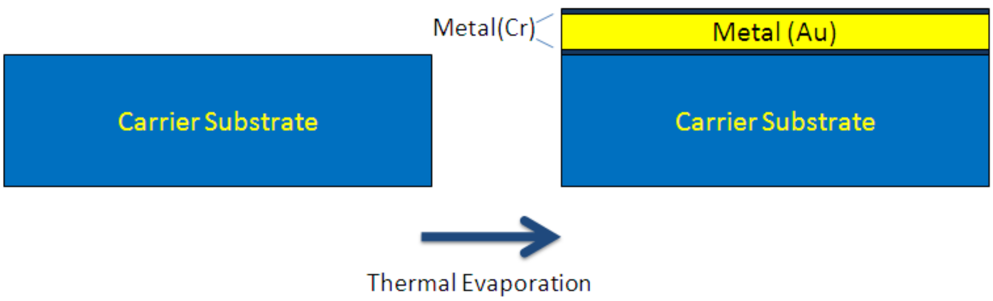

Figure 4.7 Fabrication of the bottom electrode by thermal evaporation

Evaporation is done at high vacuum condition (around 10^{-6} torr) to avoid air molecules which collides with evaporating metal molecules and scatters them before reaching to the substrate. High vacuum requires special care in chamber cleaning before the evaporation. There are several reasons making this cleaning particularly important: (1) Even small particles remaining on the vacuum parts (like the O-ring), can cause leaks or insufficient sealing. (2) The particles deposited (in a previous coating) on the inner walls of the chamber can out-gas under high vacuum. (3) Contamination may also occur because of extended pumping times in order to reach desired vacuum level. For these reasons, vacuum cleaner is used to remove loosely attached particles and flakes from the chamber and avoid contamination. After the chamber cleaning, pellets of coating materials (Au and Cr) are placed on the boats that will be heated up to several hundred (sometimes, even more) Celsius degrees during the evaporation process. Sealing the chamber, pump-down is started to obtain high vacuum conditions in the chamber. Samples are rotated during evaporation to obtain uniform film coatings and a "shutter" is used to start/stop the film coating. Material coating rate is about 0.5 Å /sec.

4.4.3 Coating of Dielectric Layers

Dielectric layers have a crucial role in this fabrication. They should have low leakage (high resistance) values to enable successful measurements and should be uniform so that all devices on the wafer show nearly identical performance. For this reason, we use SiO_2 with a very thin (~21 nm) Al_2O_3 over it as the dielectric layers. SiO_2 will later hold the recognition elements by some chemical processes; however, its surface leakage is very high due to reasons that will be discussed shortly. An additional layer of high quality Al_2O_3 film is coated to solve this problem.

SiO_2 is coated by plasma enhanced chemical vapor deposition (PECVD) technique. In this technique, chemical reaction occurs between the reactant gases

(200 sccm SiH_4 and 200 sccm N_2O) at very low pressures (0.45 Torr). Thanks to the RF powered (10 Watts) plasma, reaction can happen at low temperatures (250°C) since energetic electrons in the plasma satisfy additional energy for the chemical reaction. This is why the technique is given the name "plasma enhanced". PECVD system (VAKSIS, CVD-Handy) at UNAM is used for this coating. The coating thickness is measured with ellipsometer (J. A. Woolam V-VASE). The thickness is about 168 nm at the center and radially increases through the edge becoming around 340 nm at the edge. This non-uniformity decreased the number of identical devices on a wafer. Moreover, the film exhibits high current leakage (low resistance) and an additional dielectric layer with higher quality is needed to increase the overall resistance of the dielectric layers.

Very thin layer of Al_2O_3 is used for this purpose. It is coated with atomic layer deposition (ALD) technique. The advantage of this technique is to provide highly dense (high resistivity) and uniform dielectric films. This technique exposes the surface with two chemical gases (called precursors) sequentially. This is different than PECVD where the surface is exposed to both gases at the same time. In ALD technique, film is coated layer by layer over the sample and this offers angstrom scale accuracy in film thickness. Al_2O_3 film is coated by ALD system (Cambridge Nanotech, Savannah 100) at 250°C. Ellipsometry measurements show high uniformity with 22±1 nm film thickness on the whole wafer surface. Although the film has very high quality, ALD cannot replace the existing SiO_2 layer since the recognition elements attach to SiO_2 not Al_2O_3. However, this can be circumvented by updating the surface functionalization and biotinylation protocols explained in section 4.5. In that case, dielectric layer thickness should be made thinner since it is not efficient to use ALD for thick (more than 50nm) coatings. However, then filling a nanogap gap with those much small dimensions would be problematic [71]. There is definitely room for development in defining the optimum dielectric layer thickness.

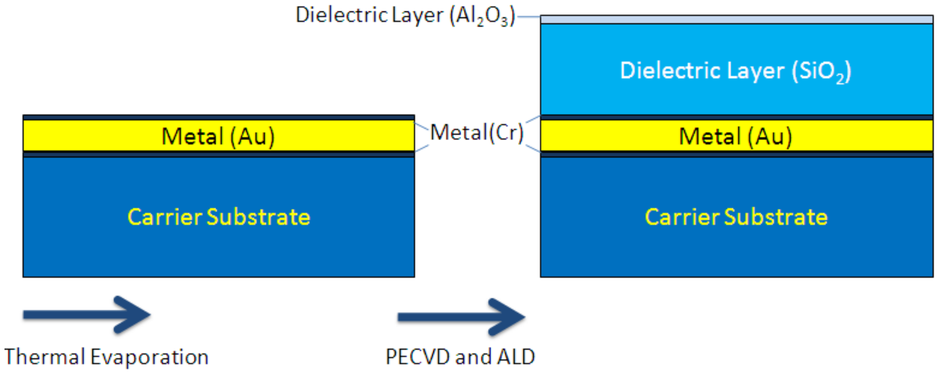

Figure 4.8 Fabrication of the dielectric layers. SiO_2 is enhanced with a thin Al_2O_3 film to improve film quality in terms of current leakage.

4.4.4 Patterning the Upper Electrode

Before the evaporation of the upper electrode, photolithography process is used to transfer the layout on to the substrate. The photo mask is designed by using the Layout Editor (GNU GPL) software and produced by the mask writer (Heidelberg Instruments DWL-66) at UNAM.

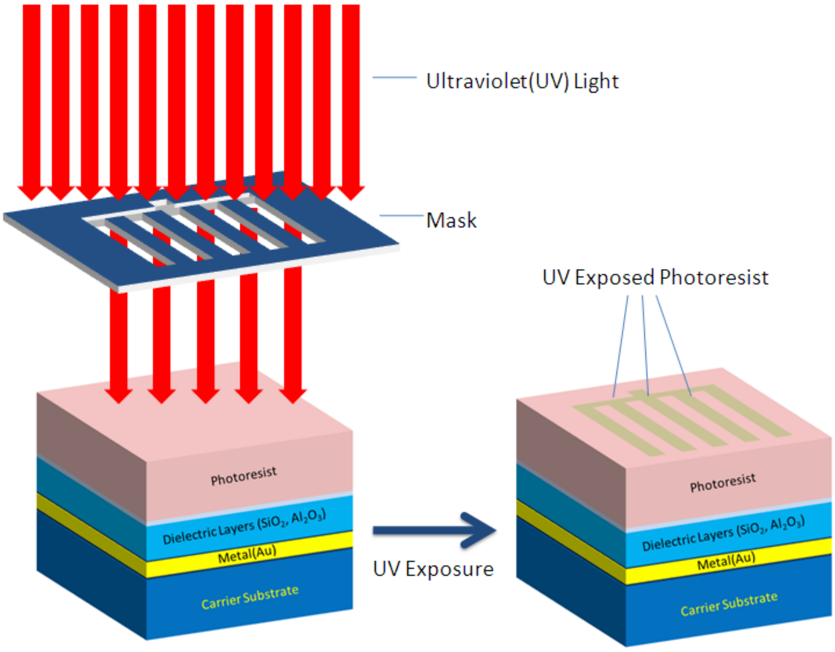

Figure 4.9 Photolithography is used to transfer upper electrode layout on two the wafer.

Photoresist is the central character of the photolithography process. It is a photosensitive material, which is insoluble to the chemical solution called photoresist developer. However, when photoresist is exposed to ultraviolet light it becomes soluble in the photoresist developer. This light-sensitive behavior of the photoresist is used to transfer the pattern on the photo mask to the wafer. Photolithography is started by surface dehydration of the sample on a hot plate at 110°C for about 5 minutes. This is necessary for removing the humidity off the surface, obtaining repeatable photoresist coverage; thus, improving the resolution of the process. HMDS (Hexametyldisilazane) is spin-coated at used 5000 rpm for 40 seconds for promoting photoresist adhesion to the surface. Photoresist (AZ5214E of AZ Electronic Materials) is spin-coated at 5000 rpm for 50 seconds producing 1.3-μm-thick photoresist layer on the surface. Pre-exposure bake is used to remove aqueous solvents in the photoresist. Photo mask is aligned over the sample and exposed with 50 mJ of ultraviolet light by the mask aligner (Electronic Vision Group EVG620). Post-exposure bake might be used for improving the resolution; but it is not used since the minimum feature size in the photo mask (10 μm) is obtained without this bake. After the exposure, AZ400K developer (AZ400K:H_20=1:4) is used to dissolve exposed photoresist leaving the desired pattern on the surface. Post-bake is not preferred since it would harden the photoresist and make the subsequent lift-off process more difficult.

4.4.5 Metallization and Lift-off of the Upper Electrode

Similar to bottom electrode, upper electrode is evaporated with thermal evaporation (VAKSIS, PVD Vapor–3S Thermal). First, 10 nm of Cr is evaporated for promoting adhesion of Au. This is followed by 120 nm Au evaporation.

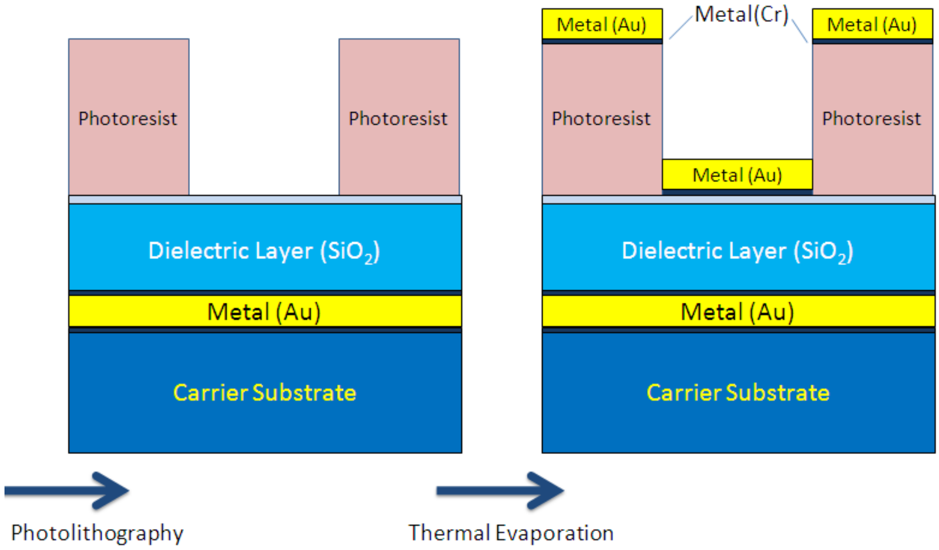

Figure 4.10 Evaporation of the upper electrode

After evaporation, the sample is left in acetone ($(CH_3)_2CO$) for the process called "lift-off". During lift-off, acetone attacks to photoresist and dissolves it; thereby, the part of the metal that sits on the photoresist lifts off. This process can take several hours. To improve the attack of acetone, we use ultrasonic agitation shortly. After the liftoff process, we get the patterned upper electrode structure.

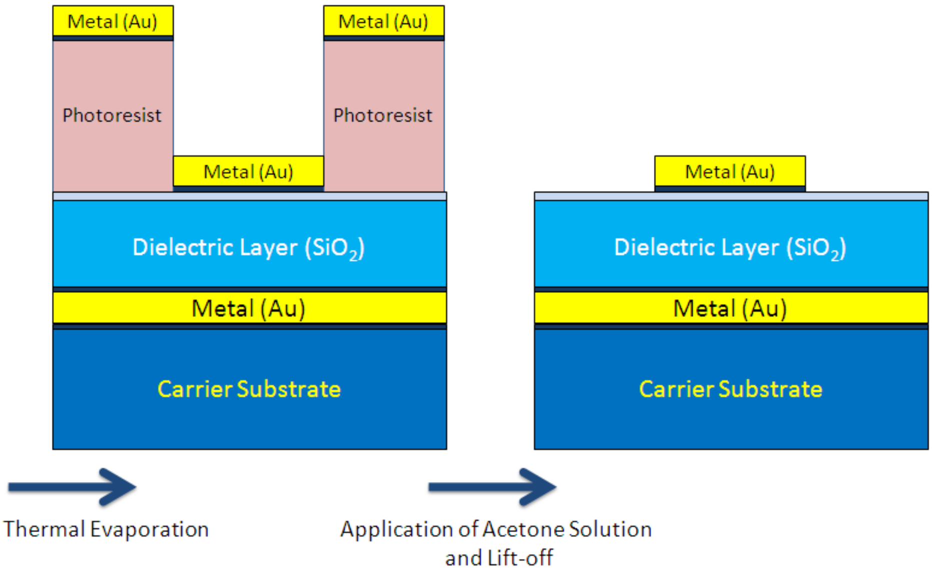

Figure 4.11 Illustration of the lift-off process

4.4.6 Nanogap formation

Wet etching is used to form nanogap. SiO_2 and Al_2O_3 are etched by using diluted hydrofluoric acid (HF) solution (38-40% HF:H_20=1:70). In this process, upper electrode acts like a mask because HF does not etch Au.

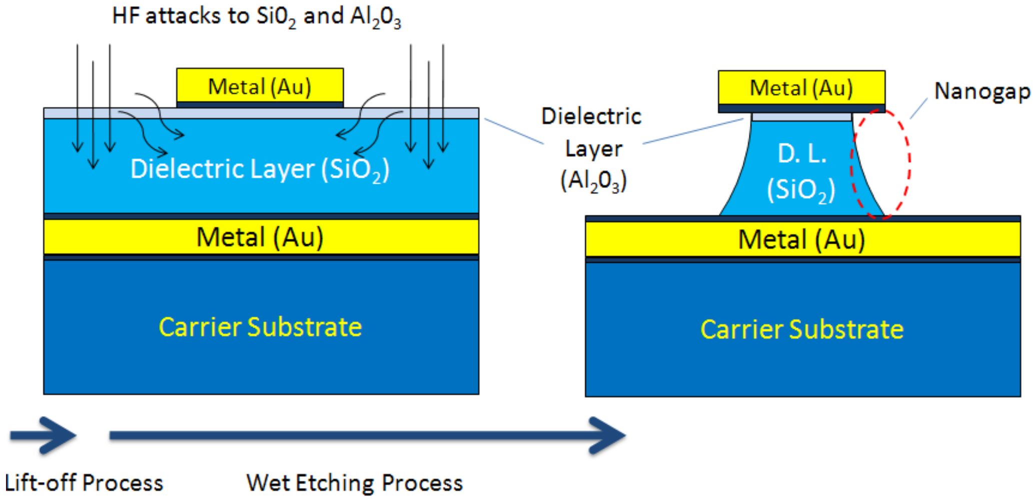

Figure 4.12 Wet Etching Process

The etch time is very important in wet etching. Process development on test samples showed the etch rates as 20-24 nm/min for Al_2O_3 and 23-28 nm/min for SiO_2. The undercut depth can be controlled or adjusted by impedance measurements after wet etching. The relation of the device capacitance with the total etching time will be analyzed in the next chapter.

Microscopy based characterization is performed to prove formation of layers and nanogap. Scanning electron microscope (FEI Nova Nanosem 430 and Nova 600i Nanolab) is used to get micrographs. Sensors are diced into pieces by a diamond scribe for taking cross-sectional images.

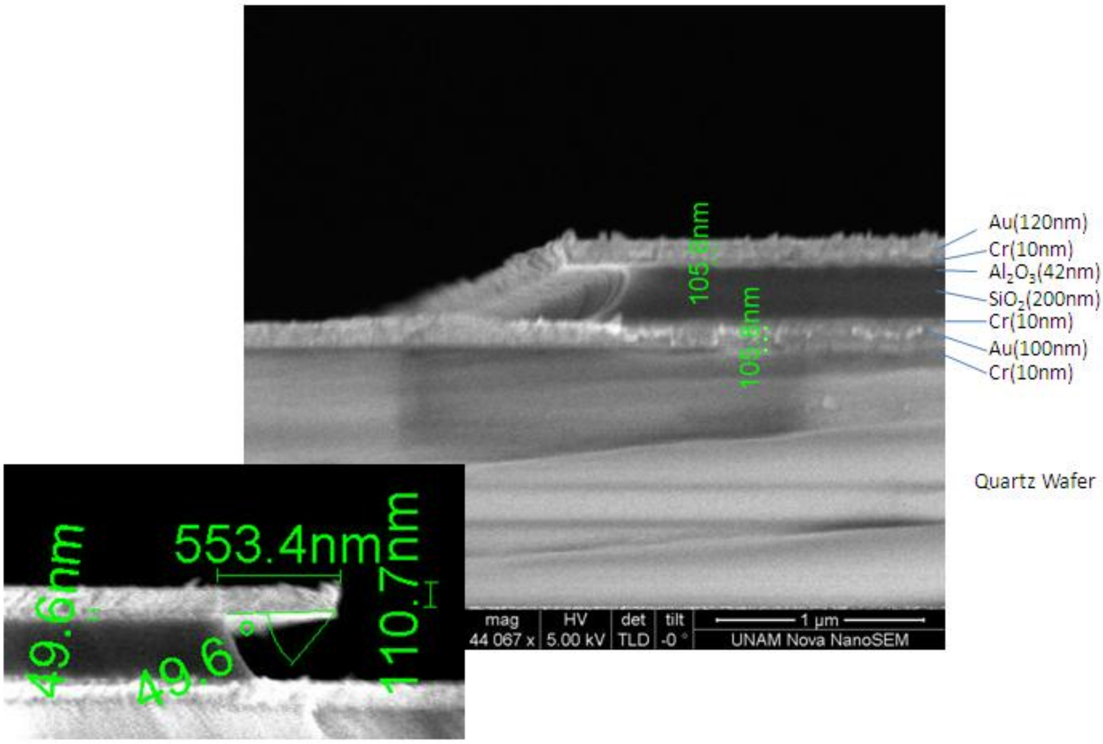

Figure 4.13 Scanning electron micrographs of the fabricated biosensors (before surface functionalization)

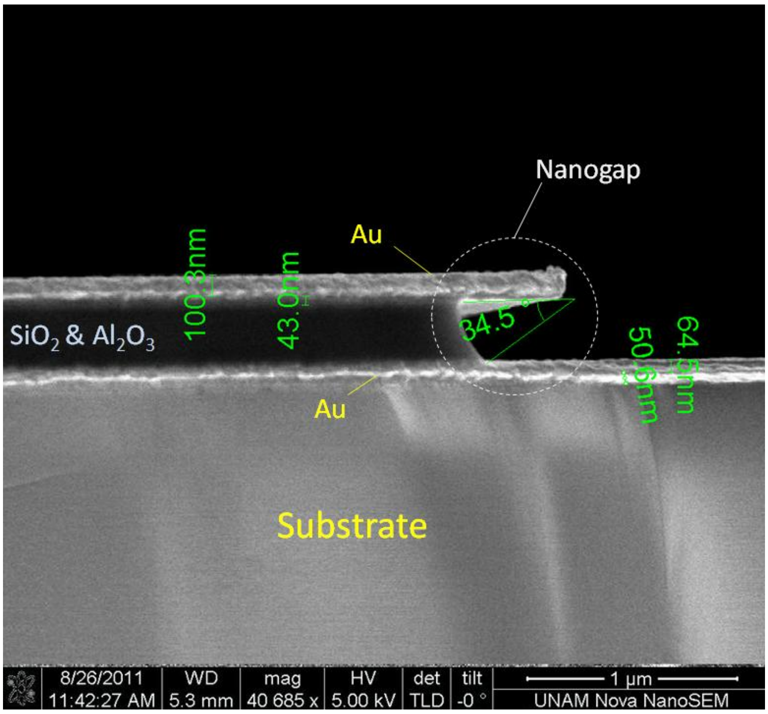

Figure 4.14 A scanning electron micrograph of the fabricated biosensors (before surface functionalization)

In addition to these, biosensors with SiO_2 as the only dielectric material are also produced (Figure 4.15). Nanogap formation is successfully achieved in these biosensors; however, they showed poor performance due to the current leakage of SiO_2.

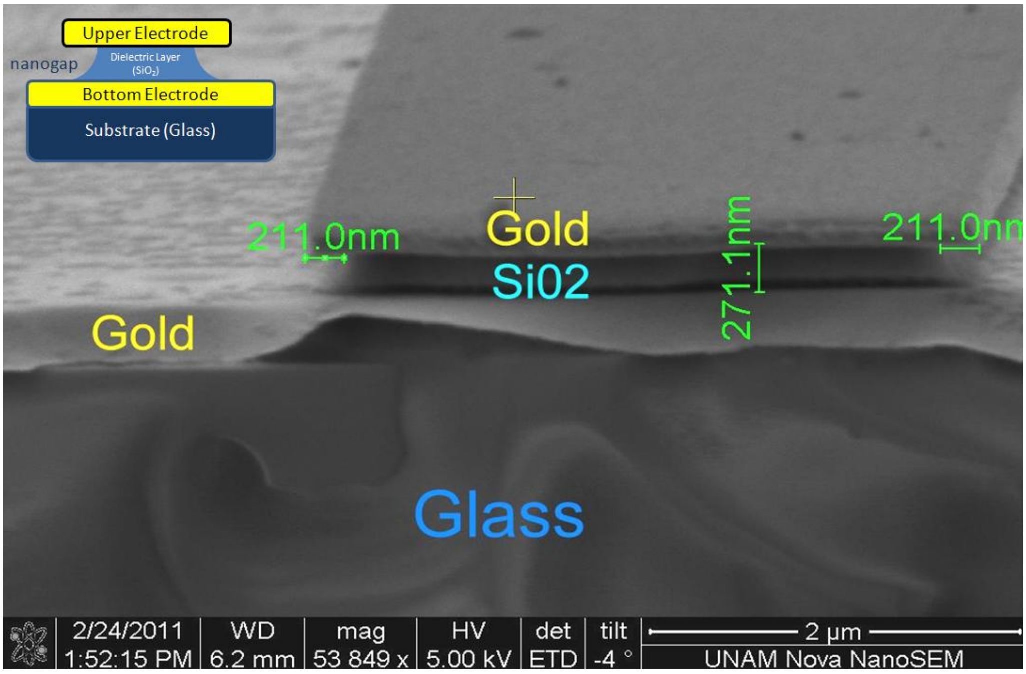

Figure 4.15 Scanning electron micrographs of a biosensor with SiO_2 as the only dielectric material

4.5 Sensor Surface Functionalization and Biotinylation

Fabricated sensors are exposed to “surface functionalization” and “biotinylation” processes for recognition elements to be placed into the nanogap. Dr. Mustafa Özgür Güler’s research team assists us in realizing the chemical reactions involved in these processes. Biomimetic Materials Laboratory at UNAM is used for this purpose.

In this work, streptavidin and biotin are studied as target molecule - recognition element pair. This is because streptavidin and biotin are known to have one of the strongest non-covalent interaction in the nature [70]. In the literature, this interaction is commonly used as a proof-of-concept procedure for sensor technology [72], [73].

Streptavidin-biotin complex is resistant to organic solvents, denaturants, detergents, extreme temperatures and pH. This is especially useful for biosensing applications, where environmental conditions may be harsh. Thus, streptavidin-biotin pair gives us the opportunity of verifying the efficient operation of nanogap concept in impedimetric sensing for point-of-care biosensing applications.

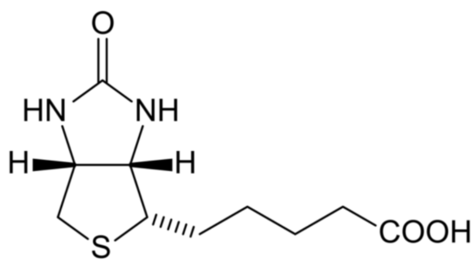

a) Chemical structure of biotin. It has carboxyl group (COOH) at the end.

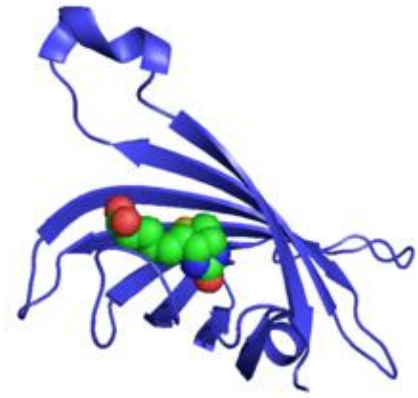

b) Monomeric streptavidin (ribbon diagram) with biotin (spheres) on it.

Figure 4.16 Streptavidin and biotin.

As far as the dimensions are concerned, biotin layer is about 3 nm, although this may increase by several nanometers due to the additional layers used in functionalization of the surface [50]. Streptavidin, on the other hand, is about 5.0 x 4.5 x 4.5 nm in size according to atomic force microscopy (AFM) measurements [74].

The operation of the biosensor is based on detecting the effective dielectric constant change in the nanogap when the target proteins (streptavidin) are bound to the recognition elements (biotin). Therefore, biotin should be anchored to the walls of the nanogap prior to the application of streptavidin. However, biotin cannot bind directly to the SiO_2 layer.

For this purpose, *surface functionalization* procedure is necessary to chemically modify the surface so that biotin molecules can bind to it. This is done by coating the surface with a self-assembled monolayer (SAM).

In the literature, various SAMs are used for functionalization purposes like lipids [75], aromatic molecules [76], DNA [77] and peptides [78]. In this work, APTS (Aminopropyltrimethoxysilane) functionalization procedure is used since it is a well-known, highly efficient surface functionalization procedure [79–83]. APTS is a molecule with ethoxy and amine groups at its ends.

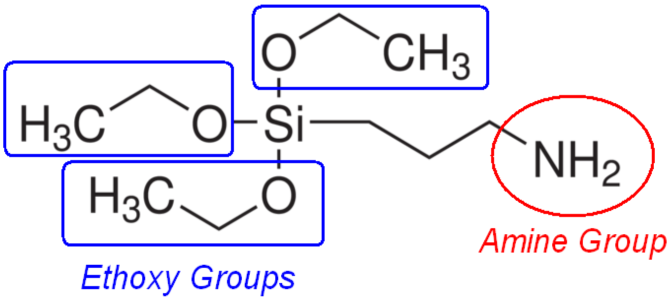

Figure 4.17 APTS molecule

SiO_2 surface has free hydroxyl (-OH) groups formed in few hours in ambient conditions due to moisture in the air. APTS can bind to this hydroxyl groups via its ethoxy groups. On the other hand, APTS has free amine (-NH_2) groups which can form peptide bonds with the free carboxyl groups of biotin (Figure 4.16a). Therefore, APTS can function like a “connection cable” between SiO_2 surface and biotin molecules.

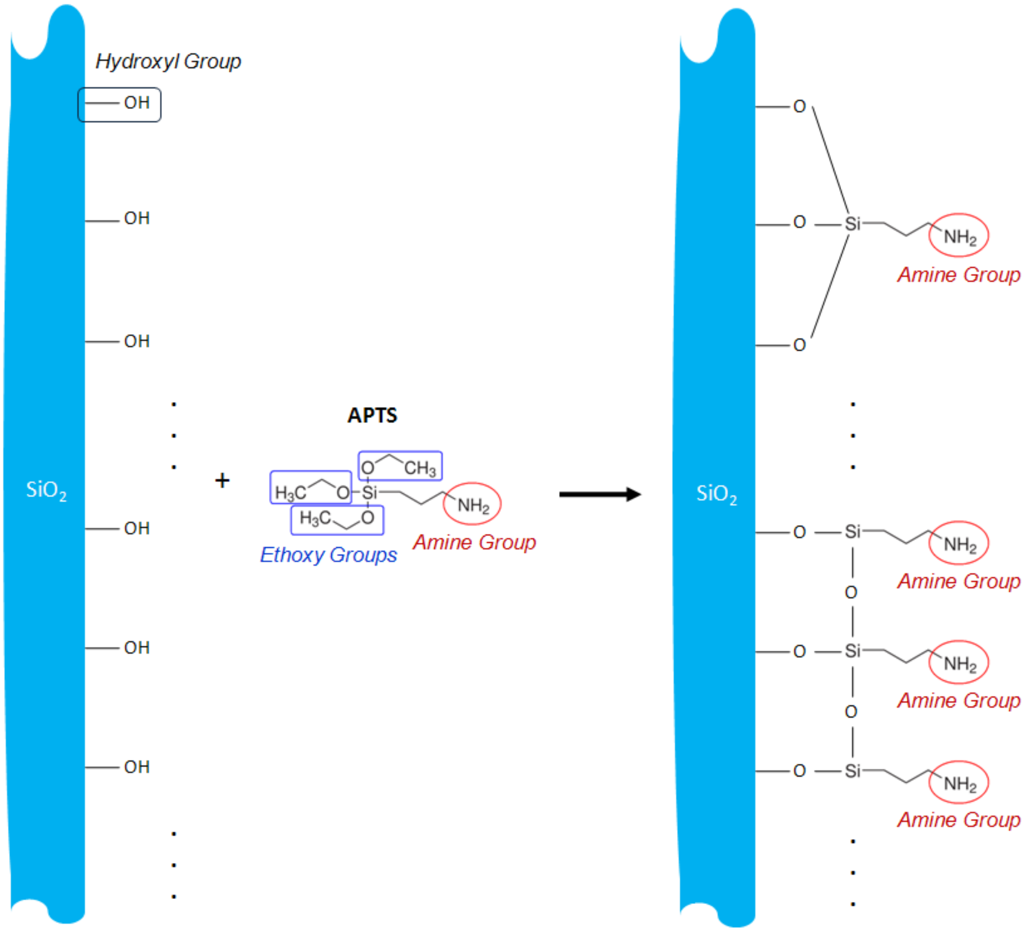

Figure 4.18 After the surface functionalization procedure,
APTS binds to SiO_2 surface thanks to its ethoxy groups

Prior to surface functionalization, the sample is cleaned thoroughly with acetone ($(CH_3)_2CO$), 50% methanol (CH_3OH) / toluene ($C_6H_5CH_3$) mix and 100% toluene ($C_6H_5CH_3$) respectively (all purchased from Merck). APTS is purchased from Sigma-Aldrich and 5% APTS (0.213 mM) solution is prepared in toluene. The cleaned sample is immersed into this solution at room temperature for about 5 hours to realize the surface functionalization reaction. This is followed by exhaustive toluene and methanol rinse and nitrogen blow-dry.

Surface properties of the sample are investigated by X-ray Photoelectron Spectroscopy (XPS) measurements. The measurements are taken by monochromated high-performance XPS spectrometer (Thermo, K-Alpha) at UNAM. Since the SiO_2 layer in the nanogap is under the upper electrode, XPS cannot take measurements from it. Thus, measurements are performed on prepared test samples with bare SiO_2 surfaces. These surfaces are functionalized in an identical manner with the fabricated sensors. The presence of N (nitrogen) atoms is investigated on the surfaces as an indicator of APTS. Surface functionalization procedure explained above should be selective to SiO_2 with respect to Au so that biotin molecules (thus, later streptavidin molecules) do not bind to Au electrodes. Thus, to verify the selectivity, bare Au surfaces are also prepared in an identical manner with the surface functionalization procedure explained above. Similarly, the presence of N atoms is investigated as APTS indicator. The results show N atoms only on the SiO_2 surface as expected (Figure 4.19).

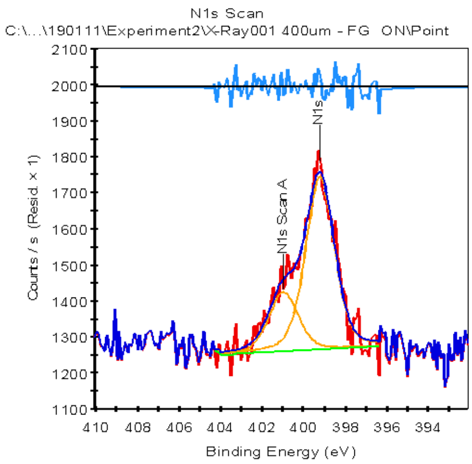

a) Sample with SiO_2 surface

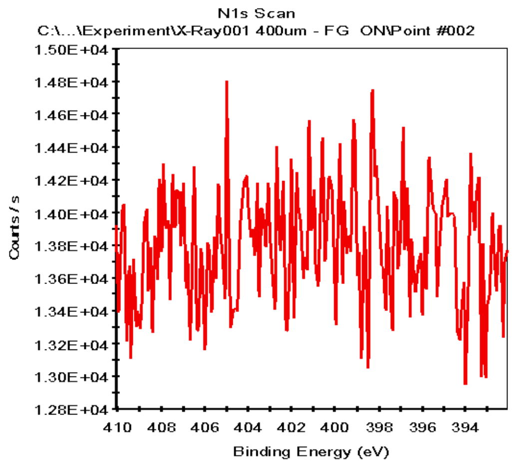

b) Sample with Au surface

Figure 4.19 XPS results after the surface functionalization of test samples.
Presence of N is attributed to presence of APTS. (a) The sample with SiO_2 surface shows peaks related to N atoms. In the figure, N1 corresponds to N-C bonds and N1scanA corresponds to C-N+. (b) No N related peak is observed on the sample with Au surface.

Following the surface functionalization, *biotinylation* process is started to fix biotin molecules to functionalized walls of the nanogap. Since the reaction between free carboxyl groups of the biotin and free amine groups of APTS on the surface is a peptide binding reaction, traditional peptide coupling of amino acid in "Solid Phase Peptide Synthesis Method" was mimicked [84]. Biotinylation solution is prepared by the ingredients and ratios from another study on peptide coupling reactions conducted by Dr.Guler's(our collaborator) research group [85]. Biotinylation solution is prepared by dissolving 2 mol biotin (purchased from Sigma-Aldrich), 1.95 mol O-Benzotriazole-N,N,N',N'-tetramethyl-uronium-hexafluoro-phosphate (HBTU, purchased from ABCR), 3 mol *N*,*N*-Diisopropylethylamine (DIEA, purchased from Merck) in 30 ml Dimethylformamide (DMF, purchased from Sigma-Aldrich) which is appropriate solvent for peptide binding reactions. This amount of biotin is sufficient to coat more than ten times the whole APTS on the surface. HBTU and DIEA are used for the activation of the carboxyl groups of biotin for biotinylation.

After washed with DMF, the sample is immersed into this solution at room temperature for about 2 hours. At the end, the sample is washed with dichloromethane (DCM, purchased from Merck), ethanol, DDW (double distilled water) and blow-dried with nitrogen.

As a result of biotinylation process, free amine groups of the functionalized sample surface (Figure 4.18) form bonds with carboxyl groups of biotin (Figure 4.16a). This is verified by XPS measurements by an approach similar to the verification of surface functionalization. Test samples with bare SiO_2 and Au are prepared by following the surface functionalization and biotinylation processes as described earlier. S (sulphur) atoms are investigated on the surface, indicating the presence of biotin molecules (Figure 4.20).

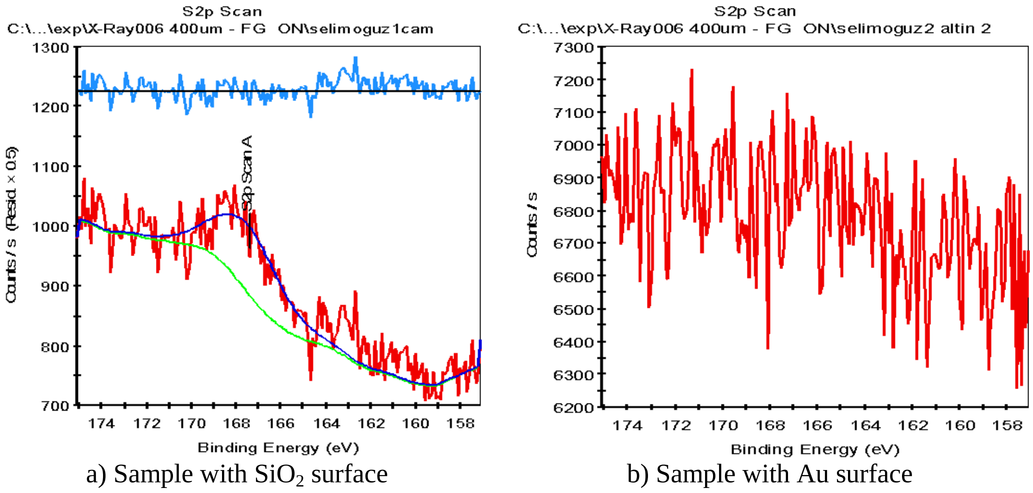

Figure 4.20 XPS results after the biotinylation of test samples. Presence of S atoms indicates biotin molecules. Results indicate that biotin molecules exist only on the sample with SiO_2 surface as expected.

After surface functionalization and biotinylation processes, sample is ready for label-free streptavidin detection (Figure 4.21).

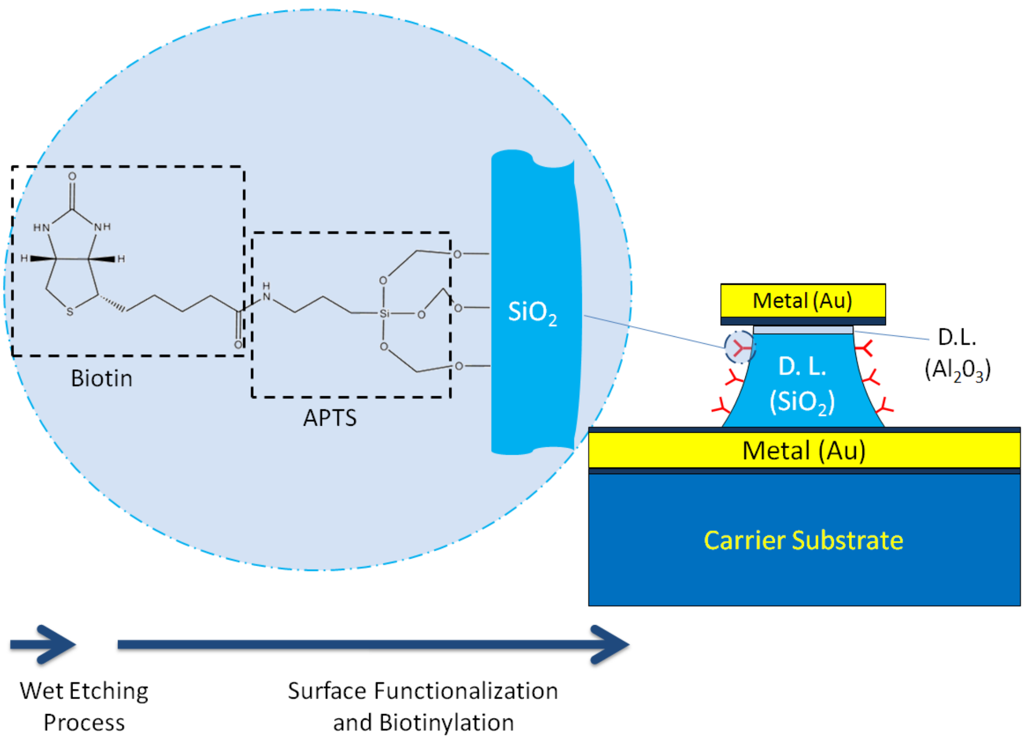

Figure 4.21 Biotin is anchored to the walls of nanogap by surface functionalization and biotinylation processes.

4.6 Conclusion

Impedimetric sensing combined with the nanogap offers appealing features for point-of-care applications like label-free and sensitive detection. When the planar and vertical nanogap fabrication techniques in the literature are considered, vertical nanogap is more advantageous due to low-cost and high yield thin film growth techniques.

This chapter explained the design, fabrication, surface functionalization and biotinylation steps of the biosensors considered in this work. Efficiencies of the steps are verified by SEM and XPS analysis. Next chapter will analyze the overall efficiency of these nanogap based biosensors by impedance measurements.

Chapter 5

Results and Discussion

5.1 Introduction

In this chapter, impedance measurements will be performed on the produced nanogap based impedimetric biosensors. The chapter starts with the introduction of the impedance measurement setup. While earlier reports on impedimetric biosensors are generally limited to very high frequencies (>100 MHz) of operation with relatively expensive instruments to eliminate the parasitic contribution of the ions (electrical double layer) in the solution, this design utilizing the nanogap configuration can be operated at low-frequencies (1 kHz – 100 kHz). Required measurement equipments are relatively low cost when compared to their RF counterparts like network analyzer. Moreover, at GHz frequencies, even the metal lines carrying the signal may become problematic due to inductive losses. Thus, special care is required for RF signal handling as well as impedance matching issues to avoid signal reflections. Not only low frequency sensors are easier to handle, but also they are more amenable to chip-integration, which is especially important for point-of-care biosensor applications.

The chapter will follow by the performance metrics related to the produced biosensors. Results of the sensitivity and reliability tests will be presented and discussed. The overall goal is to assess the applicability of nanogap based impedimetric biosensors to point-of-care, early cancer detection applications.

5.2 Measurement Setup

Impedance measurements of the produced biosensors are performed at UNAM cleanroom facility. A parameter analyzer capable of low-frequency impedance measurements (Keithley 4200-SCS with 4200-CVU) and a manual probe station (Cascade PM-5) are used for this purpose.

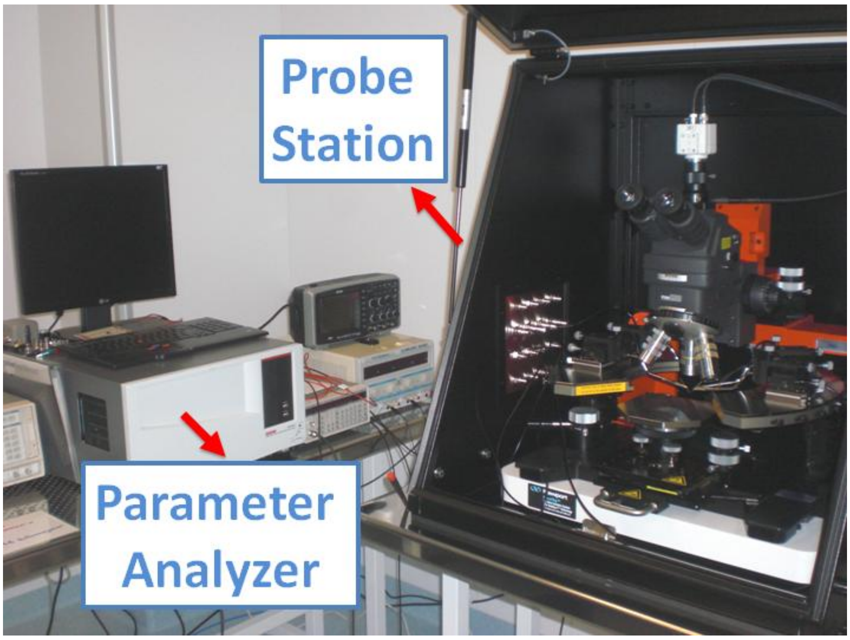

Figure 5.1 The picture from the dark room of UNAM cleanroom facility shows the equipments used for impedance measurements.

The sample is mounted on the vacuum chuck of probe station, and by the help of micromanipulators, micro-needle tips are precisely positioned and connected to the upper and bottom electrode pads for electrical connection to the parameter analyzer.

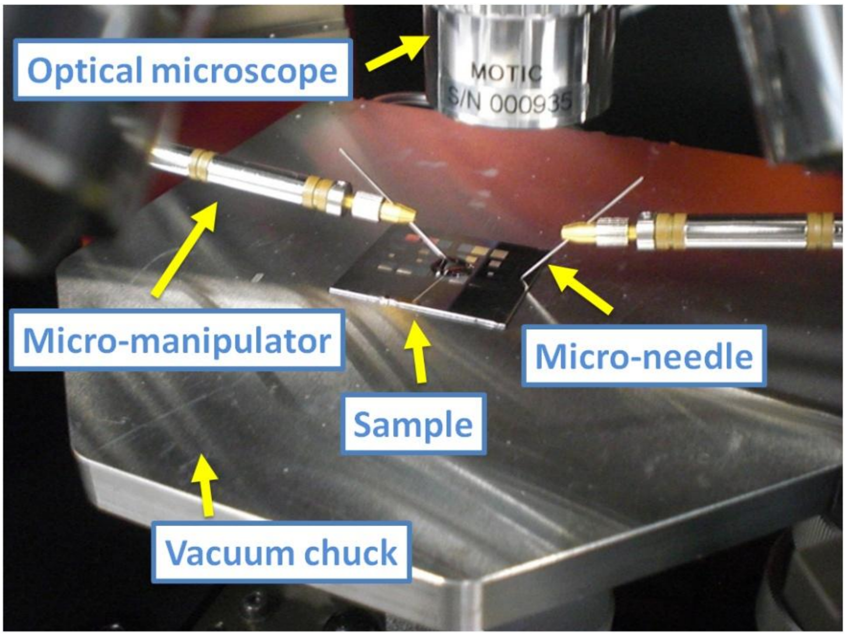

Figure 5.2 Sample on the vacuum chuck with micro-needle tips for electrical connection to the parameter analyzer.

Electrical connection between the CVU module of the parameter analyzer and probe station is done via coaxial cables to prevent any interference from the environment (Figure 5.3).

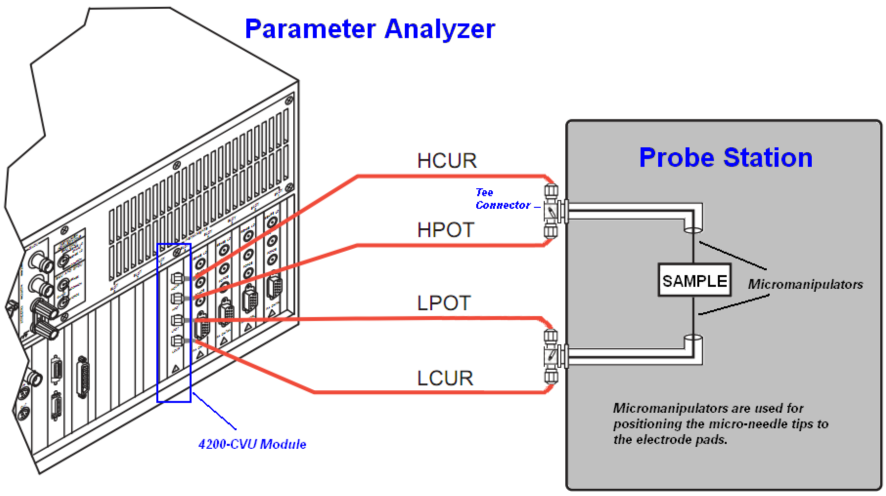

Figure 5.3 Schematics of the parameter analyzer connections to the probe station. (adapted from [86])

Parameter analyzer utilizes the measurement principle of sourcing AC voltage across the sample and measuring the resulting AC current. It is possible to extract impedance out of these measurements as explained in Section 3.1.

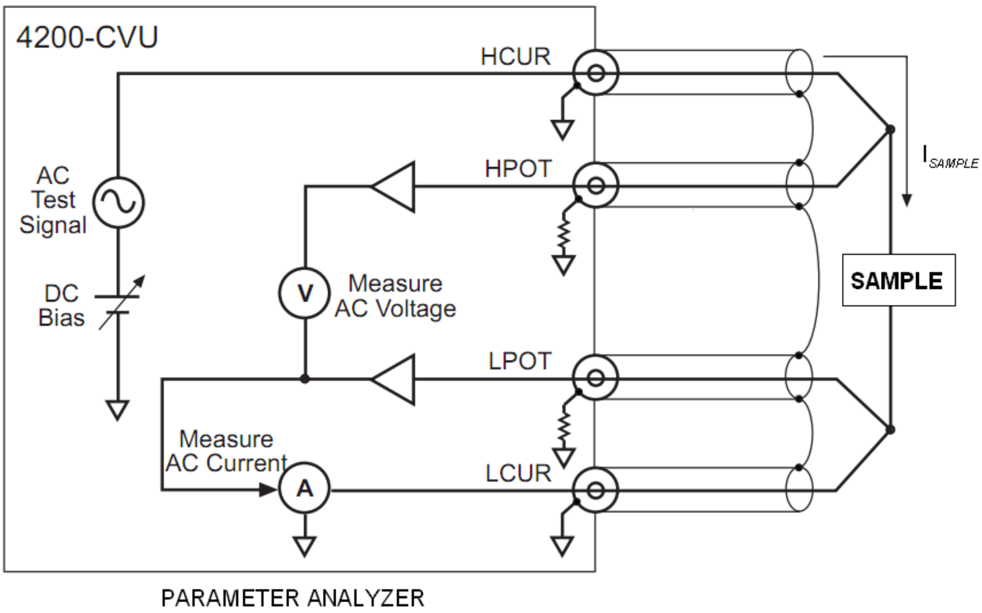

Figure 5.4 Simplified measurement circuit of the parameter analyzer (adapted from [87])

Any parasitic effect caused by the connection between parameter analyzer and probe station can be corrected by open and short connection compensation procedures performed prior to the measurements. Open correction is started after lifting the two micro-needle tips so that they are separated from each other and anywhere else. During this stage, parameter analyzer generates and stores the correction compensation data for open conditions. Short correction is started after making the two micro-needle tips touch each other like crossed swords and ended by the generation of the short correction compensation data.

The parallel capacitance and resistance model in Figure 4.5 is introduced to the parameter analyzer, so that measured impedance values are converted to Cp and Rp. In the following sections, Cp versus frequency and Cp versus time data will be analyzed, since when the target proteins are bound to the recognition elements, the dielectric constant (so, the capacitance) of the nanogap will change. On the other hand, Rp is observed to be unstable with respect to time; probably due to ionic movements in the solution resulting from the alternating electric field.

Applied AC voltage signal amplitude is 10 mV_{rms}. This is the advantage of impedimetric sensing over IV spectroscopy where DC voltage sweep up to several Volts are used. As far as biosensing applications are concerned, high voltages would damage the biological structures like proteins. Moreover, system may respond nonlinearly at resulting high electric fields and harmonics of the excitation frequency may be produced.

5.3 Sensitivity Tests

5.3.1 Sensitivity to the target protein

In this part, streptavidin – biotin pair is studied for verifying the efficient operation of nanogap concept in impedimetric sensing for point-of-care applications. Streptavidin (target protein, derived from *streptococcus avendii* bacterium) and biotin (recognition molecule, Vitamin H) are known to have one of the strongest non-covalent interaction in the nature [70]. This biomolecular system is also used in certain disesases for diagnosis purposes [50].

Streptavidin is purchased from Sigma-Aldrich and used in phospate-buffered saline solution (PBS, pH 7.4) to avoid protein denaturality. PBS solution is prepared by dissolving 2 g of KCl, 80 g NaCl, 2.4 g of KH_2PO_4 and 14.4 g of K_2HPO_4 in 1000 mL of double distilled water (DDW) (all purchased from Merck). Streptavidin is prepared in different concentrations starting from 100 µg/mL and decreasing by ten fold till 10 ng/mL.

Concentration	µg (in 50 µL)	Pmole	Protein (#)	Molar conc. (µM)
100 µg/mL	5.00E+00	8.20E+01	4.93E+13	1.64E+00
10 µg/mL	5.00E-01	8.20E+00	4.93E+12	1.64E-01
1 µg/mL	5.00E-02	8.20E-01	4.93E+11	1.64E-02
100 ng/mL	5.00E-03	8.20E-02	4.93E+10	1.64E-03
10 ng/mL	5.00E-04	8.20E-03	4.93E+09	1.64E-04

Table 5.1 Streptavidin concentrations used in this work with their equivalences in other notations.

Before the application of streptavidin, the biotinylated sample is rinsed with deionized (DI) water and placed on the vacuum chuck of probe station for the reference measurement. The reference measurement is taken with DI water as the medium filling the nanogap of the sample. This is because dielectric constant of DI water is much larger than that of streptavidin and this contrast makes the detection easier. DI water of about 30 μL is introduced by a micropipette to the sample (Figure 5.5). This volume is more than enough to coat the entire sensor. This is verified by impedance measurements in which adding an additional volume of DI water does not change the result.

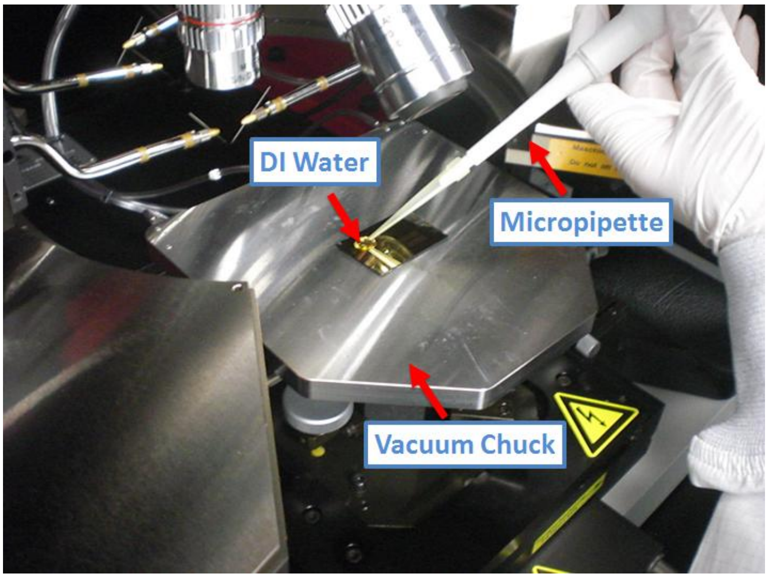

Figure 5.5 Introduction of DI Water to the sample by a micropipette.

Impedance measurements are performed for the frequency range of 1 kHz – 100 kHz. The frequency sweep is done at 19 frequencies (1 kHz, 2 kHz …, 10 kHz, 20 kHz, … 100 kHz). Although parameter analyzer allows a wider range up to 10 MHz, (100 kHz – 10 MHz) range is not used since reliable results could not be obtained probably due to cable inductances. The impedances of cable inductances ($j2\pi fL$, series connected) become dominant at high frequencies and thus, the measured impedance increases sharply at high frequencies. Similar effect is observed on the test measurements of commercial ceramic capacitors and also reported in the literature for a similar setup [71]. At the end of the measurement, the sample is rinsed with DI water and blow dried with nitrogen, and results are denoted as *"before streptavidin"* which will then be compared with those obtained after the application of streptavidin.

Streptavidin solution is introduced by a micropipette and incubated for about 10 hours. This duration is quite sufficient for streptavidin immobilization to the walls in the nanogap and it can be shortened by a systematic study. As far as point-of-care applications are considered, this duration could be shortened down to several minutes if these sensors are integrated with microfluidic systems and target solution is passed over the nanogap many times. To our knowledge, there is no specific duration suggested in the literature which ensures the completion of this immobilization. For example, whereas 15 min is used in [88], 4 hours is used in [50]. However, the concentration is also important in determining this duration. As an example, former study applies 2.5μM streptavidin solution for 15 minutes and latter study applies 300 nM streptavidin solution for 4 hours. Thus, considering that minimum concentration in this work is 164 pM (Table 5.1), 10 hours of incubation duration seems reasonable. Future work would be analyzing impedance response for the minimum concentration used with respect to incubation time. This would help in minimizing the preferred incubation duration.

During the incubation, the sample is preserved in a vacuum-sealed container to avoid evaporation. This is followed by washing the sample using DI water and blow-drying with nitrogen gun. From a broader perspective, this step is also helpful for satisfying selectivity in point-of-care biosensors. Molecules which attach to the surface by non-specific binding may exist in the nanogap and they will be removed by washing the sample. At the end of this step, streptavidin is immobilized to the walls of the nanogap by the strong intermolecular attractions with the biotin.

After immobilization, the sample is placed on the vacuum chuck for the second impedance measurement which will be denoted as *"after streptavidin"* in the following figures. This measurement is done in the same frequency range and compared with the reference measurement to detect presence of streptavidin. The results are shown in Figure 5.6 where capacitance changes with respect to frequency of the applied signal are observed for the five different streptavidin concentrations. As expected, capacitances for all frequencies decrease after streptavidin since the streptavidin proteins have less dielectric constant than the water molecules they displaced. (Table 5.3)

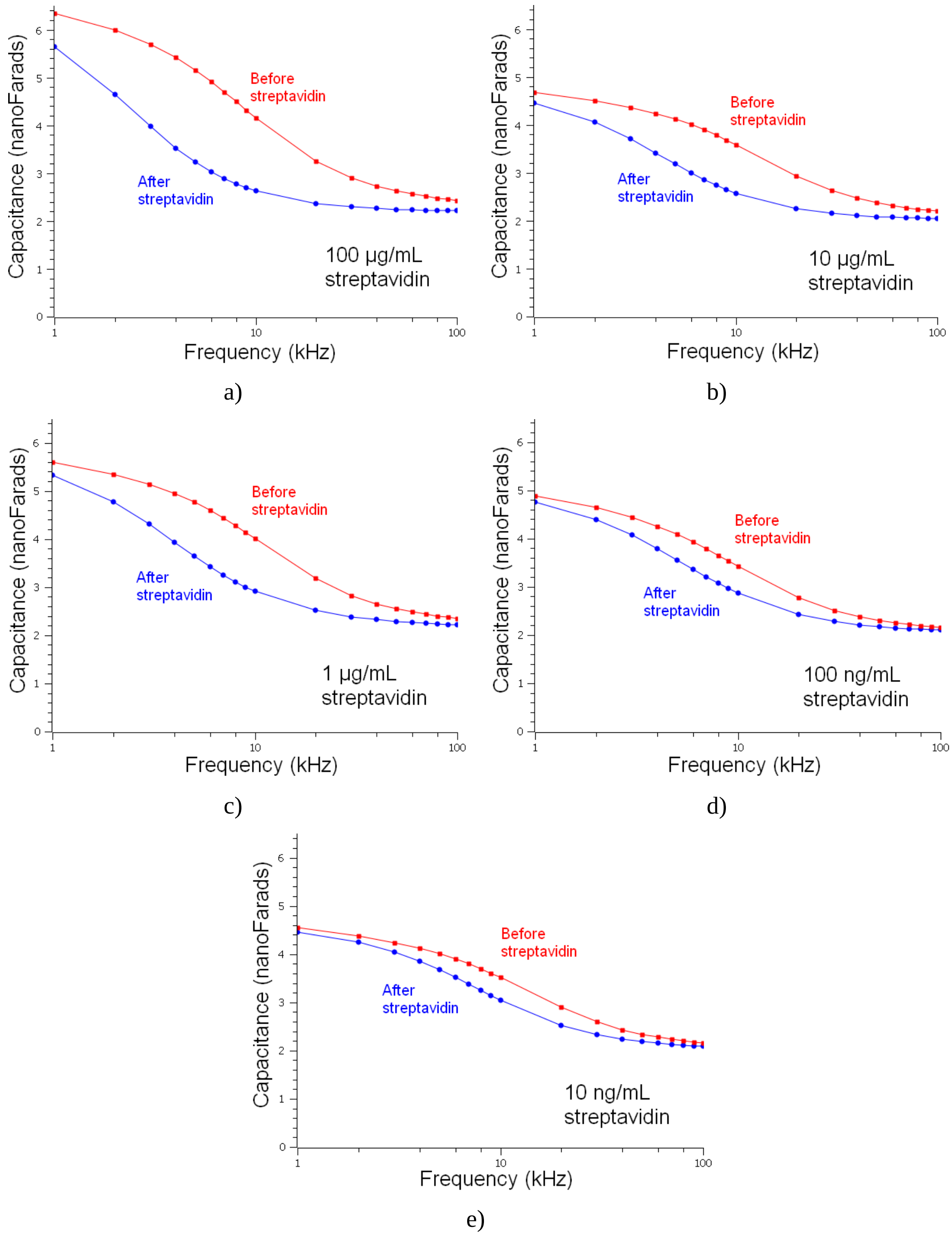

Figure 5.6 Capacitance (*Cp*) versus frequency (*f*) plots for different concentrations of streptavidin solution. For all concentrations, significant changes in the capacitances are observed after streptavidin proteins are bound to the biotin molecules.

As seen in Figure 5.6, “before streptavidin” plots are not the same for all cases. This is expected because the measurements are done on different sensors of the same wafer and PECVD SiO_2 dielectric film is non-uniform (Section 4.4.3). Thus, as the radial distance of a sensor to the wafer center increases, its dielectric layer thickness increases, and as a result, capacitance of the sensor decreases.

It is observed that for the highest streptavidin concentration (100 μg/mL) maximal capacitance change is approximately 1.93 nF, whereas this is 475 pF for the lowest streptavidin concentration (10 ng/mL). So, the biosensor can detect the presence of streptavidin within this range. Upper and lower limits of detection are out of the concentration range considered in this work and dynamic range covers the whole concentration range of 100 μg/mL to 10 ng/mL. However sensitivity to streptavidin concentration data cannot be extracted since the results are not comparable due to different “before streptavidin” plots.

In Table 5.2, the detection range observed in this work is compared with the other works on streptavidin-biotin detection in the literature. To the best of our knowledge, this is the first nanogap based impedimetric sensor showing streptavidin detection. The detection range is comparable even with that of its optical counterparts, although the utilized measurement technique is much more economical. This suggests that in the future impedimetric, disposable, lab-on-a-chip biosensors may support or even replace the current, expensive, optical based laboratory equipments and bring the point-of-care testing technology to healthy-looking (with no cancer symptoms) people enabling early cancer detection.

Structure	Detected Signal	Detection Range		Year	Ref.
		Lower Limit	Upper Limit		
Interferometer	Light Phase Shift	100 ng/mL	50 μg/mL	2011	[89]
Dielectric Modulated Field Effect Transistor	Threshold Voltage	20 μg/mL		2007	[50]
Vertically Placed Electrodes	Current	100 ng/mL	20 μg/mL	2007	[90]
Nanotube Based Field Effect Transistor	Current	170 ng/mL		2003	[88]
Optical Fiber	Light Intensity	6.5 ng/mL	2 μg/mL	2002	[91]
Nanowire Based Field Effect Transistor	Current	1.7 ng/mL	17 μg/mL	2001	[92]
Vertically Placed Electrodes	**Capacitance**	**< 10 ng/mL**	**> 100 μg/mL**	**This work**	

Table 5.2 Label-free biosensors in the literature for detecting streptavidin concentrations. Collecting data, 100 ng/mL streptavidin is taken equivalent to ~1.5 nM (see Table 5.1)

Results are consistent with the theoretical estimations. Using the dimensions in Table 4.1 and Figure 4.11 (undercut length is taken as 500 nm), *Cp* is calculated as explained in Section 4.3. The resultant *Cp* is 2.22 nF, which is the addition of C_{dl} (0.90 nF) and C_{ng} (1.32 nF). This is very close to the observed capacitance values in Figure 5.6, especially at high frequencies. Although nanogap design and DI water measurement medium are preferred to avoid electrical double layer; it seems that it is not completely eliminated. However, at higher frequencies, the effect of electrical double layer is less significant due to ionic relaxation (ions cannot respond quickly enough to form electrical double layer) and thus, parallel plate model (Figure 4.5), which assumes no electrical double layer, seems to fit better to the measured results.

In Figure 5.6, the most significant capacitance changes are observed at around 10 kHz. This is a low frequency region in the sense that the effect of electrical double layer is still valid. Thus, incremental change with respect to high frequencies can be attributed to the alteration of electrical double layer when streptavidin is bound to the dielectric layer in between.

However, when the dimensions are compared: streptavidin is about 5 nm in size and undercut depth is in the order of 100 nanometers. Thus, there is very small intersection region with electrical double layers when immobilized on the walls of the nanogap (Figure 5.7).

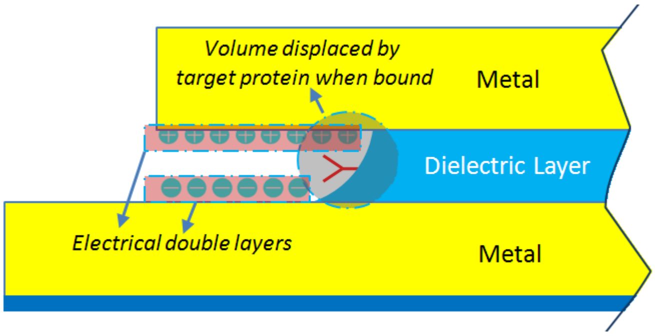

Figure 5.7 Electrical double layers and the volume displaced after the binding of target protein.

Considering that streptavidin can only displace very small portion of the double layer on the electrodes, it is not easy to relate observed high capacitance change at low frequencies with electrical double layer. To enlighten this, further investigation may be conducted on different designs. For example, the electrodes, instead of dielectric layers, can be used for immobilization as in Figure 5.11b. In that case, displacement of electrical double layer will be much more significant when target molecules are bind to the metal surface. Analyzing the capacitance change after this would give further insight about the effect of electrical double layer in these nanogap sensors.

5.3.2 Sensitivity to the dielectric constant of the solution

The operation principles of the nanogap based impedimetric biosensors studied in this work depend directly on detecting change in effective dielectric constant of the nanogap. Thus, sensitivity of the sensor output to unit change in dielectric constant of the nanogap is also analyzed.

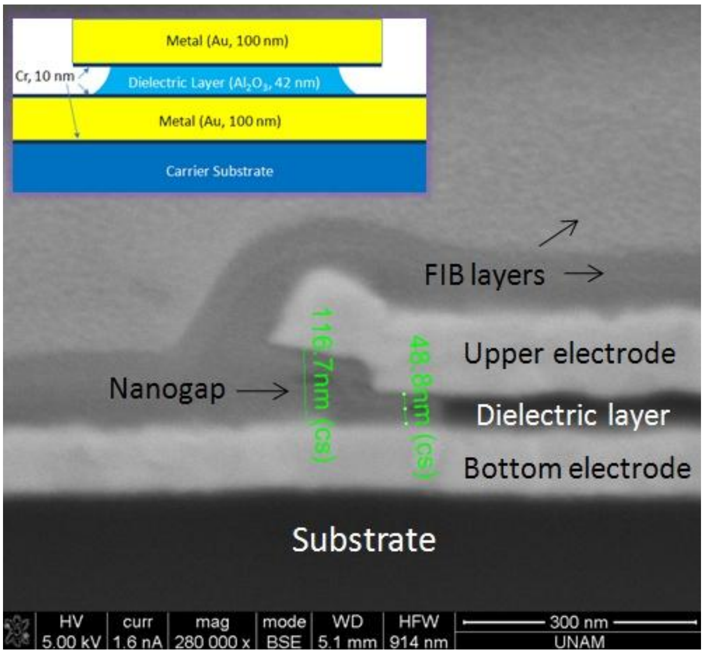

Figure 5.8 Electron micrograph image taken by focused ion beam (FIB, FEI Nova 600i Nanolab) at UNAM. FIB layers coated are only for cross-sectional (cs) imaging purposes.

For this analysis, the same sensor layout in Figure 4.2d is used; however, this time, SiO_2 layer is not coated since functionalization procedure or target molecule detection is not necessary for this analysis. Thus, dielectric layer used in this design is only atomic layer deposited Al_2O_3.

Figure 5.8 shows the cross-sectional electron micrograph image of the produced sensors. Upper electrode seems to be bended upwards, which is due to lift-off process in fabrication. Although not a problem for our analysis, this could be avoided by using negative tone lithography technique [93], which is more suitable for lift-off purposes.

In this analysis, *Cp* response is analyzed at a single frequency of 10 kHz. 10 kHz is preferred since it is one of the frequencies at which high capacitance change occurs after the application of streptavidin as seen in Figure 5.6.

Solutions	**Dielectric constant (ϵ_r)**
Deionized(DI) Water	80
Methanol	33
Isopropanol(IPA)	18

Table 5.3 Solutions used in this analysis with their dielectric constants (ϵ_r) [47]

Three different solutions (DI Water, Methanol and IPA) are chosen so that their vapor pressures are low enough to avoid evaporation during the measurements and their dielectric constants **(ϵ_r)** are quite different from each other enabling large ϵ_r range analysis (Table 5.3). After probing the sample on vacuum chuck, capacitance measurement is started. Referring to Figure 5.9, the steps are: (1) Dry (medium is air) measurements are being taken (2) Solution is applied by a micropipette. (3) Probes are lifted and sample is rinsed with DI water and dried by a nitrogen gun. (4) To verify repeatability, measurement continues with Step 1.

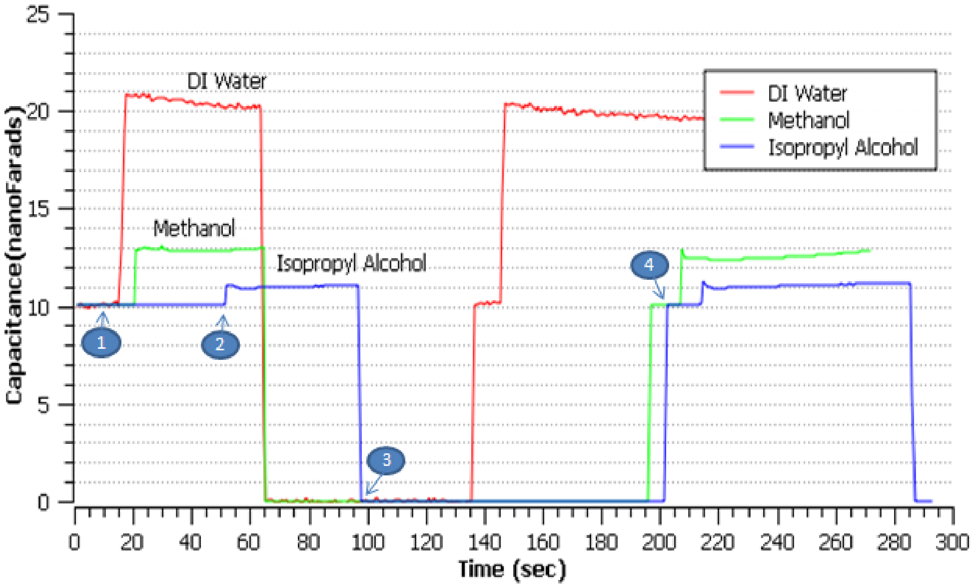

Figure 5.9 *Cp* vs. time for different solutions at 10 kHz.

Results show that dielectric constant of nanogap has significant effect on the overall capacitance and that this change is repeatable, which is quite important although not much analyzed in the literature [7] . Sensors proved repeatable for at least six dry-wet cycles. This is not shown in Figure 5.9 to keep coherency of this section. Repeatability analysis will be done in section 5.4.2.

In order to obtain average C_p values, which will then be used in sensitivity analysis, averaging is done over three sensor outputs considering their minimum and maximum values in a time window of more than 30 seconds. This is done after the solution is applied and stabilization is satisfied. (Table 5.4)

Device	**Air (dry) ϵ_r=1**		**IPA ϵ_r=18**		**Methanol ϵ_r=33**		**DI Water ϵ_r=80**	
	Min.	Max.	Min.	Max.	Min.	Max.	Min.	Max.
#2	9.9	10.2	10.9	11.1	12.3	12.9	19.4	20.8
#8	10.0	10.0	11.0	11.3	12.4	13.6	19.5	21.1
#9	10.0	10.1	10.8	11.1	12.5	14.3	19.4	20.6
Average	**10.0**		**11.0**		**13.0**		**20.1**	

Table 5.4 *Cp* (in nF) values are obtained from three sensors and averaged for sensitivity analysis.

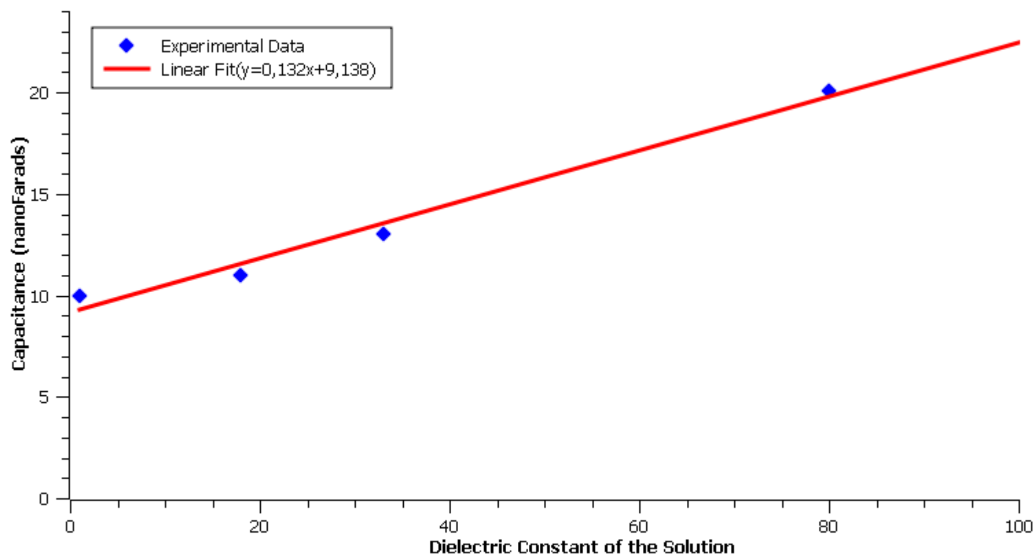

Figure 5.10 Average C_p values of Table 5.4 is plotted with respect to dielectric constant of the related solution (Experimental Data) and fitted by a line (Linear Fit).

When analyzed with respect to dielectric constants of the related solutions, C_p values exhibit linear change as expected also by the *Cp-Rp* model (Figure 4.5). The linear fit shown in Figure 5.10 indicates that sensitivity of C_p with respect to unit change in dielectric constant is 132 pF, which is well above the resolution limit of commercial and low-cost capacitance chips [94]. The linear response with high sensitivity also offers benefits for other sensor applications like gas or chemical sensors [95–97].

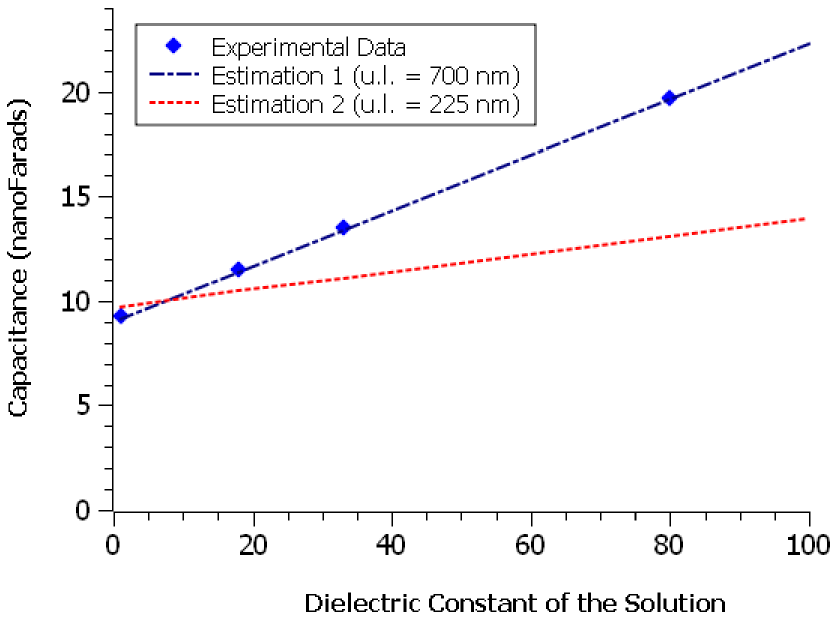

Figure 5.11 Experimental and estimated C_p vs. ϵ_r values

Using the dimensions in Figure 5.8, *Cp* values are estimated using the undercut length as the fitting parameter. The finger width is taken 11.91 μm (obtained by FIB measurements) instead of its layout value of 10 μm, since it increased due to the bending observed at the edges of fingers (Figure 5.8). Bending also changes the height of the some portion of nanogap; however, the height is assumed constant and equal to 42 nm (height of dielectric layer) for the simplicity of the modeling. It is observed that the estimation fits well with the experimental data when the undercut length is 700 nm (Figure 5.10, Estimation1). However, this is too much for the undercut length in the electron micrograph (Figure 5.8). The high undercut length can be attributed to fringing fields; however, there is no support for not neglecting fringing fields in these structures, where separation distance (42 nm) is relatively very low with respect to finger width (11.91 μm).

Another calculation (Estimation 2) is done by using the undercut length obtained from SEM image in Figure 5.8, which is around 225 nm. The estimation result with this undercut length is shown in Figure 5.11 (Estimation 2). Observed capacitance is higher than estimated one, especially at higher frequencies. The difference cannot be due to the crude approximation made in nanogap height, since this approximation will yield a decrease in the difference between experimental and estimated values, not an increase. That is, a more detailed modeling of the nonuniform nanogap height will decrease the estimated capacitance and, this will increase the difference with experimental data. The difference can be attributed to the effect of electrical double layer which is also observed in Section 5.3.1. Electrical double layer shields the applied electric field and increases the capacitance observed. If this experiment were conducted at higher frequencies like 100 kHz, the ions would not be able to respond to quickly changing electric field, and experimental C_p values probably would be lower (this is observed in Figure 5.6) and closer to estimated C_p values with undercut length of 225 nm; however, high frequencies are not preferred in this Section since this would also decrease the sensitivity according to Figure 5.6.

The sensitivity can be adjusted by the undercut length. At the ultimate case, where almost no Al_2O_3 remains, sensitivity is calculated to be around 1250 pF per unit change in dielectric constant. Increasing the undercut has disadvantages though: (1) This may result in collapse of the fingers. (2) Liquids may not fill the undercut due to fluid mechanical problems [71]. (3) As far as the biosensors in this work is considered, using dielectric layer walls for immobilization does not change the volume displaced even if the undercut is increased (Figure 5.12a); on the other hand, by changing surface functionalization procedure as in Figure 5.12b, sensitivity can be improved by increasing undercut length. Nevertheless, it is not easy to develop a surface functionalization procedure which will only coat the parts of the metal within the nanogap.

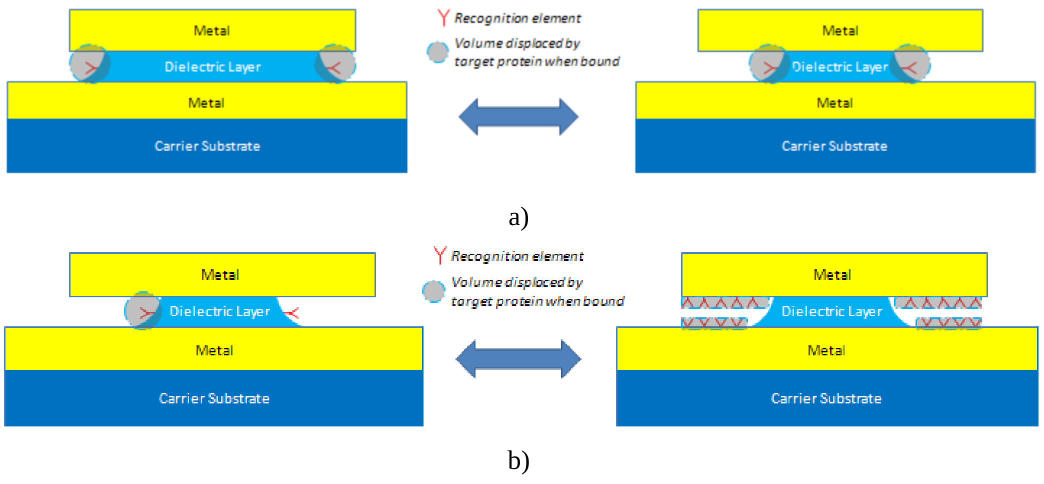

Figure 5.12 Discussion on possible effects of longer undercut length with and without a different surface functionalization technique a) With the current surface functionalization procedure, increasing the undercut length does not change the volume displaced by target protein when bound to the recognition element. b) By changing the surface functionalization procedure so that recognition elements are anchored to the base and ceiling of the nanogap, it is possible to increase the volume displaced and get a more sensitive sensor.

Effect of undercut length on the capacitance is frequently used during the fabrication for measuring the undercut length, instead of the impractical and invasive method of taking cross-sectional electron micrograph image of the undercut. The measured C_p change after successive etch processes is illustrated in Figure 5.13. Note that although 10 kHz is used in this figure, for undercut length measurement purposes high frequencies like 100 kHz should be used to avoid the effect of electrical double layer and fit the undercut length more accurately.

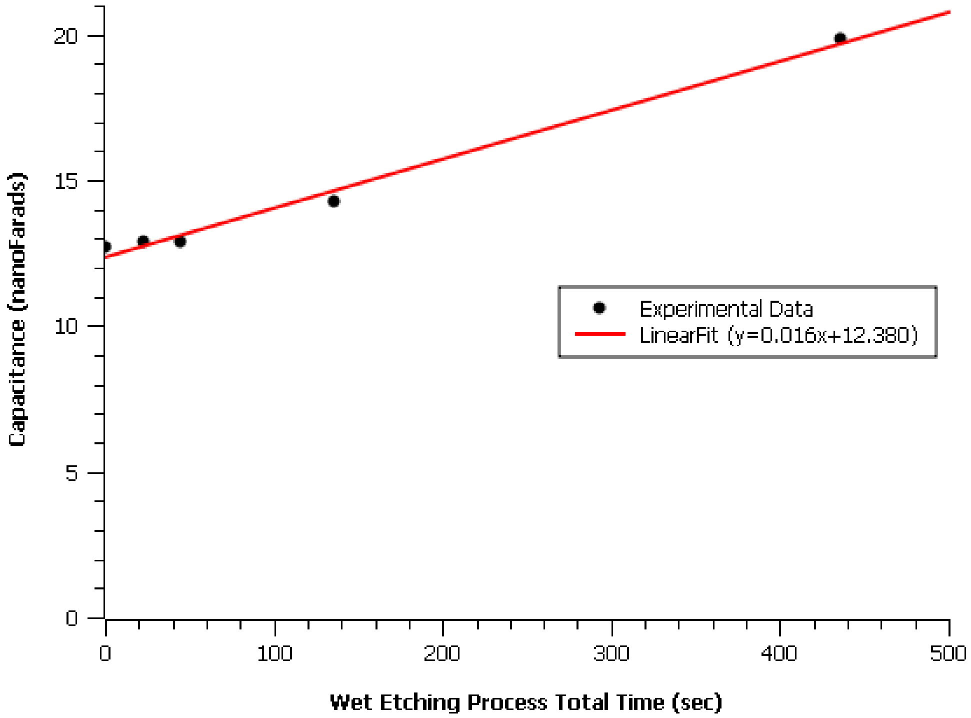

Figure 5.13 C_p versus dielectric layer wet etching time.

Measurements performed in DI water at 10 kHz after successive etch processes.

Sensitivity is also dependent on the dimensions of the fingers and the electrode distance. Increasing the area of fingers will increase the sensitivity; however, this will also increase the area of nanogap walls and in biosensing applications with very low concentration of target proteins, this will decrease the performance since then not all of the walls could be coated. Actually, it is the advantage of nanogap based sensing to be able to maximize the capacitive change while keeping the sensing region (where target molecules are bound to) minimal. Thereby, very low concentrations of target protein can be detected and obviously, there is the promise of single molecule detection biosensors. Decreasing the electrode distance is also possible for high sensitivity purposes; however, as the distance approaches to several nanometers undercut filling of the liquid might be problematic as well as any congestion in undercut entry due to molecules (proteins, hormones, ions etc.) in the target solution.

5.4 Reliability Tests

Reliability tests consist of stability and repeatability verifications, which are at least as important as sensitivity tests for commercialization purposes; unfortunately, they are generally not reported in literature [7].

5.4.1 Verification of stability

Stability tests are done after the biotinylation of sensors shown in Figure 4.13. The sample is mounted on the vacuum chuck and probed by micromanipulators. Shortly after starting *Cp* vs. time measurement, DI water is placed over the sample by a micropipette. Signal response is observed for about 20 minutes, which is a quite long duration considering point-of-care applications where single impedance measurement is enough and can be completed within a second after stabilization is satisfied. However, it is meaningful to test stability for long durations considering clinical applications where constantly monitoring the concentration of target molecules with respect to time is needed. Monitoring the glucose level of a diabetic patient is an example of this kind of an application.

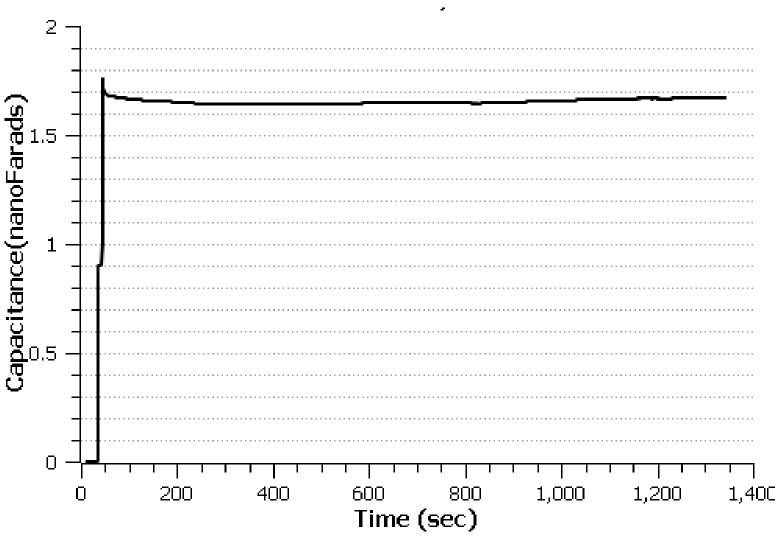

Figure 5.14 C_p vs. time is analyzed for more than 20 minutes for stability verification. DI water is used as the medium and excitation frequency is 50 kHz.

As seen in Figure 5.14, signal stabilization is satisfied shortly after the application of DI water around 1.67 nF within a tolerance band of ±0.03nF. Signal is sustained within this tolerance range during the 20 minutes time interval considered. Small changes in the capacitance might be due to non-static ionic distribution created by the rapidly changing electric field.

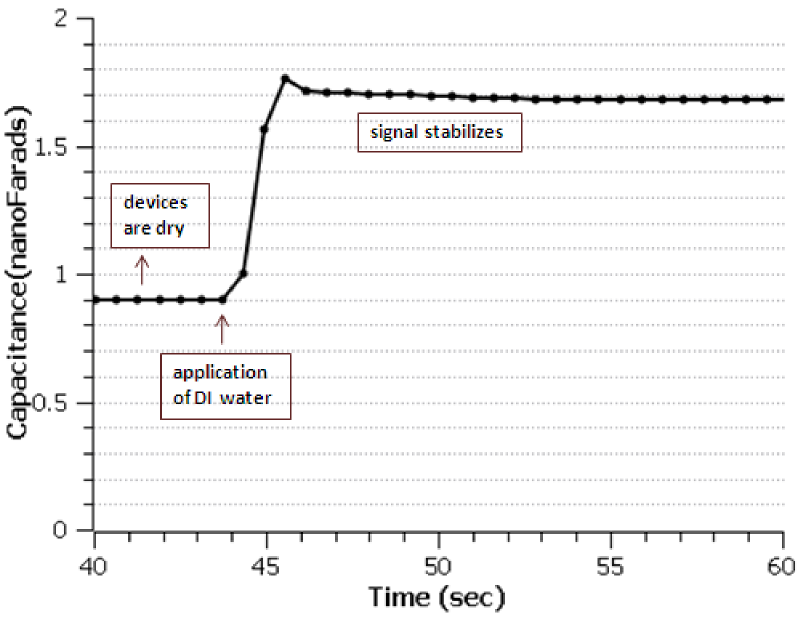

Figure 5.15 A closer view of the duration before and after the application of DI water in Figure 5.14.

The response time is measured by analyzing the change in signal response at the instant of DI water application. It is observed to be less than 10 seconds in Figure 5.15. This is mainly the time for liquid filling the nanogap and can be even shortened if solution is introduced by an integrated microfluidic system. Stability is tested and verified on several additional sensors on the wafer. The observed tolerance bands and response times are promising for point-of-care applications

5.4.2 Verification of repeatability

Repeatability is tested by changing the measurement medium from air to DI water (by wetting with a micropipette) and DI water to air (by drying with a nitrogen gun). The followed steps are similar to that explained in Figure 5.16.

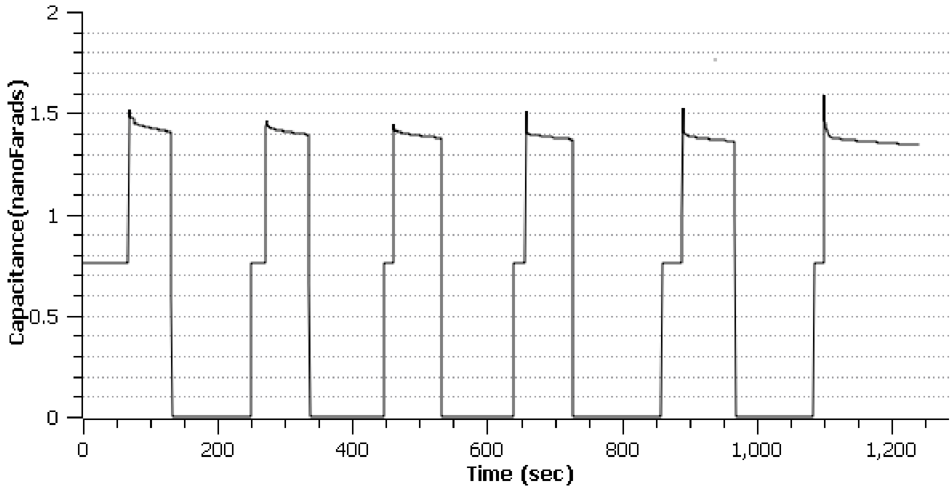

Figure 5.16 C_p vs. time measurements are performed by repeating the dry-wet cycle six times to investigate repeatability performance of the sensors.

As seen in Figure 5.16, the observed C_p response is reasonably repeatable; however it decreases by about 0.01 nF (less than 1%) in each cycle. It is difficult to explain this without considering any change in the physical dimensions of the sensors due to pressure applied on sensors, especially when drying with nitrogen. The pressure might be slightly bending the suspended fingers of the nanogap. However, this should be analyzed further to have an accurate insight. Hopefully, this effect produces a tolerable change in the C_p response and the sensor repeatability is verified.

Similar tests are also done on other sensors on the same wafer and similarly, stable and repeatable results are observed. Since the sensors do not have identical dielectric thicknesses due to non-uniform PECVD SiO_2 (section 4.4.3), each sensor stabilizes on a different C_p range which is expected. On the other hand, thanks to uniform Al_2O_3 coating, sensors produced with only Al_2O_3 exhibited very close *Cp* values as seen in Table 5.4.

5.5 Conclusion

This chapter started with the introduction of the measurement setup used to perform low-frequency impedance analysis on the biosensors. Nanogap allows the low frequency measurements, which gives the opportunity of chip-integrality for point-of-care biosensors.

Sensitivity tests showed the detection of various streptavidin concentrations from 100 μg/mL to 10 ng/mL is possible. To the best of our knowledge, this is the first nanogap based impedimetric sensor showing streptavidin detection. Sensitivity to dielectric constant of the nanogap medium is found to be 132 pF per unit change in dielectric constant. This much of capacitive change can be detected by integrating these biosensors with a low-cost commercial capacitance chip like AD7147A™ (sold at $1.25) [94]. Finally, reliability tests proved the stable and repeatable operation of the sensors, which are essential for any biosensor platform.

Chapter 6

Conclusions

Despite lots of research going on to find a hope, cancer is still a major cause of death in today's world. It has been reported that cancer has biomarkers in human body and detecting these biomarkers timely can pave the way for early detection and successful treatments. Point-of-care biosensors are promising for this mission. If they can achieve sensitivity and reliability with a low-cost and simple platform, they can address a large mass of people who are at the early stages of cancer without any clear symptoms yet.

Impedimetric sensing is an efficient method and it can be utilized for point-of-care biosensor applications. However, electrical double layer formed due to ions in the solution of interest is problematic since it shields the applied electric field. Traditionally, high frequencies (>100 kHz) are preferred to eliminate electrical double layer. However, this is not desired due to parasitic and inductive effects at those frequencies as well as cost associated with high frequency systems. This thesis demonstrates a technique which paves the way for low frequency (1 kHz – 100 kHz) measurements.

This technique requires a nanogap based biosensor structure, which is also helpful in minimizing the measurement volume. Also, measurement protocol is designed such that after the application of target solution, DI water medium is used for obtaining electrical double layer free measurements. This is also beneficial in increasing the dielectric constant contrasts between the target molecules and medium of measurement and thereby, improving sensitivity.

Moreover, this measurement protocol includes DI water rinse step, which serves the purpose of selectivity by removing the unspecifically bound molecules from the measurement medium.

The technique is demonstrated by performing the design, fabrication, surface functionalization and biotinylation stages of a nanogap based biosensor. Label-free detection of streptavidin proteins are achieved for 100 µg/mL, 10 µg/mL, 1 µg/mL, 100 ng/mL and 10 ng/mL concentrations of streptavidin. Thereby, to our knowledge, for the first time the application of nanogap based impedimetric biosensors in streptavidin protein detection is demonstrated. Detection range is comparable with the other sensor platforms like optical ones. This is promising for replacing commercial optical biosensor platforms with low-cost, label-free, nanogap based impedimetric biosensors in the future. These biosensors are also appealing since they are operating at 10 mV_{rms} and offer low-power platforms.

Sensitivity to the dielectric constant of target medium is 132 pF per unit change in dielectric constant. This can be tailored by the geometry (for instance, undercut length) of the design according to application. Thus, this sensor platform can also find potential applications in chemical or gas sensors. Reliability is also tested by stability and repeatability measurements and positive results are observed.

These sensors can be further improved by optimizing sensor dimensions such as dielectric layer thickness and undercut length. Other surface functionalization techniques such as placing recognition elements on the electrodes, instead of the dielectric layer, can be tested. These would enhance sensitivity results even further and lower concentrations can be detected. Another path for the future work would be studying on a new target molecule like a specific cancer biomarker. In that case, a recognition element related to that specific type of cancer should be used and instead of the biotin in this work, that recognition element should be attached to the surface. Thus, a different surface functionalization procedure is going to be required. However, since the electrical detection platform will be the same, quick results can be obtained by using this work and only changing the surface functionalization procedure according to the new recognition element. The dynamic range can be tailored by the sensor geometry according to the required dynamic range of the studied cancer biomarker.

Finally, the current platform can be integrated with a microfluidic system and a low-cost commercial capacitance chip. This combination can offer novel and beneficial systems for the purpose of point-of-care and early cancer detection. It may be possible to search for multiple types of cancer on a single chip. This can be achieved with a sensor-array scheme by functionalizing different pixels with different types of recognition elements.

In the future, point of care biosensors can be in the shape of a wristwatch or necklace, periodically monitoring our blood over skin for cancer biomarkers and set off the alarm bells when the enemy is observed on the horizon. Maybe in the future, human will win the battle of cancer. Early detection would be a key component in this achievement and point-of-care biosensors would be an essential part of early detection. Maybe in the future, thanks to point-of-care biosensor technology, winning cancer will be so easy that a simple notification like *"Risk detected. Visit your doctor."* in a wristwatch embedded with a point-of-care biosensor will save the life of the one wearing this watch.

In the pursuit of this dream, this thesis investigated nanogap based label-free impedimetric biosensors as promising candidates and demonstrated that they offer compelling attributes for point-of-care and early cancer detection.

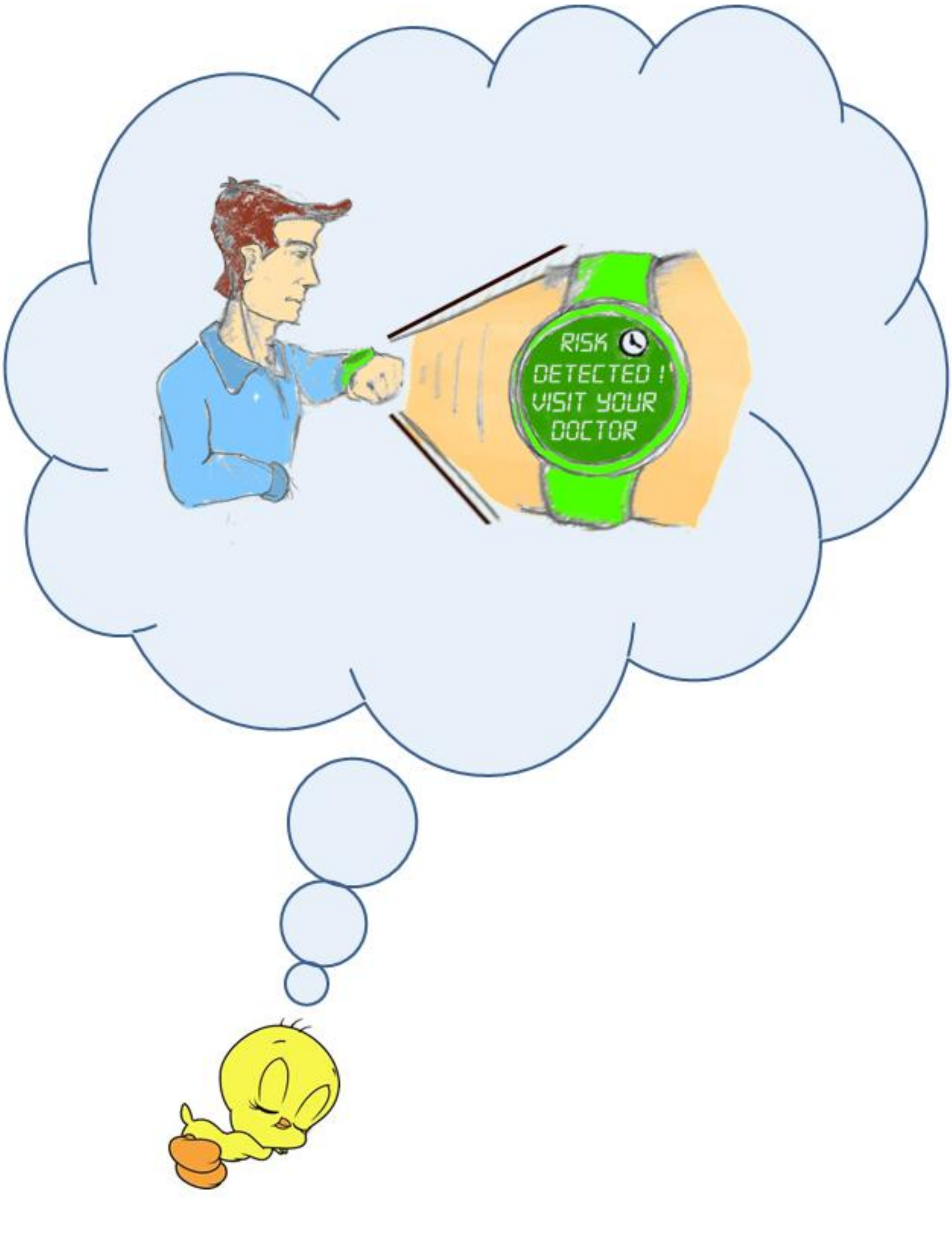

Figure 6.1 Biosensor embedded wristwatch as one of
the dream products of the work in this thesis
(the man is drawn by Fırat Yılmaz)

BIBLIOGRAPHY

[1] "WHO | Cancer," *WHO*. [Online].
Available: http://www.who.int/mediacentre/factsheets/fs297/en/.
[Accessed: 07-Jun-2012].

[2] "GLOBOCAN 2008." [Online].
Available: http://globocan.iarc.fr/. [Accessed: 07-Jun-2012].

[3] C. Leaf, "Why We're Losing The War On Cancer (And How To Win It)," *Fortune*, vol. 149, no. 84, pp. 76–82, 2004.

[4] S. Mousa, "Biosensors: the new wave in cancer diagnosis," *Nanotechnology, Science and Applications*, p. 1, Dec. 2010.

[5] S. A. Soper, K. Brown, A. Ellington, B. Frazier, G. Garcia-Manero, V. Gau, S. I. Gutman, D. F. Hayes, B. Korte, J. L. Landers, D. Larson, F. Ligler, A. Majumdar, M. Mascini, D. Nolte, Z. Rosenzweig, J. Wang, and D. Wilson, "Point-of-care biosensor systems for cancer diagnostics/prognostics," *Biosensors and Bioelectronics*, vol. 21, no. 10, pp. 1932–1942, Apr. 2006.

[6] I. E. Tothill, "Biosensors for cancer markers diagnosis," *Seminars in Cell & Developmental Biology*, vol. 20, no. 1, pp. 55–62, Feb. 2009.

[7] J. S. Daniels and N. Pourmand, "Label-Free Impedance Biosensors: Opportunities and Challenges," *Electroanalysis*, vol. 19, no. 12, pp. 1239–1257, 2007.

[8] D. Therriault, "Biosensors: Filling the gap," *Nature Nanotechnology*, vol. 2, no. 7, pp. 393–394, 2007.

[9] A. P. F. Turner, "Biosensors--Sense and Sensitivity," *Science*, vol. 290, no. 5495, pp. 1315–1317, Nov. 2000.

[10] C. for D. and R. Health, "Recently-Approved Devices - GlucoWatch G2 Biographer - P990026/S0008." [Online].
Available:http://www.fda.gov/medicaldevices/productsandmedicalprocedure

s/deviceapprovalsandclearances/recently-approveddevices/ucm083294.htm. [Accessed: 07-Jun-2012].

[11] “ApexBio Taiwan.” [Online]. Available: http://www.apexbio.com/. [Accessed: 07-Jun-2012].

[12] “OneTouch® | More power to you™.” [Online]. Available: http://www.onetouch.com/. [Accessed: 07-Jun-2012].

[13] J. P. Chambers, B. P. Arulanandam, L. L. Matta, A. Weis, and J. J. Valdes, “Biosensor recognition elements,” *Curr Issues Mol Biol*, vol. 10, no. 1–2, pp. 1–12, 2008.

[14] M. A. Cooper, “Label-free screening of bio-molecular interactions,” *Anal Bioanal Chem*, vol. 377, no. 5, pp. 834–842, Nov. 2003.

[15] J. Lin, F. Yan, and H. Ju, “Noncompetitive enzyme immunoassay for carcinoembryonic antigen by flow injection chemiluminescence,” *Clinica Chimica Acta*, vol. 341, no. 1–2, pp. 109–115, 2004.

[16] S.-F. Chou, W.-L. Hsu, J.-M. Hwang, and C.-Y. Chen, “Development of an immunosensor for human ferritin, a nonspecific tumor marker, based on surface plasmon resonance,” *Biosensors and Bioelectronics*, vol. 19, no. 9, pp. 999–1005, 2004.

[17] X. Fan, I. M. White, S. I. Shopova, H. Zhu, J. D. Suter, and Y. Sun, “Sensitive optical biosensors for unlabeled targets: A review,” *Analytica Chimica Acta*, vol. 620, no. 1–2, pp. 8–26, Jul. 2008.

[18] D. L. Graham, H. A. Ferreira, and P. P. Freitas, “Magnetoresistive-based biosensors and biochips,” *Trends Biotechnol.*, vol. 22, no. 9, pp. 455–462, Sep. 2004.

[19] D. R. Baselt, G. U. Lee, M. Natesan, S. W. Metzger, P. E. Sheehan, and R. J. Colton, “A biosensor based on magnetoresistance technology,” *Biosensors and Bioelectronics*, vol. 13, no. 7–8, pp. 731–739, Oct. 1998.

[20] D. . Graham, H. . Ferreira, P. . Freitas, and J. M. . Cabral, “High sensitivity detection of molecular recognition using magnetically labelled biomolecules and magnetoresistive sensors,” *Biosensors and Bioelectronics*, vol. 18, no. 4, pp. 483–488, Apr. 2003.

[21] F. Montaigne, A. Schuhl, F. N. Van Dau, and A. Encinas, "Development of magnetoresistive sensors based on planar Hall effect for applications to microcompass," *Sensors and Actuators A: Physical*, vol. 81, no. 1–3, pp. 324–327, Apr. 2000.

[22] M. Tondra, M. Porter, and R. J. Lipert, "Model for detection of immobilized superparamagnetic nanosphere assay labels using giant magnetoresistive sensors," *Journal of Vacuum Science Technology A: Vacuum, Surfaces, and Films*, vol. 18, no. 4, pp. 1125 –1129, Jul. 2000.

[23] S.-H. Chen, V. C. H. Wu, Y.-C. Chuang, and C.-S. Lin, "Using oligonucleotide-functionalized Au nanoparticles to rapidly detect foodborne pathogens on a piezoelectric biosensor," *Journal of Microbiological Methods*, vol. 73, no. 1, pp. 7–17, Apr. 2008.

[24] J. H. Chua, R.-E. Chee, A. Agarwal, S. M. Wong, and G.-J. Zhang, "Label-Free Electrical Detection of Cardiac Biomarker with Complementary Metal-Oxide Semiconductor-Compatible Silicon Nanowire Sensor Arrays," *Anal. Chem.*, vol. 81, no. 15, pp. 6266–6271, 2009.

[25] X. Dong, Y. Shi, W. Huang, P. Chen, and L.-J. Li, "Electrical Detection of DNA Hybridization with Single-Base Specificity Using Transistors Based on CVD-Grown Graphene Sheets," *Advanced Materials*, vol. 22, no. 14, pp. 1649–1653, 2010.

[26] F. N. Ishikawa, H.-K. Chang, M. Curreli, H.-I. Liao, C. A. Olson, P.-C. Chen, R. Zhang, R. W. Roberts, R. Sun, R. J. Cote, M. E. Thompson, and C. Zhou, "Label-Free, Electrical Detection of the SARS Virus N-Protein with Nanowire Biosensors Utilizing Antibody Mimics as Capture Probes," *ACS Nano*, vol. 3, no. 5, pp. 1219–1224, 2009.

[27] B. Gu, T. J. Park, J.-H. Ahn, X.-J. Huang, S. Y. Lee, and Y.-K. Choi, "Nanogap Field-Effect Transistor Biosensors for Electrical Detection of Avian Influenza," *Small*, vol. 5, no. 21, pp. 2407–2412, 2009.

[28] H.-S. Lee, K. S. Kim, C.-J. Kim, S. K. Hahn, and M.-H. Jo, "Electrical detection of VEGFs for cancer diagnoses using anti-vascular endotherial growth factor aptamer-modified Si nanowire FETs," *Biosensors and Bioelectronics*, vol. 24, no. 6, pp. 1801–1805, Feb. 2009.

[29] T. An, K. S. Kim, S. K. Hahn, and G. Lim, "Real-time, step-wise, electrical detection of protein molecules using dielectrophoretically aligned

SWNT-film FET aptasensors," *Lab on a Chip*, vol. 10, no. 16, p. 2052, 2010.

[30] J. C. Rife, M. M. Miller, P. E. Sheehan, C. R. Tamanaha, M. Tondra, and L. J. Whitman, "Design and performance of GMR sensors for the detection of magnetic microbeads in biosensors," *Sensors and Actuators A: Physical*, vol. 107, no. 3, pp. 209–218, Nov. 2003.

[31] P. Jiang and Z. Guo, "Fluorescent detection of zinc in biological systems: recent development on the design of chemosensors and biosensors," *Coordination Chemistry Reviews*, vol. 248, no. 1–2, pp. 205–229, Jan. 2004.

[32] H. Yu, F. Yan, Z. Dai, and H. Ju, "A disposable amperometric immunosensor for α-1-fetoprotein based on enzyme-labeled antibody/chitosan-membrane-modified screen-printed carbon electrode," *Analytical Biochemistry*, vol. 331, no. 1, pp. 98–105, Aug. 2004.

[33] P. Forrer, R. Tamaskovic, and R. Jaussi, "Enzyme-linked immunosorbent assay for measurement of JNK, ERK, and p38 kinase activities," *Biol. Chem.*, vol. 379, no. 8–9, pp. 1101–1111, Sep. 1998.

[34] B. B. Haab, "Methods and applications of antibody microarrays in cancer research," *Proteomics*, vol. 3, no. 11, pp. 2116–2122, Nov. 2003.

[35] "Prevalence of Prostate Cancer among Men with a Prostate-Specific Antigen Level ≤4.0 ng per Milliliter," *New England Journal of Medicine*, vol. 351, no. 14, pp. 1470–1470, 2004.

[36] L. Määttänen, A. Auvinen, U.-H. Stenman, T. Tammela, S. Rannikko, J. Aro, H. Juusela, and M. Hakama, "Three-Year Results of the Finnish Prostate Cancer Screening Trial," *JNCI J Natl Cancer Inst*, vol. 93, no. 7, pp. 552–553, Apr. 2001.

[37] C. D. Chin, V. Linder, and S. K. Sia, "Lab-on-a-chip devices for global health: Past studies and future opportunities," *Lab on a Chip*, vol. 7, no. 1, p. 41, 2007.

[38] A. Romani, N. Manaresi, L. Marzocchi, G. Medoro, A. Leonardi, L. Altomare, M. Tartagni, and R. Guerrieri, "Capacitive sensor array for localization of bioparticles in CMOS lab-on-a-chip," in *Solid-State Circuits Conference, 2004. Digest of Technical Papers. ISSCC. 2004 IEEE International*, 2004, pp. 224 – 225 Vol.1.

[39] T. Vilkner, D. Janasek, and A. Manz, “Micro Total Analysis Systems. Recent Developments,” *Anal. Chem.*, vol. 76, no. 12, pp. 3373–3386, 2004.

[40] A. Kim, C. S. Ah, C. W. Park, J.-H. Yang, T. Kim, C.-G. Ahn, S. H. Park, and G. Y. Sung, “Direct label-free electrical immunodetection in human serum using a flow-through-apparatus approach with integrated field-effect transistors,” *Biosensors and Bioelectronics*, vol. 25, no. 7, pp. 1767–1773, Mar. 2010.

[41] C. A. Marquette and L. J. Blum, “State of the art and recent advances in immunoanalytical systems,” *Biosensors and Bioelectronics*, vol. 21, no. 8, pp. 1424–1433, Feb. 2006.

[42] J. J. Carr and J. M. Brown, *Introduction to Biomedical Equipment Technology*, 3rd ed. Prentice Hall, 2000.

[43] J. S. Wilson, Lee, Y. H., and Mutharasan R., *Sensor Technology Handbook*. Newnes, 2005.

[44] A. royale des sciences Paris, *Histoire de l’Academie royale des sciences*. De l’imprimerie royale, 1788.

[45] D. K. Cheng, *Fundamentals of Engineering Electromagnetics*, 1st ed. Prentice Hall, 1992.

[46] Nevill, J.T., “Impedance Spectroscopy-Based Biosensors,” PhD, Bioengineering, University of California, Berkeley.

[47] “Dielectric constants of various materials.” [Online]. Available: http://www.clippercontrols.com/pages/Dielectric-Constant-Values.html. [Accessed: 07-Jun-2012].

[48] “Alumina (Al2O3) Atomic Layer Deposition (ALD).” [Online]. Available: https://www.mems-exchange.org/catalog/P3487/. [Accessed: 07-Jun-2012].

[49] G. Cogin Schwartz, Y.-S. Huang, and W. J. Patrick, “The effective dielectric constant of silicon dioxides deposited in the spaces between adjacent conductors,” *Journal of the Electrochemical Society*, vol. 139, no. 12, pp. L118–L122.

[50] H. Im, X.-J. Huang, B. Gu, and Y.-K. Choi, “A dielectric-modulated field-effect transistor for biosensing,” *Nature Nanotechnology*, vol. 2, no. 7, pp. 430–434, 2007.

[51] P. Van Gerwen, W. Laureys, G. Huyberechts, M. De Baeck, K. Baert, J. Suis, A. Varlan, W. Sansen, L. Hermans, and R. Mertens, “Nanoscaled interdigitated electrode arrays for biochemical sensors,” in *Solid State Sensors and Actuators, 1997. TRANSDUCERS ’97 Chicago., 1997 International Conference on*, 1997, vol. 2, pp. 907 –910 vol.2.

[52] D. K. Cheng, *Field and Wave Electromagnetics*, 2nd ed. Addison-Wesley, 1989.

[53] H. Morgan and N. G. Green, *AC Electrokinetics: Colloids and Nanoparticles*, 1st ed. Research Studies Pr, 2002.

[54] G. L. Bullard, H. B. Sierra-Alcazar, H. L. Lee, and J. L. Morris, “Operating principles of the ultracapacitor,” *Magnetics, IEEE Transactions on*, vol. 25, no. 1, pp. 102 –106, Jan. 1989.

[55] Z. Zhang, O. C. Thomsen, M. Andersen, J. D. Schmidt, and H. R. Nielsen, “Analysis and Design of Bi-directional DC-DC Converter in Extended Run Time DC UPS System Based on Fuel Cell and Supercapacitor,” in *Applied Power Electronics Conference and Exposition, 2009. APEC 2009. Twenty-Fourth Annual IEEE*, 2009, pp. 714 –719.

[56] V. Paladini, T. Donateo, A. de Risi, and D. Laforgia, “Super-capacitors fuel-cell hybrid electric vehicle optimization and control strategy development,” *Energy Conversion and Management*, vol. 48, no. 11, pp. 3001–3008, Nov. 2007.

[57] Y. Liu, M. Liu, W. M. Lau, and J. Yang, “Ion Size and Image Effect on Electrokinetic Flows,” *Langmuir*, vol. 24, no. 6, pp. 2884–2891, 2008.

[58] A. McBride, M. Kohonen, and P. Attard, “The screening length of charge-asymmetric electrolytes: A hypernetted chain calculation,” *The Journal of Chemical Physics*, vol. 109, no. 6, pp. 2423–2428, Aug. 1998.

[59] R. Parsons, “The electrical double layer: recent experimental and theoretical developments,” *Chem. Rev.*, vol. 90, no. 5, pp. 813–826, 1990.

[60] H.-J. Butt, K. Graf, and M. Kappl, *Physics and Chemistry of Interfaces*. Wiley-VCH, 2006.

[61] X. Chen, Z. Guo, G.-M. Yang, J. Li, M.-Q. Li, J.-H. Liu, and X.-J. Huang, "Electrical nanogap devices for biosensing," *Materials Today*, vol. 13, no. 11, pp. 28–41, Nov. 2010.

[62] J. T. Nevill, D. Di Carlo, P. Liu, K. H. Jeong, and L. P. Lee, "Detection of protein conformational changes with a nanogap biosensor," in *Solid-State Sensors, Actuators and Microsystems, 2005. Digest of Technical Papers. TRANSDUCERS '05. The 13th International Conference on*, 2005, vol. 2, pp. 1668 – 1671 Vol. 2.

[63] "Charge Relaxation in Uniform Conductors." [Online]. Available: http://web.mit.edu/6.013_book/www/chapter7/7.7.html. [Accessed: 07-Jun-2012].

[64] X. Liang and S. Y. Chou, "Nanogap Detector Inside Nanofluidic Channel for Fast Real-Time Label-Free DNA Analysis," *Nano Lett.*, vol. 8, no. 5, pp. 1472–1476, 2008.

[65] E. Finot, E. Bourillot, R. Meunier-Prest, Y. Lacroute, G. Legay, M. Cherkaoui-Malki, N. Latruffe, O. Siri, P. Braunstein, and A. Dereux, "Performance of interdigitated nanoelectrodes for electrochemical DNA biosensor," *Ultramicroscopy*, vol. 97, no. 1–4, pp. 441–449, Oct. 2003.

[66] B. Liu, J. Xiang, J.-H. Tian, C. Zhong, B.-W. Mao, F.-Z. Yang, Z.-B. Chen, S.-T. Wu, and Z.-Q. Tian, "Controllable nanogap fabrication on microchip by chronopotentiometry," *Electrochimica Acta*, vol. 50, no. 15, pp. 3041–3047, May 2005.

[67] Y. Fan, X. Chen, A. D. Trigg, C. Tung, J. Kong, and Z. Gao, "Detection of MicroRNAs Using Target-Guided Formation of Conducting Polymer Nanowires in Nanogaps," *J. Am. Chem. Soc.*, vol. 129, no. 17, pp. 5437–5443, 2007.

[68] U. Schlecht, A. Malavé, T. M. A. Gronewold, M. Tewes, and M. Löhndorf, "Detection of Rev peptides with impedance-sensors — Comparison of device-geometries," *Biosensors and Bioelectronics*, vol. 22, no. 9–10, pp. 2337–2340, Apr. 2007.

[69] C. Ionescu-Zanetti, J. T. Nevill, D. Di Carlo, K. H. Jeong, and L. P. Lee, "Nanogap capacitors: Sensitivity to sample permittivity changes," *Journal of applied physics*, vol. 99, no. 2.

[70] M. Wilchek and E. A. Bayer, in *Avidin-Biotin Technology*, vol. Volume 184, Academic Press, 1990.

[71] L. P. Lee, "Nanogap Biomolecular Junction," May 2004.

[72] M. B. González-García, C. Fernández-Sánchez, and A. Costa-García, "Colloidal gold as an electrochemical label of streptavidin-biotin interaction," *Biosens Bioelectron*, vol. 15, no. 5–6, pp. 315–321, Aug. 2000.

[73] R. A. Williams and H. W. Blanch, "Covalent immobilization of protein monolayers for biosensor applications," *Biosens Bioelectron*, vol. 9, no. 2, pp. 159–167, 1994.

[74] A. L. Weisenhorn, F.-J. Schmitt, W. Knoll, and P. K. Hansma, "Streptavidin binding observed with an atomic force microscope," *Ultramicroscopy*, vol. 42–44, Part 2, no. 0, pp. 1125–1132, Jul. 1992.

[75] J. Spinke, M. Liley, F.-J. Schmitt, H.-J. Guder, L. Angermaier, and W. Knoll, "Molecular recognition at self-assembled monolayers: Optimization of surface functionalization," *The Journal of Chemical Physics*, vol. 99, no. 9, p. 7012, Nov. 1993.

[76] A. Shaporenko, K. Adlkofer, L. S. O. Johansson, M. Tanaka, and M. Zharnikov, "Functionalization of GaAs Surfaces with Aromatic Self-Assembled Monolayers: A Synchrotron-Based Spectroscopic Study," *Langmuir*, vol. 19, no. 12, pp. 4992–4998, Jun. 2003.

[77] C. Boozer, J. Ladd, S. Chen, Q. Yu, J. Homola, and S. Jiang, "DNA directed protein immobilization on mixed ssDNA/oligo(ethylene glycol) self-assembled monolayers for sensitive biosensors.," *Analytical chemistry*, vol. 76, no. 23, pp. 6967–72, Dec. 2004.

[78] C. Duschl, A. F. Sévin-Landais, and H. Vogel, "Surface engineering: optimization of antigen presentation in self-assembled monolayers.," *Biophysical journal*, vol. 70, no. 4, pp. 1985–95, Apr. 1996.

[79] F. Zhang and M. P. Srinivasan, “Self-assembled molecular films of aminosilanes and their immobilization capacities,” *Langmuir*, vol. 20, no. 6, pp. 2309–2314, Mar. 2004.

[80] J.-K. Kim, D.-S. Shin, W.-J. Chung, K.-H. Jang, K.-N. Lee, Y.-K. Kim, and Y.-S. Lee, “Effects of polymer grafting on a glass surface for protein chip applications,” *Colloids and Surfaces B: Biointerfaces*, vol. 33, no. 2, pp. 67–75, Jan. 2004.

[81] A. Ahluwalia, D. De Rossi, C. Ristori, A. Schirone, and G. Serra, “A comparative study of protein immobilization techniques for optical immunosensors,” *Biosens Bioelectron*, vol. 7, no. 3, pp. 207–214, 1992.

[82] E. L. Schmid, T. A. Keller, Z. Dienes, and H. Vogel, “Reversible Oriented Surface Immobilization of Functional Proteins on Oxide Surfaces,” *Anal. Chem.*, vol. 69, no. 11, pp. 1979–1985, 1997.

[83] A. Ulman, “Formation and Structure of Self-Assembled Monolayers,” *Chem. Rev.*, vol. 96, no. 4, pp. 1533–1554, Jun. 1996.

[84] R. B. Merrifield, “Solid Phase Peptide Synthesis. I. The Synthesis of a Tetrapeptide,” *J. Am. Chem. Soc.*, vol. 85, no. 14, pp. 2149–2154, 1963.

[84] H. Acar, R. Garifullin, and M. O. Guler, “Self-assembled template-directed synthesis of one-dimensional silica and titania nanostructures.,” *Langmuir: the ACS journal of surfaces and colloids*, vol. 27, no. 3, pp. 1079–84, Feb. 2011.

[86] Keithley Instruments Inc., “Model 4200-CVU Start Up Guide.” Nov-2007.

[87] Keithley Instruments Inc., “Model 4200-SCS Semiconductor Characterization System Reference Manual.” Sep-2011.

[88] A. Star, J.-C. P. Gabriel, K. Bradley, and G. Grüner, “Electronic Detection of Specific Protein Binding Using Nanotube FET Devices,” *Nano Lett.*, vol. 3, no. 4, pp. 459–463, 2003.

[89] R. Bruck, E. Melnik, P. Muellner, R. Hainberger, and M. Lammerhofer, “Spin coated thin-film polymer waveguide Mach-Zehnder interferometer for label-free streptavidin detection,” in *Information Photonics (IP), 2011 ICO International Conference on*, 2011, pp. 1 –2.

[90] D.-Y. Jang, Y.-P. Kim, H.-S. Kim, S.-H. K. Park, S.-Y. Choi, and Y.-K. Choi, “Sublithographic vertical gold nanogap for label-free electrical detection of protein-ligand binding,” *Journal of Vacuum Science & Technology B: Microelectronics and Nanometer Structures*, vol. 25, no. 2, pp. 443–447, 2007.

[91] S.-F. Cheng and L.-K. Chau, “Colloidal Gold-Modified Optical Fiber for Chemical and Biochemical Sensing,” *Anal. Chem.*, vol. 75, no. 1, pp. 16–21, 2002.

[92] Y. Cui, Q. Wei, H. Park, and C. M. Lieber, “Nanowire Nanosensors for Highly Sensitive and Selective Detection of Biological and Chemical Species,” *Science*, vol. 293, no. 5533, pp. 1289–1292, Aug. 2001.

[93] D. De Simone, E. Tenaglia, P. Piazza, A. Vaccaro, M. Bollin, G. Capetti, P. Piacentini, and P. Canestrari, “Potential applications of negative tone development in advanced lithography,” *Microelectronic Engineering*, vol. 88, no. 8, pp. 1917–1922, Aug. 2011.

[94] “Capacitance to Digital Converters | A/D Converters | Analog Devices.” [Online]. Available: http://www.analog.com/en/analog-to-digital-converters/capacitance-to-digital-converters/products/index.html. [Accessed: 07-Jun-2012].

[95] E. S. Snow, F. K. Perkins, E. J. Houser, S. C. Badescu, and T. L. Reinecke, “Chemical Detection with a Single-Walled Carbon Nanotube Capacitor,” *Science*, vol. 307, no. 5717, pp. 1942–1945, Mar. 2005.

[96] S. Chopra, K. McGuire, N. Gothard, A. M. Rao, and A. Pham, “Selective gas detection using a carbon nanotube sensor,” *Applied Physics Letters*, vol. 83, no. 11, p. 2280, 2003.

[97] J. Li, Y. Lu, Q. Ye, M. Cinke, J. Han, and M. Meyyappan, “Carbon Nanotube Sensors for Gas and Organic Vapor Detection,” *Nano Lett.*, vol. 3, no. 7, pp. 929–933, 2003.